UNIFORM MULTILAYER GRAPHENE FOR SPACE PLASMA

INSTRUMENTATION

by

Michael LePere, B.S.

A thesis submitted to the Graduate Council of
Texas State University in partial fulfillment
of the requirements for the degree of
Master of Science
with a Major in Engineering
December 2020

Committee Members:

Ravi Droopad, Chair

Qingkai Yu

Yihong Chen

FAIR USE AND AUTHOR'S PERMISSION STATEMENT

Fair Use

Duplication Permission

ACKNOWLEDGEMENTS

I would like to thank Dr. Qingkai Yu, Dr. Ravi Droopad, Dr. Zhihong Liu, and Dr. Dalim

Mia. Their support and guidance has guided me through the work completed in this

thesis.

TABLE OF CONTENTS

Page

CHAPTER

LIST OF TABLES

LIST OF FIGURES

Figure   **Page**

LIST OF ABBREVIATIONS

Abbreviation	Description
PMMA	poly(methyl methacrylate)
TOF	time-of-flight
ENA	energetic neutral atom
CVD	chemical vapor deposition
HFTCVD	hot filament chemical vapor deposition
RIE	reactive ion etch
SEM	scanning electron microscopy
AFM	atomic force microscopy
EDX	energy-dispersive x-ray spectroscopy
XPS	x-ray photoelectron spectroscopy
TEM	transmission electron microscopy
HRTEM	high-resolution transmission microscopy
NPC	nanoporous carbon
IPA	isopropanol alcohol
GFET	graphene field effect transistor
FLG	few layer graphene
DI	deionized
PC	pure copper
CNA	copper-nickel alloy

PCC   pure copper with carbon cover

MFC   mass flow controller

ABSTRACT

With plasma being the most common state of matter in the universe, it is no wonder why astronomers and the like are very interested in studying plasma. Scientists have sent many probes, shuttles, and spacecraft into our solar system with the purpose to study the plasma surrounding or composing the celestial bodies around Earth, including the plasma giant we call the Sun. To collect data and information from these celestial bodies, spacecraft are equipped with space plasma instruments which detect plasma or ions. One of the common components of these instruments is the use of carbon as a foil to take advantage of two properties which occur between foils and particles: charge conversion and secondary electron emission. Carbon foils have been used for decades in space plasma instrumentation to detect ions and energetic neutral atoms and have allowed researchers to obtain a better understanding of space plasma and have resulted in many scientific advancements. However, the use of these foils produces adverse effects such as angular scattering and energy straggling during detection phases which inhibits the performance of these instruments. These issues are correlated with incident angle, energy, mass of the projectile and foil thickness. With the discovery of graphene, studies have indicated that graphene foils are a promising replacement for carbon foils due to their incredible strength and extreme thinness. These results have shown that graphene foils have similar charge state distributions to carbon foils, decrease angular scattering, and lower average energy loss. Such results indicate that graphene may soon replace carbon foils and create new opportunities for space research. However, due to the current

transfer processes during the manufacture of graphene foils, most commonly using poly(methyl methacrylate) (PMMA), impurities present on the foils impede the detection process in space plasma instruments. This is due to the difficulties in removing the transfer layer, leaving a residual film. This research will focus on current transfer processes and the production of uniform multilayer graphene for its implementation in space plasma instruments. Producing a more uniform multilayer graphene will reduce the potential for contamination and defects by allowing for a transfer process which does not require a transfer layer.

1. INTRODUCTION

Plasma is a state of matter which can be described as an ionized gas made up of positively charged ions and free electrons. These ions and free electrons result in a net-zero electrical charge; however, they are electrically conductive, and their behavior can be controlled by long-range electromagnetic fields. In areas of low pressure, such as the upper atmospheres of planets, and very high temperatures, such as stars, plasma can be found. Plasma also constitutes over 99% of the matter found in the universe, and therefore has been in the forefront of space science and astrophysics.

Solar wind, planetary atmospheres and their magnetic fields influence the way space plasma interacts and is described through magnetohydrodynamics to model its behavior. To get a better understanding of the composition of plasma surrounding planets, instrumentation was developed and placed on spacecraft to detect these ions.

Carbon foils have become a crucial component in many space plasma instruments such as coincidence and time-of-flight (TOF) measurements in plasma spectrometers, plasma mass spectrometers, and energetic neutral atom (ENA) imagers. These carbon foils can be utilized to take advantage of two main processes that occur due to interaction with ions and neutral atoms: (1) particle-induced secondary emission, which allows for coincidence and TOF measurements, and (2) particle charge state modification, which allows ENAs to be measured (Allegrini, Ebert, & Funsten, 2016).

Unfortunately, the interaction of the foil with the incident particle creates several adverse effects which can inhibit the detection and measurements of the particles. To minimize these adverse effects, using the thinnest foils possible is appropriate. With the discovery and development of graphene, space plasma instrument devices may become

more accurate and sensitive to plasma by using this new material.

Graphene is a one atomic layer thick carbon material arranged in a hexagonal lattice. Being one atomic layer thick and a carbon material, it could prove to be a perfect replacement to even the state-of-the-art carbon foils (~20 atoms thick) because it is not only incredibly thin but is also incredibly strong (Young modulus ~1 TPa), increasing the likelihood of survival during a rocket launch into space (Allegrini, Ebert, & Funsten, 2016).

While graphene may be a perfect material to replace carbon foils in space plasma instruments, its implementation into such instruments proves to be difficult. The production of graphene can be completed in many different ways; most require it to be grown on a metal substrate, typically copper. One such process to produce graphene is through chemical vapor deposition (CVD) at a high temperature, typically around 1,000°C. Once this process is completed, the graphene must then be transferred to the desired target location, such as an arbitrary substrate. While graphene is considered as one of the strongest materials in the world, it is very fragile, or brittle, on a scale that makes it usable in most technologies. Thus, a support layer must be utilized to maintain integrity during the transfer process. Once the graphene is transferred, the support layer must be removed to utilize the outstanding characteristics of the material. However, the removal process can prove to be an incredible challenge since the support layer must be removed in its entirety. Current cleaning processes are unable to fully remove the support layer and the underlying contaminates during the growth process.

One of the most common methods of transferring graphene is with the use of poly-methyl-methacrylate (PMMA) due to its strong interaction with graphene, however,

as mentioned previously, this process is unable to remove the PMMA in its entirety. I propose a process which will remove the necessity to utilize a transfer layer by creating a consistent multilayer graphene sturdy enough to be transferred without the need for a transfer layer using CVD.

The added layers of graphene will promote an overall structural integrity which can allow for a reasonable strength to transfer the graphene without the need for a transfer layer. This would reduce the chances of tears or breaks occurring in the graphene, as well as reducing the potential of contamination by not using a transfer layer. For space plasma instruments, such as plasma mass spectrometers, the foil must ideally contain no breaks or tears, no contamination, and be multi-layer to promote secondary electron emission.

Most commonly, graphene is produced using CVD. This work will produce graphene using CVD with the goal of maximizing uniformity with multi-layer graphene. Once the sample is produced, the sample will be examined using Raman spectroscopy and XPS. These techniques have proven to provide good information regarding uniformity, number of layers, and chemical composition of the carbon and substrate.

To promote the growth of uniform multi-layer graphene, the use of nickel and a carbon cover were used. The results of these samples have been compared to that of pure copper samples. The use of nickel increases the carbon saturation limit while the carbon cover was used to create a temperature gradient to promote an increase in the number of graphene layers as well as uniformity. More information regarding this is in Chapter 3.

1.1 Applications

With the discovery of graphene, the world of opportunities for graphene-based devices and systems are nearly endless due to its incredible electrical and thermal conductivity and strength. Medical, military, industrial, electrical, mechanical, and many more fields are open to new developments with graphene.

Aerospace is yet another field that is incorporating graphene. Aftab, Shaikh, Saifullah, Hussein, & Ahmed (2019) covers new aerospace applications such as improved barrier performance on space craft, and surface technology to reduce ice and erosion. Graphene oxide also has many incredible characteristics such as high stability and can be made into covering large surface area. Graphene can be used as fuel in aircraft, separate water from fuel tanks, and dissipate heat.

Due to graphene's thin nature, it can be incorporated easily into flexible electronic applications and organic electronics. With these characteristics, graphene can be used in display systems in aircrafts. It can also be used in antennas because of its high electrical mobility and power storage due to its high surface area and conductivity.

Since graphene is a carbon material, it is naturally compatible with biomedical technology. Because of this, extensive research has been conducted to implement graphene into applications such as energy biomaterials, polymer composites and biosensors (Cheng et al., 2019). These biosensors can be used in the diagnosis and treatment of various diseases. Graphene based nanocarriers are also a possibility to release drugs into the human body.

Though all of these applications are being introduced in new research experiments, most have yet to become a reality due to the difficulty in the

implementation process.

1.2 Limitations and Challenges

While graphene may be considered the strongest material in the known universe, it is very difficult to manufacture effectively and handle on a manageable scale. Graphene is incredibly fragile due to scaling effects, becoming weaker on a larger scale and due to its brittle nature, requiring high purity and ideally no cracks or breaks in bonds. The introduction of these defects causes the overall strength of graphene to plummet.

An experiment conducted by Giesbers et al. (2016) highlights the current difficulties and defects currently found in graphene. Typically, grain boundaries are the main culprit in defects found in graphene, limiting its applications into flexible technologies such as gas permeation, organic solar cells, OLEDs, food and medical packaging. Graphene integration will remain as a dream until a better method can be used to produce more consistent and pure graphene.

2. LITERATURE REVIEW

2.1 PMMA with Acetone Cleaning
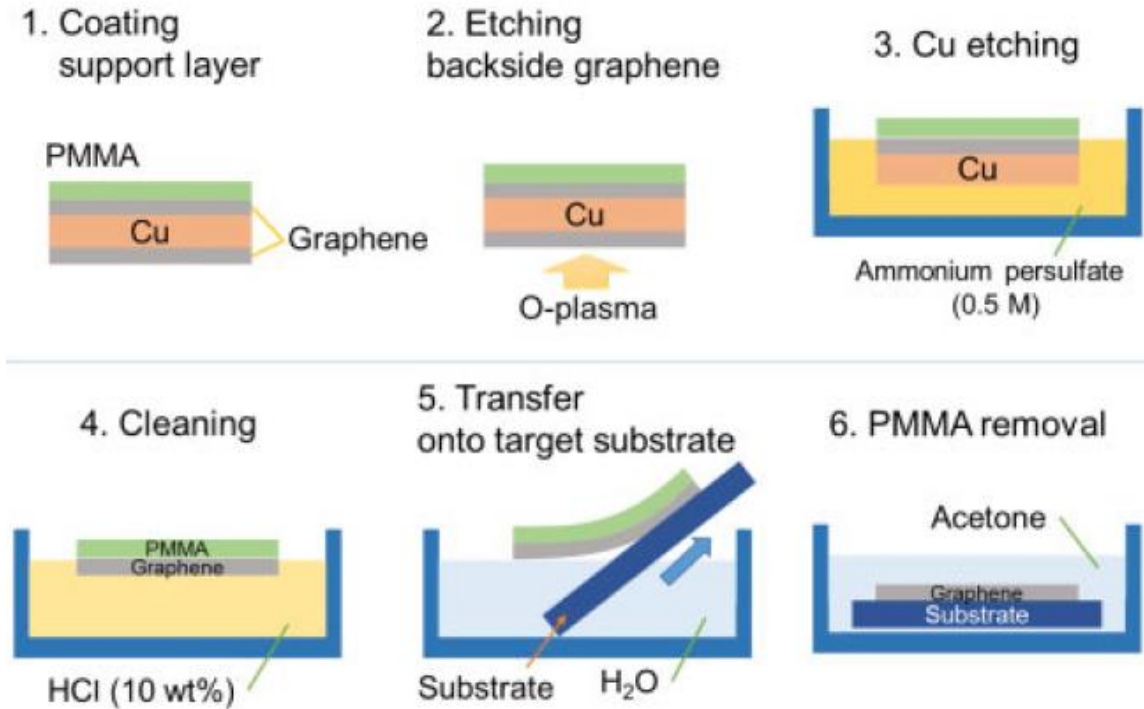
Figure 2.1. Diagram of transfer method using PMMA. Retrieved from Yasunishi et al., 2016.

Yasunishi et al. (2016) performed an experiment to transfer graphene. Using CVD grown graphene on a copper substrate, PMMA is spin coated onto one side of the copper/graphene foil. Once the PMMA is applied, an oxygen plasma is used through a reactive ion etch (RIE) to remove the graphene from the non-PMMA side. Next, the copper is etched away using ammonium persulfate, leaving only a layer of graphene and PMMA. Graphene and PMMA is cleaned of the etchant using hydrochloric acid and water then finally transferred to the target substrate. Once the graphene has been transferred to the target substrate, acetone is used to remove the PMMA. Figure 2.1 is a schematic detailing this transfer process.

This process succeeds in its ability to transfer the graphene to the target substrate

without damaging the integrity of the graphene, however, the use of acetone fails at completely removing the PMMA. Scanning electron microscopy (SEM) and atomic force microscopy (AFM) were used to check for residual particles in this process.
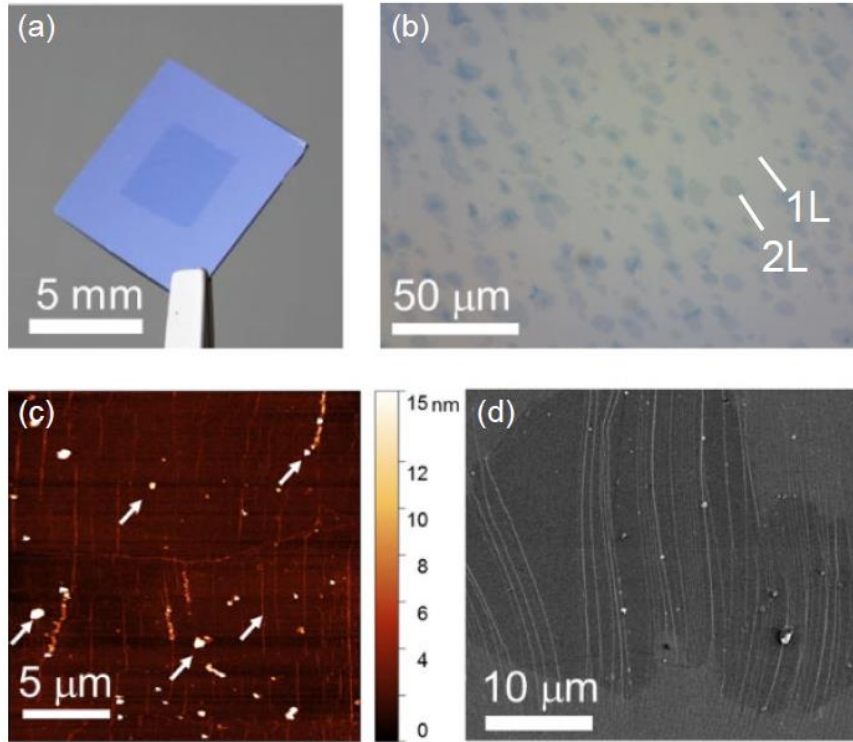
Figure 2.2. Images of graphene transferred onto silicon substrate. (a) Photograph, (b) micrograph, (c) AFM image, (d) SEM image. Retrieved from Yasunishi et al., 2016.

The residual particles remaining on the graphene can be seen in Figure 2.2. The arrows in (c) indicate the remaining PMMA that failed to be removed with the acetone. These particles can be verified to be PMMA through the use of energy-dispersive X-ray spectroscopy (EDX). It should be noted that while PMMA does remain after the acetone treatment, other contaminates such as silicon, magnesium, aluminum, and titanium are also found using EDX. The origin of these particles is believed to be from the quartz tube of the CVD furnace during the graphene growth phase and the copper foil used as a growth substrate. The utilization of a buffered hydrofluoric acid (BHF), a well-known

7

etchant for oxides, is able to reduce these particles by a factor of four.

2.2 PMMA Transfer Using Low Molecular Weight

The molecular weight of PMMA also influences the contamination amount after the removal process. An experiment conducted by Kim et al. (2016) demonstrated the contamination concentration of varying molecular weights of PMMA and found that a higher molecular weight produced a higher contamination. This is due to an increase in van der Waals attractions of longer polymer chains associated with higher average molecular weight. Potential other solutions to remove this PMMA involve processes such as oxygen plasma or ultrasound cleaning. However, these processes can easily damage the graphene.

In electronic applications of graphene, PMMA residuals can result in a p-doping effect and reduced carrier mobility, which degrades device performance. Optimizing the average molecular weight of the PMMA can reduce the degrading effects without increasing a thermal budget to do so.

2.3 Hexane Transfer
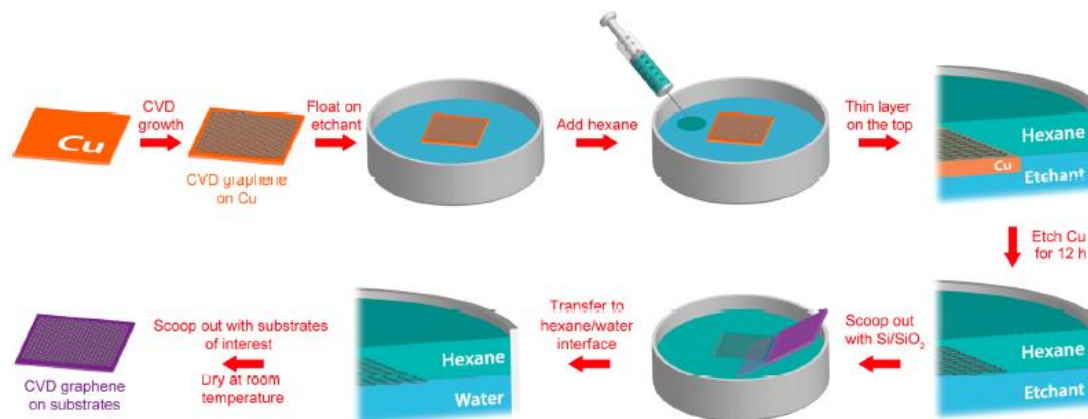
Figure 2.3. Transfer process of graphene using hexane. Retrieved from G. Zhang et al., 2016.

In this process, no polymer is utilized during the transfer and thus there is no need

for a cleaning process to remove a polymer. Instead, hexane is utilized to reduce the

surface tension placed on the graphene to maintain its integrity (G. Zhang et al., 2016).

Once the copper substrate is etched and the graphene is cleaned, the graphene is

transferred to the target substrate. The residual particles from the quartz CVD tube still

remain, however, there is no residual polymer since one was never used. This transfer

method is more difficult than a PMMA transfer and may not be suitable to all

applications, but it does result in a cleaner transfer. Figure 2.3 outlines the schematic for

the hexane transfer process.

2.4 PMMA Removal with Thermal Annealing
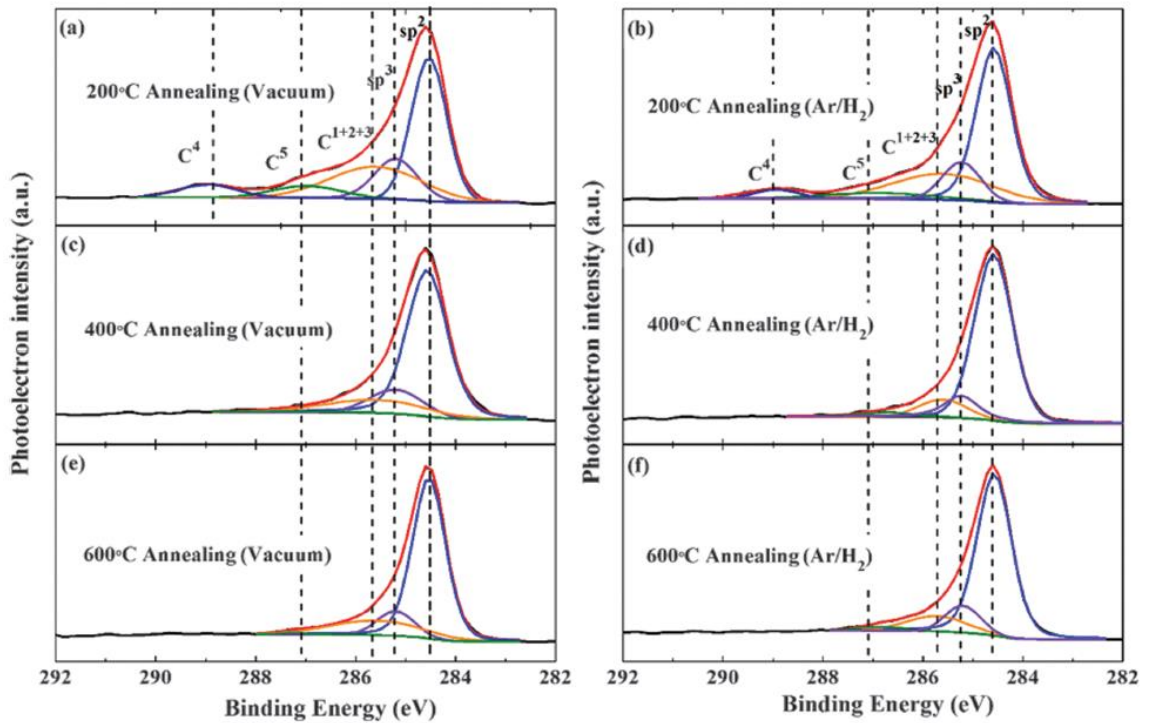
Figure 2.4. XPS spectrum of the transferred graphene after annealing process. (a), (c), and (e) indicate the XPS after vacuum annealing. (b), (d), (f) indicate XPS spectrum after Ar/H$_2$ annealing. Retrieved from Ahn, Kim, Ganorkar, Kim, & Kim, 2016.

9
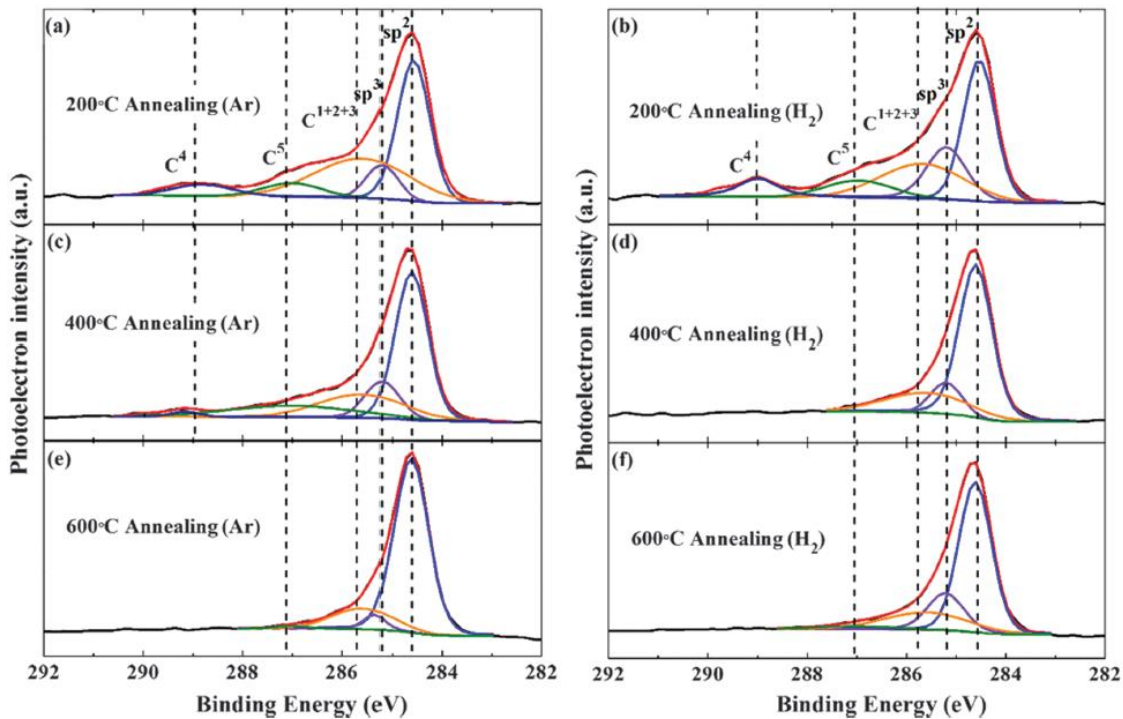
Figure 2.5. XPS spectrum of the transferred graphene after annealing process. (a), (c), and (e) indicate the XPS after Ar annealing. (b), (d), (f) indicate XPS spectrum after H_2 annealing. Retrieved from Ahn, Kim, Ganorkar, Kim, & Kim, 2016.

Utilizing a PMMA transfer, a thermal annealing process is used in addition to acetone to remove the PMMA by Ahn, Kim, Ganorkar, Kim, & Kim (2016). Using a vacuum chamber, a vacuum, Ar, H_2, and a mixture Ar/H_2 is used at different temperatures to remove the PMMA. A reaction occurs between the ambient gas at an elevated temperature with the PMMA causing it to decompose. Higher temperatures result in an increase in the removal of the PMMA. The XPS spectrum in Figures 4 and 5 indicate the carbon 1s reactions to graphene and PMMA. A lower photoelectron intensity indicates a lower amount of PMMA on the graphene surface.

The results from this experiment indicate a removal of PMMA, however, not completely. Some side effects are produced with this technique such as the production of amorphous carbon, which jeopardizes the integrity of the graphene. However, the use of

10

argon did not produce any amorphous carbon.

2.5 PMMA Removal with Radiolized Water at High Temperatures
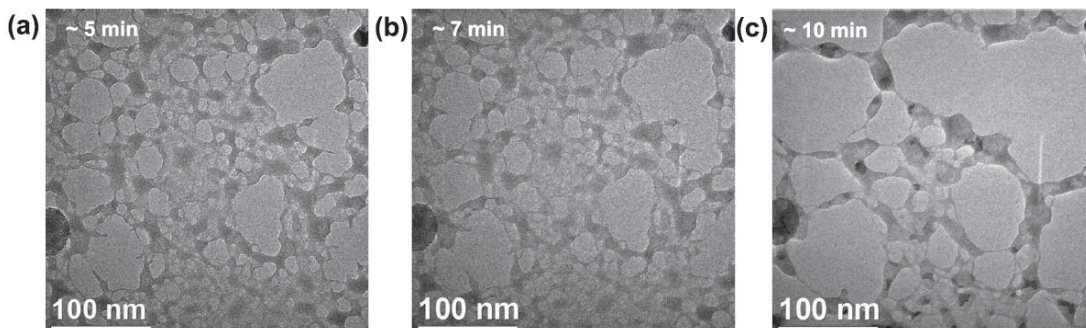
Figure 2.6. TEM imaging of PMMA removal over time. Retrieved from Islam et al., 2017.

Radiolized water, created by using an electron beam (e-beam), can be used to selectively decompose and remove PMMA and leave the graphene unaffected (Islam et al., 2017). At high temperatures (800°C), PMMA exposed to radiolized water decomposes and is removed from the surface of the graphene. This process is very effective at removing the PMMA locally (~0.02 μm^2), however, it cannot be used on a large scale. It is also ineffective in locations where inorganic particles are located. PMMA removal over exposure time can be seen in Figure 2.6 above.

2.6 Rosin-enabled Graphene Transfer
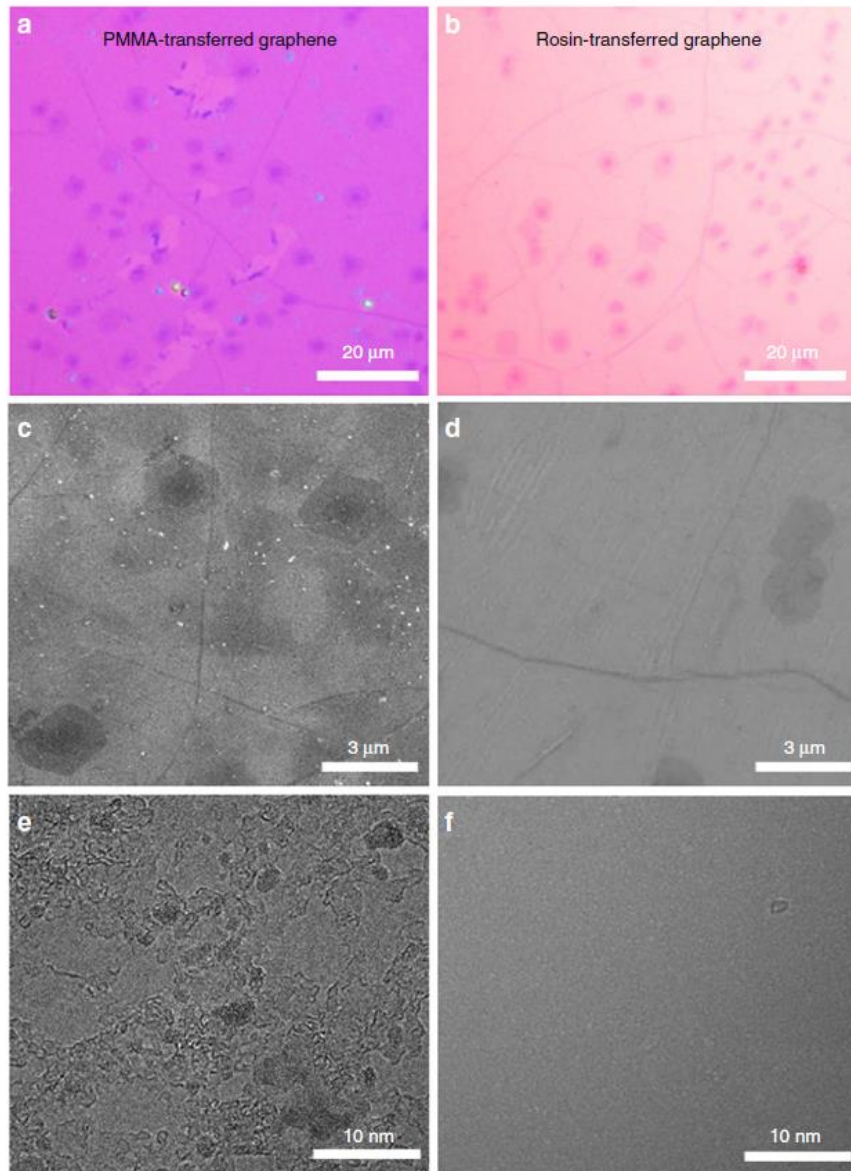
Figure 2.7. Surface characterization of graphene transferred by PMMA and rosin. (a, b) OM, (c, d) SEM, and (e, f) HRTEM. (a, c, e) PMMA and (b, d, f) rosin-transferred graphene. Retrieved from Z. Zhang et al., 2017.

Naturally, rosin has a weak interaction with graphene, but strong enough support strength, allowing it to be used as a support layer and be removed with more ease as compared to PMMA. It also has better solubility as compared to PMMA. In this transfer technique, instead of PMMA, a rosin solution with high viscosity is applied using a spin

coating technique to create a uniform film over the graphene (Z. Zhang et al., 2017).

Once the copper substrate is etched, the rosin is removed using acetone and banana oil

solutions. In Figure 2.7, optical microscopy (OM), SEM, and high-resolution

transmission electron microscopy (HRTEM) are used to characterize the transfer of

graphene by PMMA and rosin. One can clearly see, while the graphene is not perfectly

clean, the rosin transferred graphene has less contaminants than the PMMA transferred

graphene. This transfer technique can be used on a large scale as well, allowing for more

versatile applications of graphene-based technology.

2.7 PMMA Transfer with Platinum-metal Catalysis Cleaning
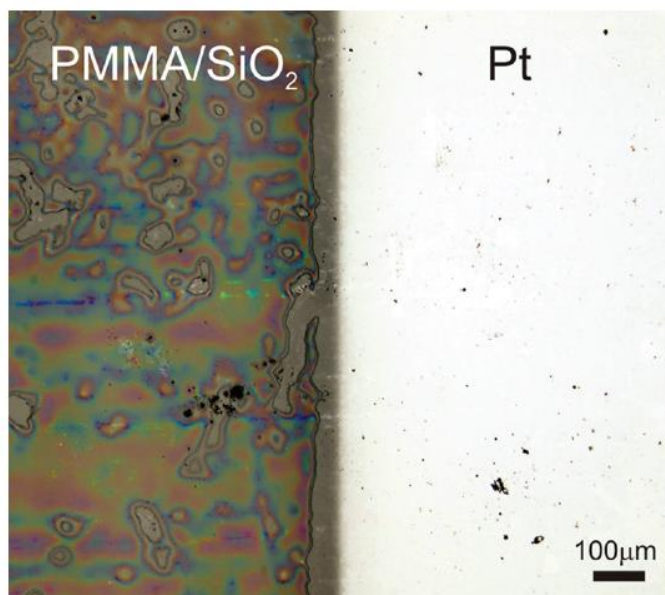
Figure 2.8. Light optical microscopy image of platinum-catalysis cleaning. Retrieved
from Longchamp, Escher, & Fink, 2013.

Platinum is well known in catalysis and interestingly, platinum has a catalytic

property in its reaction with PMMA (Longchamp, Escher, & Fink, 2013). Using the same

transfer method as outlined in PMMA with Acetone Cleaning, the PMMA and graphene

foil is placed onto a platinum-coated 50nm thick silicon nitride membrane. Next, the

sample is placed onto a conventional hot plate to be thermally annealed in air at 175-300°C. An increased temperature allows for a lower time needed to achieve complete PMMA degradation. Figure 2.8 shows the optical microscopy image of the platinum-catalytic reaction with the PMMA. On the platinum surface, no visible PMMA can be seen, however, PMMA still remains on the silicon dioxide surface, indicating the catalytic reaction.

The catalytic properties to selectively degrade the PMMA can be attributed to the platinum's ability to dissociate adsorbed H_2 into atomic hydrogen, effectively breaking up the PMMA polymer chain. Platinum even in the vicinity of the PMMA allows for decomposition to occur. Because of this, this process is more easily accessible in laboratories and does not require any special equipment.

2.8 Crack-free Transfer for Gas Mixture Separation
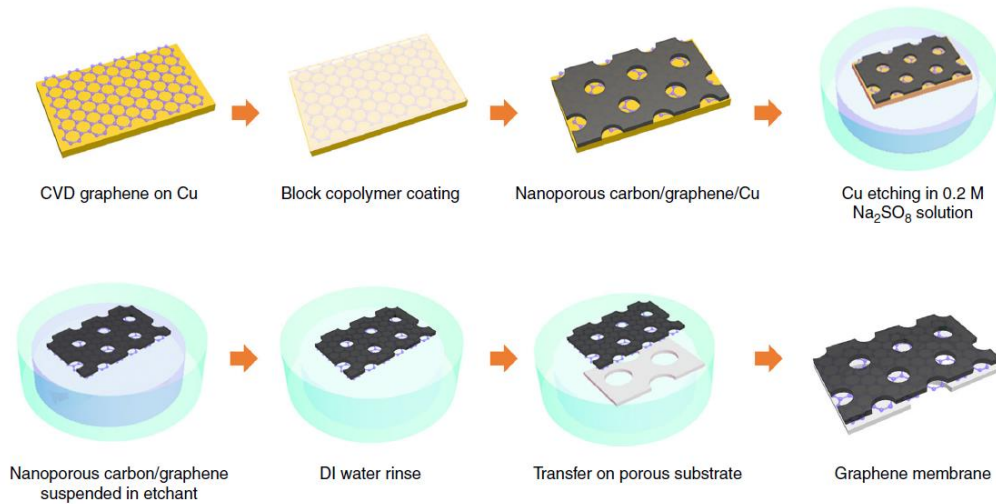
Figure 2.9. Schematic of graphene membrane by nanoporous carbon (NPC) assisted transfer method. Retrieved from Huang et al., 2018.

An important characteristic which must be achieved for many graphene-based technologies is for the graphene to be crack-free, including the foils in space plasma

instruments. This transfer method focuses on achieving the most consistent, crack-free graphene possible using nanoporous carbon (NPC) for a gas separation application. Huang et al. (2018) performed this experiment to solve the problem of significant cracks or tears occurring when using a porous support. Their solution was the utilization of NPC grown on top of the graphene. Once the graphene was grown it was used in a gas separation application and was found to have an H_2/CH_4 selectivity of 25. Figure 2.9 displays this transfer process to achieve this application.

2.9 Direct Transfer of Graphene
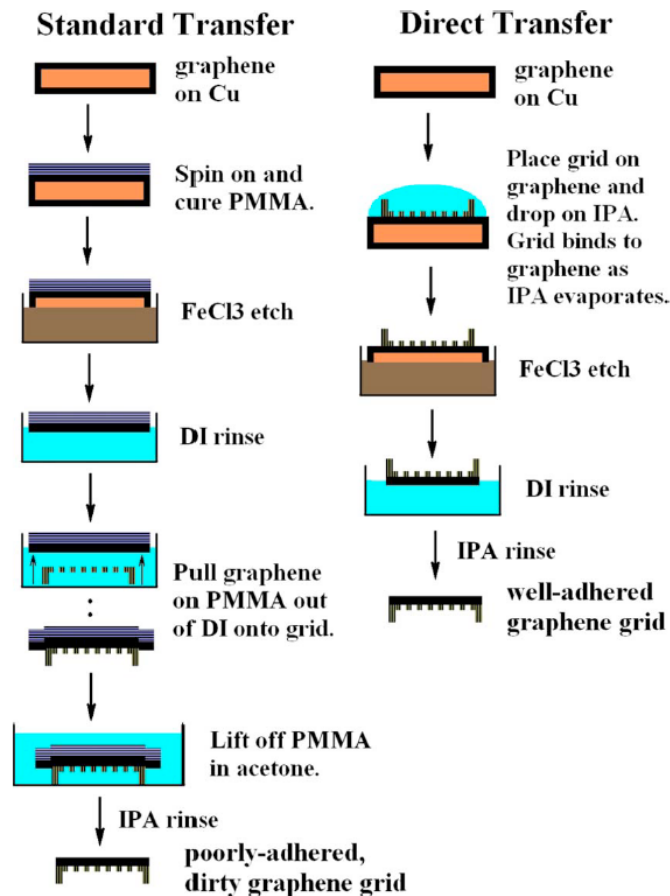
Figure 2.10. Comparison of PMMA and direct transfer of graphene to a-C TEM grids. Retrieved from Regan et al., 2010.

Regan et al. (2010) performed a simple, yet effective transfer process of placing

15

the graphene/copper foil directly onto a TEM grid. This transfer process does not involve

any polymer or transfer layer, eliminating the requirement to remove a transfer layer. It

results in a strong bond between the grid support and graphene with very low

contamination. However, intrinsic particles from the graphene growth process do still

remain. This process also cannot be used in many applications.

As seen in Figure 2.10, after one side of the graphene/copper foil is etched using

an oxygen plasma, the graphene/copper foil is placed directly onto the TEM grid.

Isopropanol (IPA) is then carefully placed onto the top of the grid to wet both the support

grid and the graphene. A 10 to 20-minute bake on a hot plate at 120°C is then used to

help evaporate and strengthen the bond between the grid and graphene. Next, the copper

foil is etched using iron chloride (FeCl$_3$). The etchant is then cleaned using deionized

water. Finally, IPA is used to remove any remaining etchant, remove organic material,

and help dry the grid.

2.10 Precise Graphene Transfer

Figure 2.11. Photographs of wafer before the transfer (a), mediator film during the transfer (b), final product after the transfer (c). Retrieved from Kireev et al., 2016.

A natural consequence of transferring graphene to a target substrate is much of

the graphene is lost due to etching. Also, if the graphene foil is large enough, cracks and

folds are very susceptible. An experiment conducted by Kireev et al. (2016) eliminates

this problem through the use of a mediator film to transfer smaller pieces of graphene

individually onto a target location. The result is a much higher utilization of all graphene with much lower defects due to folds and cracks.

The target location in this experiment was a four-inch silicon wafer with graphene field effect transistors (GFETs). A chamber was designed to align the wafer and mediator film. The mediator film was designed as an identical copy of the wafer with openings for the graphene transfers zones. PMMA is used to maintain the graphene integrity during transfer. The transfer process is as follows: (1) The wafer and mediator film is placed into the chamber and precisely aligned. (2) The chamber is filled with deionized water to approximately 2-3cm above the surface of the wafer. The mediator film is lifted with the water level. (3) PMMA/graphene foils are each placed into the opening of the mediator film one by one. (4) Finally, the water is released, lowering the mediator film back onto the wafer surface. The PMMA is removed using acetone and annealing process. The photographs of the wafer at different stages during the transfer process can be seen in Figure 2.11.

The result is a transfer technique that more efficiently utilizes more graphene. This technique can be used to produce more cost-effective graphene-based devices for commercial application. A final yield of 90% was achieved after improving on the design after several trails.

2.11 Controllable Growth of Graphene on Liquid Surfaces

Much research has been conducted on the characterization of graphene as well as how to improve the uniformity. For certain applications, multilayer graphene is preferable, but currently unattainable due to the inherent difficulty in producing uniform layers. This section will cover the characterization techniques as well as research

conducted on improving the uniformity of multilayer graphene.

During the graphene growth process, carbon atoms are diffused within a substrate, typically Cu. These atoms then arrange on the surface of the substrate to form a single, sometimes bi-layer graphene sheets. However, this process is self-limiting in that the capability to produce graphene of more layers. To address this, the use of molten or liquid surfaces has been researched as these liquid substrates offer the capabilities to form uniform graphene layers without the self-limiting factor in solid substrates. Liu and Fu (2019) reviews the research completed in this area.
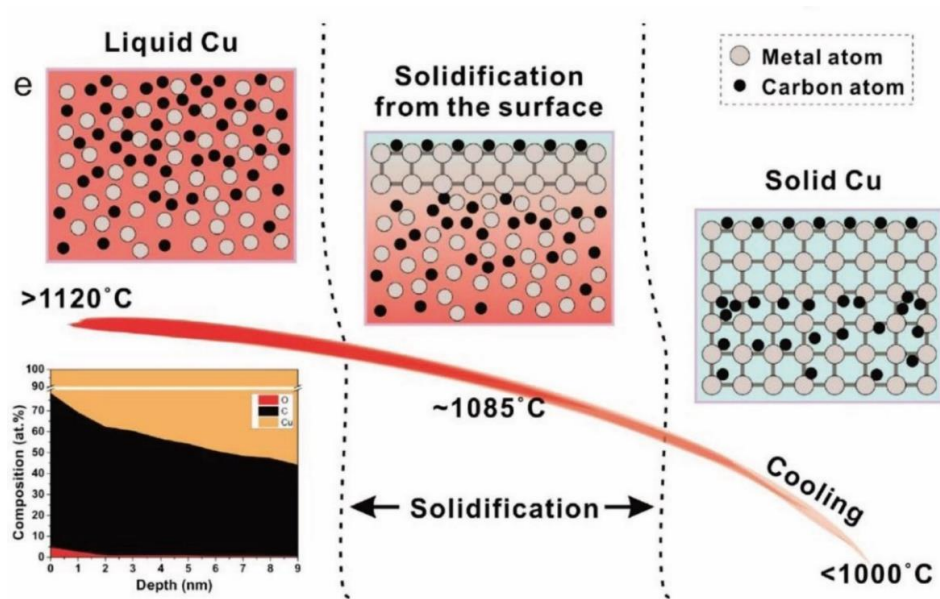
Figure 2.12. Schematic exhibition of carbon distribution in liquid Cu, solid Cu, and solidified surface of liquid Cu during solidification. Retrieved from Liu and Fu, 2019.

Figure 2.12 above illustrates the carbon distribution process in solid and liquid Cu. When Cu is brought above its melting temperature, ~1085°C, the carbon will begin to diffuse within the Cu substrate. After the temperature is decreased, the carbon will begin to form its graphene layers. Finally, once the Cu has become solidified, the graphene growth process is complete. However, while this process can produce

18

multilayer graphene, the uniformity is still low.

2.12 Growth of Single-Layer and Multilayer Graphene on Cu/Ni Alloy Substrates

One of the limiting factors of using Cu substrates is the low solubility. To address this Ni can be used to supplement Cu due to its inherent high carbon solubility. Huang and Ruoff (2020) reviewed the research conducted using Cu/Ni alloy substrates and their effect on the production of monolayer, bilayer and multilayer graphene. CVD processes using commercial Cu/Ni alloy foils, polycrystalline Cu/Ni films and foils, Cu/Ni gradient alloy, and single crystal Cu/Ni (111) substrates were reviewed and found that single crystal Cu/Ni alloy foils proved to be the most successful in producing large-scale synthesis of higher quality graphene.

The processes of using Cu/Ni have been unable to create more perfect multilayer graphene which would be suitable for applications in space plasma instruments as the resultant films are not uniform nor thick enough.

2.13 XPS Analysis of Graphene

X-ray photoelectron spectroscopy (XPS) is a great technique for characterizing carbon based materials. Since graphene is a carbon material and produced on the surface of the substrate, XPS, a surface sensitive technique, can provide elemental and chemical information for the material. Hawaldar et al. (2012) produced graphene using hot filament chemical vapor deposition (HFTCVD) and utilized XPS to determine the elemental and chemical composition of the resultant graphene using a copper substrate.

19
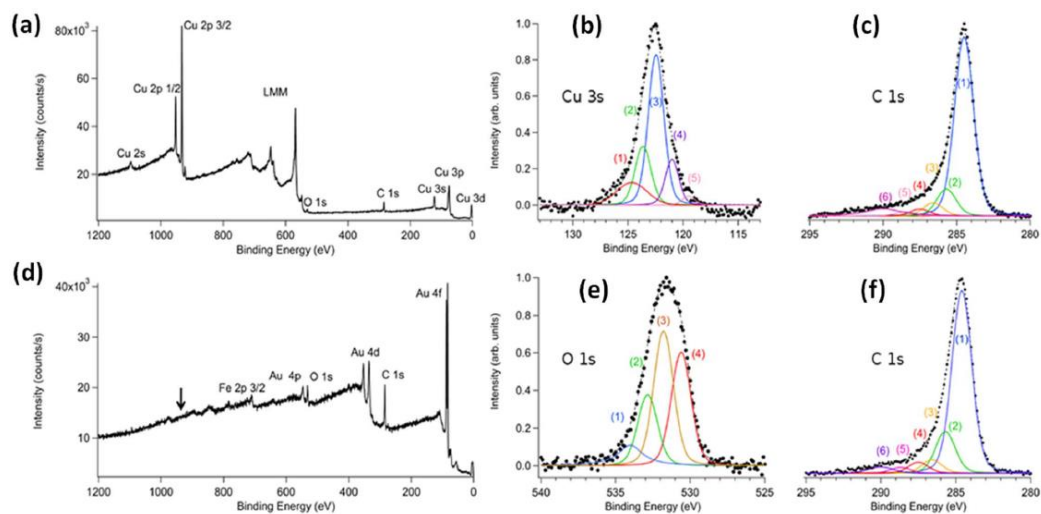
Figure 2.13. XPS data for graphene produced using HFTCVD. (a) General scan for graphene on Cu. (b) High-resolution scan for Cu 3s. (c) High-resolution scan for C 1s. (d) General scan for transferred graphene on gold-coated silica substrate. (e) High-resolution scan for O 1s. (f) High-resolution scan for C 1s.

The XPS analysis of graphene on Cu focuses on the C 1s, Cu 3s, and O 1s core level peaks. For the C 1s core level peak, this peak can be decomposed into six components; C sp2, C-OH, C-O, C=O, and O-C=O with the binding energies of 284.6, 285.7, 286.6, 287.5, 288.7, and 290 eV, respectively. The Cu 3s core level peak can be decomposed into five components, Cu=C, Cu-C, Cu-Cu, Cu-O, and Cu-OH with the binding energies of 119.5, 121.0, 122.4, 123.6, and 124.7 eV, respectively. The O 1s core level peak can be decomposed into four components, C-C=O/O-C=O, C-OH/C-O, hydroxides, C=O and other carbon complexes with the binding energies of 534, 532.9, 531.8, and 530.6 eV, respectively.

The purpose of examining these core level peaks is to receive a better understanding of the quality of the produced graphene. The chemical states of the carbon components provide an understanding of the impact of oxygen on the sample and the copper substrate.

3. EXPERIMENTATION AND METHODOLOGY

To meet the requirement of a space plasma instrument foil, the graphene must be ultra-clean, have very low roughness, have no tears or breaks in the foil, and be thin as possible. The PMMA transfer method allows for low roughness and breaks, however, the issue is in the removal of the PMMA after the transfer process to the TEM type grid. The process which I propose would ultimately skip the necessity of a transfer layer and therefore a removal process, resulting in a cleaner graphene foil. This process utilizes a new graphene produced CVD method which will allow for a direct transfer of graphene of approximately 3-5 layers which would remove the necessity of a transfer layer due to the inherent durability of the multilayer graphene.

The steps below outline the experimentation and production processes for creating the multilayer graphene foil grid for space plasma instruments.

Creating multilayer graphene: Growth of a few layer (3-5) graphene (FLG) on molten Cu.

Gas: CH_4, H_2, Ar.

Substrate: Tungsten or Al_2O_3, Cu or Cu/Ni

1)   Rinse substrate and metal(s) with IPA and DI water.

2)   Use ultrasonic for ten minutes to clean metal and substrate, then dry

3)   Place sample in quartz tube and purge the chamber for 30 minutes with Ar

4)   Slow heat the chamber to baking temperature as dictated in recipe

5)   Once bake temperature has been reached, begin flowing methane at designated rate in recipe

6)   Bake for designated time

7)   Begin slow temperature ramp down

8)   Once final temperature has been reached, either fast cool (Cu/Ni) or slow cool (Cu)

FLG will be used to enhance stability and graphene integrity during the grid transfer process. FLG provides a higher durability in the transfer process due to the inherent durability of multilayer graphene over monolayer graphene. This CVD process has shown to create 3-5 layers of graphene consistently, but also produce groups of amorphous carbon. This amorphous carbon will affect the effectiveness of space plasma instruments; however, the degree of negative influence should be fairly negligible compared to the drastic improvement in effectiveness due to the thinner nature of multilayer graphene over the currently used carbon foils.

The purity, cleanliness, uniformity and number of layers will be measured by Raman spectroscopy and XPS. Raman spectroscopy allows the experimenter to not only verify the presence and amount of various materials but can also verify the number graphene layers. XPS allows for an elemental and chemical analysis of the sample surface. Quality of the graphene and oxygen impact can be determined. The results from these experiments will be compared to three subsets of samples produced: Cu/Ni alloy, pure Cu, and pure Cu with the carbon cover.

To maintain the integrity of these experiments, all other variables must be held constant between each individual sample. Aspects which may influence results are:

1. Graphene quality

    a. CVD grown graphene on a copper substrate is subject to oxidation due to the nature of copper, which oxidizes at room temperature. Furthermore, copper does not stop oxidizing once a thick enough oxide layer has grown to halt the

oxidation process. To prevent this, the CVD grown graphene on copper must be used soon after it is exposed to the surrounding atmosphere.

b. While CVD grown graphene on a copper substrate is very common, the growth of graphene is not an easy task. Therefore, Raman spectroscopy will be used to verify the number of layers grown.

2. Outside Contamination

a. Since air contains floating particles, the graphene foil may become contaminated. Therefore, all analysis of the foils will be completed in a clean room or controlled setting where the contaminates are at a very low amount.

3.1 Equipment Overview

The CVD process utilized an OTF-1200X furnace. The copper material used was produced from UT Austin 90%/10% Cu/Ni (pre-made Cu/Ni). The other copper material and nickel material was from Alfa Aesar, 99+%. The Raman spectrometer utilized a 532nm laser and was from DXR Raman Microscope (Thermo Fisher Scientific). The XPS analysis used a Scienta Omicron XPS. Optical images were taken using a Hirox Digital Microscope.

3.2 Recipe Overview

Table 3.1: List of Recipes

Recipe	Purge Time (min)	Baking Temperature (°C)	Bake Time (min)	End Ramp Temperature (°C)	Methane Flow Rate (sccm)	Notes
1	30	1150	60	1000	100	
2	30	1150	60	N/A	N/A	Rapid cooling
3	30	1150	60	N/A	100	Rapid cooling
4	30	1150	60	N/A	50	Rapid cooling
5	30	1150	60	N/A	25	Rapid cooling
6	30	1100	60	1000	100	
7	30	1100	60	1000	50	
8	30	1100	60	1000	25	

3.3 Sample Overview

Table 3.2: Sample Overview

Sample	Sample Type	Substrate	Recipe	Notes
1	1 layer pre-made Cu/Ni	Al_2O_3	1	
2	2 layer pre-made Cu/Ni	Al_2O_3	1	
3	3 layer pre-made Cu/Ni	Al_2O_3	1	
4	4 layer pre-made Cu/Ni	Al_2O_3	1	
5	1 layer pre-made Cu/Ni	W	1	
6	1 layer pre-made Cu/Ni	W	1	Ruined Tube
7	Self-made alloy Cu/Ni (15:1)	Al_2O_3	1	1.5g:0.1g
8	Self-made alloy Cu/Ni (15:1)	Al_2O_3	1	1.5g:0.1g
9	Self-made alloy Cu/Ni (15:1)	Al_2O_3	2	1.5g:0.1g
10	Self-made alloy Cu/Ni (15:1)	Al_2O_3	2	1.5g:0.1g
11	Self-made alloy Cu/Ni (15:1)	Al_2O_3	2	1.5g:0.1g
12	Self-made alloy Cu/Ni (15:1)	Al_2O_3	2	1.5g:0.1g
13	Al_2O_3	N/A	N/A	white color
14	Al_2O_3	N/A	N/A	cream color
15	Self-made alloy Cu/Ni (15:1)	Al_2O_3	3	
16	Self-made alloy Cu/Ni (15:1)	Al_2O_3	4	
17	Self-made alloy Cu/Ni (15:1)	Al_2O_3	5	
18	Pre-made Cu/Ni	Al_2O_3	3	1.5g
19	Self-made alloy Cu/Ni (15:1)	Al_2O_3	3	Two-hour bake time 1.5g:0.1g
20	Self-made alloy Cu/Ni (15:1)	Al_2O_3	4	Two-hour bake time 1.5g:0.1g
21	Pure copper	Al_2O_3	6	1.5g
22	Pure copper	Al_2O_3	7	1.5g
23	Pure copper	Al_2O_3	8	1.5g
24	Pure copper	Al_2O_3	6	Carbon cover 1.5g
25	Pure copper	Al_2O_3	7	Carbon cover 1.5g
26	Pure copper	Al_2O_3	8	Carbon cover 1.5g

4. RESULTS & DISCUSSION

To demonstrate the effects that the carbon cover had on the uniformity of multilayer graphene, three sample types were prepared, pure copper (PC), copper-nickel alloy (CNA), and pure copper using the carbon cover (PCC). Theoretically, the CNA samples should prove to have better uniformity than the PC samples, and the PCC samples should have better uniformity than the PC samples. Initially, it was unknown to how the PCC samples would compare to the PCC samples.

The initial stages of experimentation focused on the development of graphene and identifying potential issues with the equipment and system setup. One of the major challenges which presented itself in this work was the initial ability to produce any amount of graphene on any sample type. As such, several different strategies were used to help promote this initial growth, including the use of a copper-nickel alloy, checking for system leaks, and the optimization of gas flow rates, substrate type, sample size, and sample rapid cooling.

This Discussion section will cover 26 samples produced demonstrating the effects that the strategies had on the effect of graphene growth and its overall uniformity. The end of this discussion will compare the quality and uniformity that the PC, CNA and PCC samples had on graphene growth.

4.1 Background information

4.1.1 Carbon Cover

As mentioned previously in the literature review, the graphene growth process is self-limiting in that once 1-2 layers have been formed, the further production of graphene is halted. Research has been completed on using liquid substrates to increase the carbon

solubility and uniformity and also using Cu/Ni alloy to increase carbon solubility. In

theory, one of the causes for this limiting factor in producing uniform multilayer

graphene in liquid substrates is due to the exterior of the molten Cu solidifying prior to

the interior. This causes the carbon atoms to freeze within the Cu and halt the graphene

production process. To aid in the production of multilayer graphene, the use of a carbon

cover over the Cu substrate is used to create a temperature gradient. This gradient will

cause the Cu substrate to first cool down, not at the surface, but within the Cu substrate

first, causing the carbon atoms to migrate near the surface and promote the development

of multilayer graphene. This process can be seen in Figure 4.1 below. These samples,

once produced, will be compared to the PC and CNA samples to compare the quality and

uniformity.
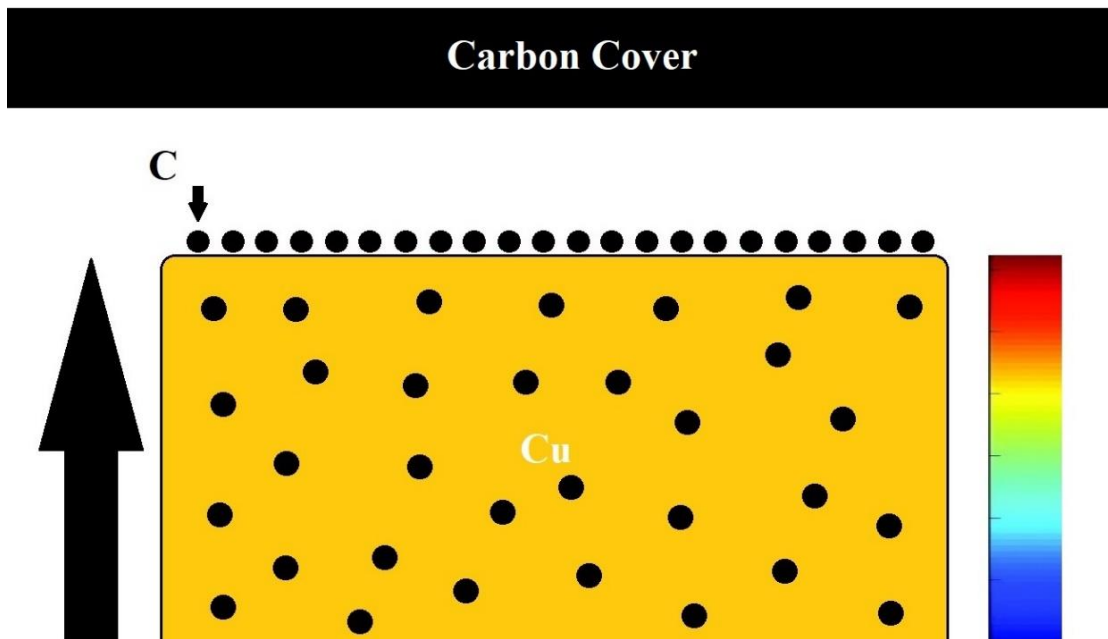
Figure 4.1. Temperature gradient in Cu to promote multilayer graphene on surface.

4.1.2 Determining the Quality and Number of Graphene Layers

Since the initial discovery of graphene, Raman microscopy has quickly become one of the most popular characterization techniques. This is due to the extreme sensitivity that graphene has with the resultant spectra. Intense research has been developed to properly characterize and understand the precise number of layers and defects present in graphene. Most commonly, graphene on a Si/SiO_2 surface with a 532nm wavelength is used. The resultant 2D band ($\sim$2690cm^{-1}), G band (1580 cm^{-1}), and D band (1350cm^{-1}) and their relative shapes and intensities can provide information such as defects and thickness among other properties.

The peak intensities ratio, I_{2D}/I_G, as well as the position and shape provide information on the thickness of the graphene (Nguyen et al. 2013). Also the I_D/I_G ratio indicates the level of disorder within the graphene layer. The ratios of I_{2D}/I_G indicate as follows:

$$3 > I_{2D}/I_G > 2: \text{Monolayer}$$

$$2 > I_{2D}/I_G > 1: \text{Double Layer}$$

$$1 > I_{2D}/I_G: \text{Multilayer}$$
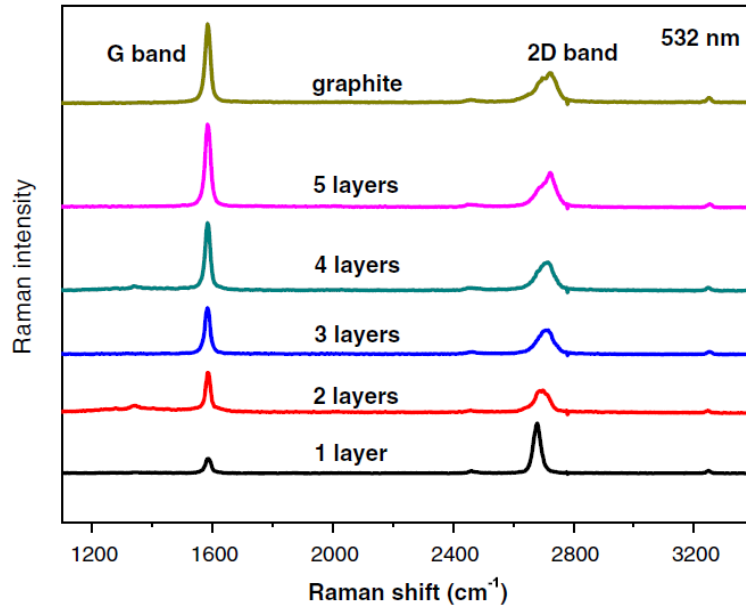
Figure 4.2. Relative shape and intensities of the G and 2D bands in graphene to determine the number of layers present. Retrieved from Liu et al., 2013.

Figure 4.2 above indicates the relative intensities and shapes of the 2D and G bands to determine the number of layers present. Using this information, the number of graphene layers can be estimated. Furthermore, the intensity of the D peak indicates disorder or defects in the graphene. In pristine, this peak will not be visible due to its crystal symmetries. Thus, this peak will occur in non-pristine graphene such as amorphous carbon.

4.1.3 Phase Diagram of Cu/Ni Alloy

As a Cu/Ni alloy is used to promote the production of graphene, a phase difference will occur as the bake temperature used is above the melting temperature of Cu but not of Ni.
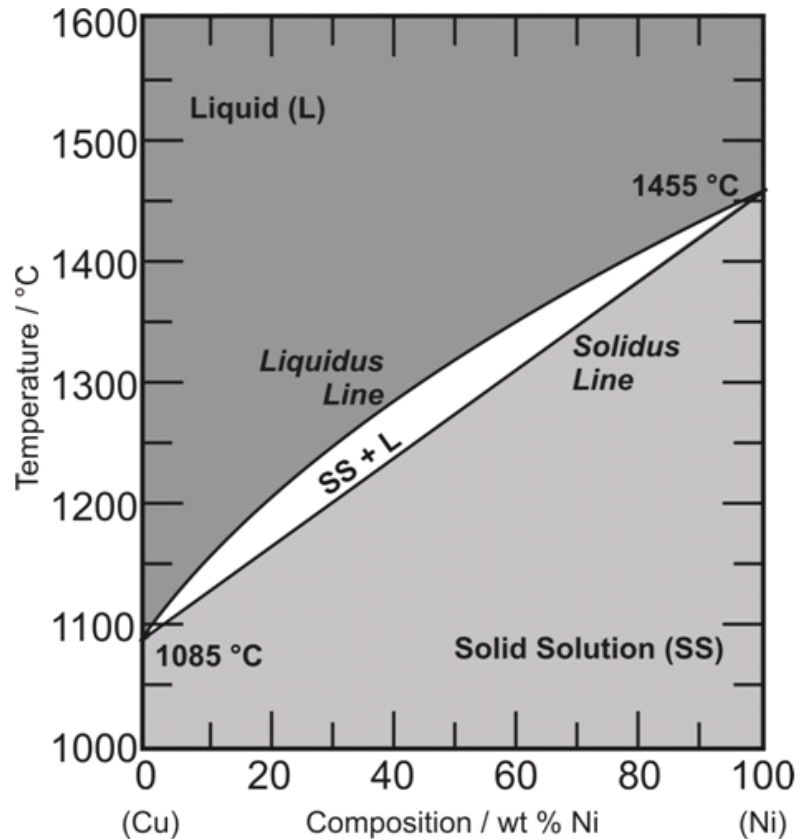
Figure 4.3. Phase diagram of Cu/Ni alloy. Retrieved from
http://www.spaceflight.esa.int/impress/text/education/Solidification/Phase_Diagrams.htm
l

While using the Cu/Ni alloy, a rapid cooling process was used to prevent the

segregation of the Cu and Ni. Segregation of these two elements can negatively impact

the carbon distribution and ultimately lead to an uneven and improper graphene on the

sample surface. To rapidly cool, the sample is pushed out of the heating zone using a

quartz rod and into the cool zone, upstream of the gas flow. This cooling process will

cool the sample by approximately 100°C/sec. This rapid cooling can prevent the

segregation of Cu/Ni to allow for more uniform graphene.

4.1.4 Troubleshooting – Oxygen Leaks

During the initial trials of producing samples, oxygen leaks has shown to be an

extensive problem. An oxygen leak can cause an adverse effect in the production of

30

graphene by causing an etching effect on the deposited carbon withing the copper

substrate. In addition, the oxygen leaks caused serious issues when tungsten was used as

a foundation substrate. In combination with the elevated temperatures, the oxygen would

react to create and deposit a tungsten oxide on the sample and the inside of the quartz

tube. This reaction would ruin a sample and would require that the tube need to be

cleaned of the deposited tungsten oxide. This can be seen in Figure 4.4 below.

Figure 4.4. Result of oxygen leak after experimentation of Sample 6. Tungsten oxide was
produced as a result of the oxygen leak, depositing on the sample surface and on the
inside of the quartz tube.

Due to the nature of an oxygen leak. The entire system must be checked to

determine the location of the leak. To complete this, the system had several swage locks

placed on different areas to isolate the several different gas lines from each other. Next, the system is pumped down and left overnight to allow the oxygen leak to occur and be identified. The next day the pressure gauge is checked to initially check if there is a leak. If no leak has occurred, each swage lock is opened one at a time until the pressure gauge indicates a change in pressure due to the leak. Once the leak has been identified and isolated to one area due to the swage lock, the defective part can be replaced. After the part has been replaced, the system can be pumped down again and left overnight. Once again, the pressure gauge is checked, and the swage locks are opened to determine if a leak is still present. This process is repeated until a stable low pressure is achieved and no obvious sign of an oxygen leak can be seen. During the process of producing samples, it was determined that a few of the mass flow controllers (MFC) and gas regulators had been the source of these gas leaks. These parts were placed and tested to ensure no more leaks were present.

An improvement of this experiment is the use of Al_2O_3 instead of W. While Cu and W are inert in their reactions with each other, Ni and W will combine at the elevated temperature to produce a Cu/Ni/W alloy. This reaction can cause detriments in the quality of producing uniform multi-layer graphene. As such, W should not be used as a base material when using Ni.

4.1.5 Strategy

To compare the effects of the usefulness of the carbon cover, three different setups were used. First, graphene was attempted to be produced using pure copper in a molten state. Second, to promote the growth of graphene, a copper-nickel alloy was used (15:1), also in a molten state. The nickel is used to help promote the absorption of carbon

within the substrate as nickel has a higher carbon absorption limit to copper. This higher absorption will help to ensure that enough carbon atoms are present to produce the graphene layers needed.

Originally, a tungsten base was used during the graphene production process due to its high melting temperature, ability to maintain strength even when in a thin sheet, and inert reaction with copper. A thinner base is important to ensure that the base has as low of a thermal absorption as possible. If the base was to maintain a high amount of thermal energy, the sample would not be able to cool uniformly and result in a more non-uniform sample. However, the use of tungsten with a copper-nickel alloy would cause a reaction with the tungsten to form a copper-nickel-tungsten alloy. This reaction may cause an adverse effect in the development of uniform multilayer graphene; therefore a different base would need to be used. The chosen base is an aluminum-oxide ceramic. To maintain consistency between the three different setups, the aluminum-oxide base was used for all three setups in all samples. Lastly, a pure copper sample using a carbon cover to create a temperature gradient was used.

4.2 Raman Spectroscopy

4.2.1 Samples 1-4

Samples 1-4 were produced to examine the effect that the total amount of alloy has on graphene growth. As such, Sample 1 uses 1 layer of the Cu/Ni alloy to Sample 4 which uses 4 layers.
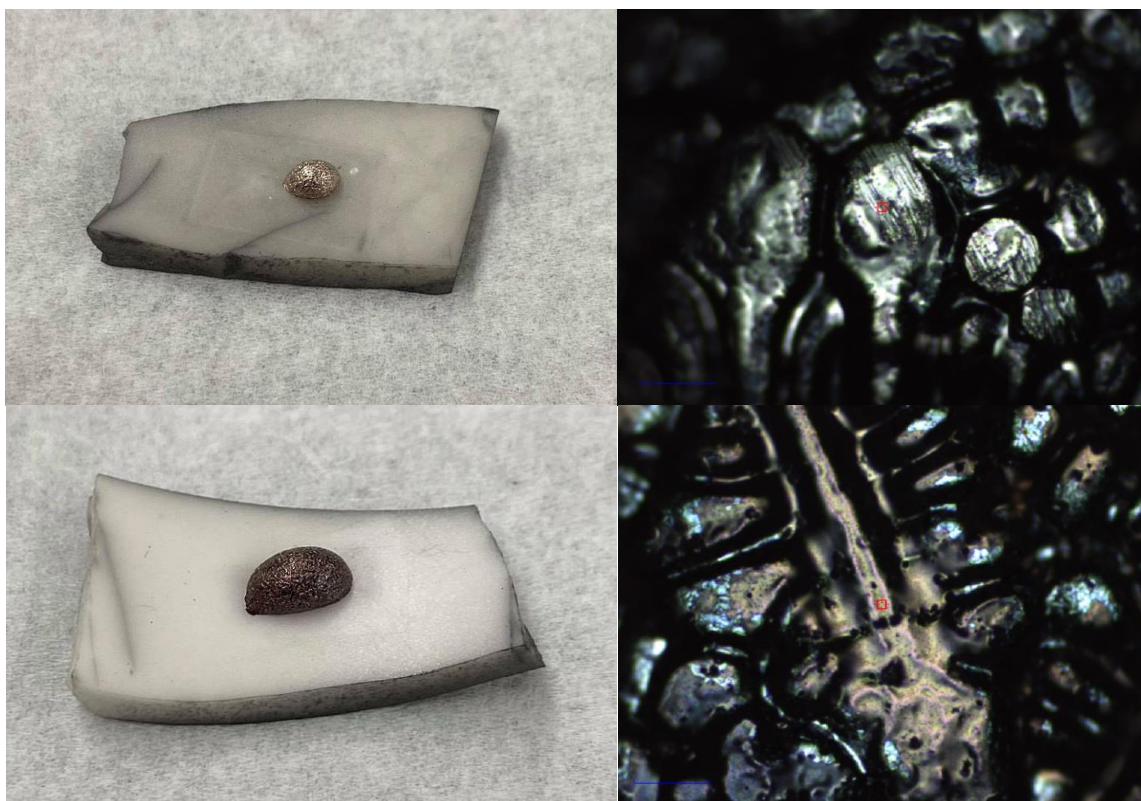
Figure 4.5. Image of Sample 1 (top left) and Sample 4 (bottom left) and at 10x magnifications (top right and bottom right). Scale bar indicates 120μm.

After initial trials proved to be unable to produce any graphene, the use of a copper-nickel alloy was utilized as nickel provides the substrate with a higher carbon concentration capacity than what can be achieved by using pure copper. This increased capacity can help to promote the growth of graphene as the initial trials suspected cause of failure was a low concentration of carbon atoms deposited during the growth phase. Figure 4.5 above are images of Sample 1 and Sample 4 after graphene growth.

After the graphene growth process, the sample was examined using Raman microscopy to determine the elemental composition and carbon arrangement on the surface. During the analysis of Samples 1-4, three distinct regions can be identified. Each of these regions were examined and compared to verify the consistency and accuracy of characterizing the region. The results of these spectra were then compared between

Samples 1-4. The results of the Raman analysis can be seen below.
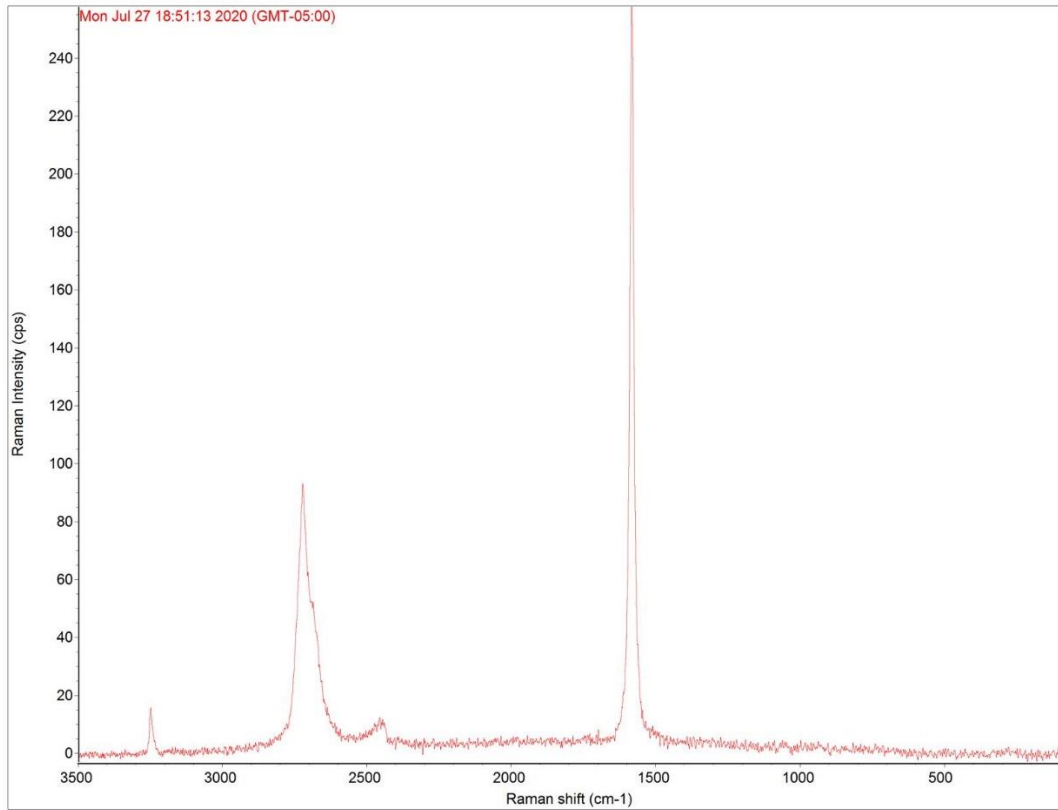
Figure 4.6. Raman Spectra of Graphene Areas in Samples 1-4.

Figure 4.6 above shows the results of the Raman spectra taken from a suspected graphene region in Sample 2. Due to the inherent similarity of all the spectra taken in these regions from all four samples, only this spectra is shown.

This spectra strongly suggests the presence of multilayer graphene given the location of the peaks and ratio of I_{2D}/I_G is 0.37. Furthermore, the shape of the 2D curve suggests that the number of layers present is approximately 5. There was no indication of a D peak in any of the spectra, suggesting little to no disorder in the graphene.
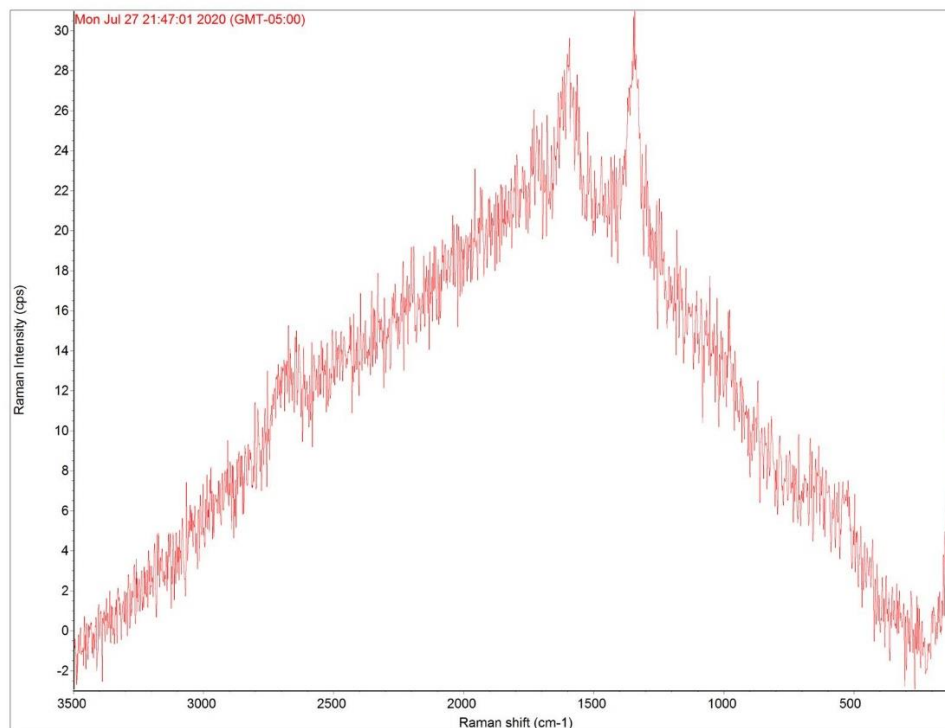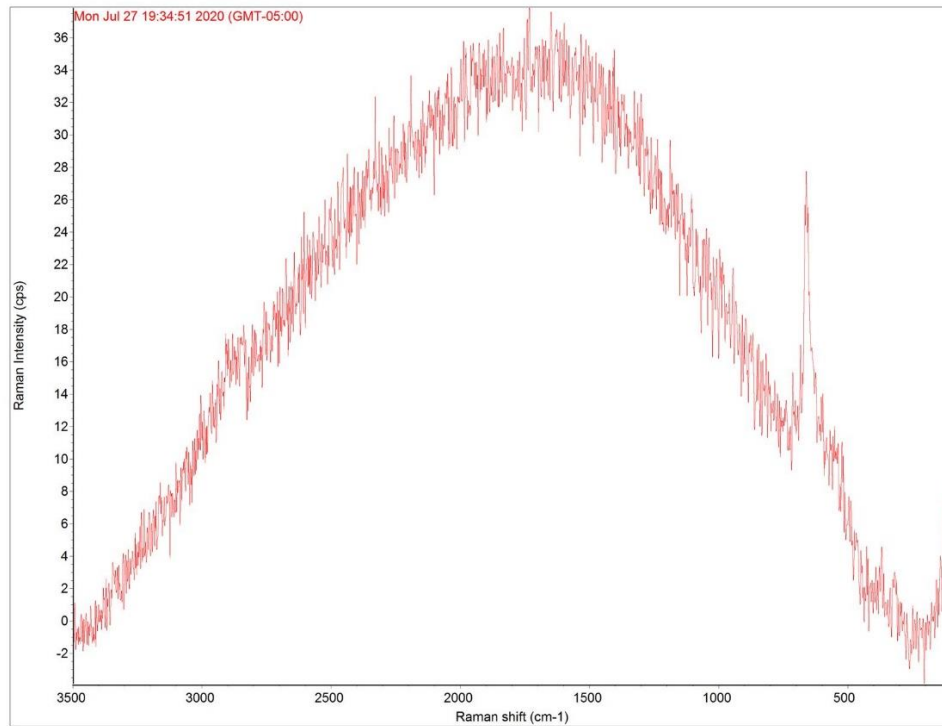
Figure 4.7. Raman Spectra of Cu/Ni Areas in Samples 1-4. Raman spectra in Sample 1 (top) and Sample 3 (bottom).

Figure 4.7 above shows the results of the Raman spectra taken from a suspected Cu/Ni regions in Sample 2. Due to the inherent similarity of all the spectra taken in these regions from all four samples, only these spectra are shown.

Due to the low intensity and broad shape of the spectra, there is no indication of graphene present. However, the bottom spectra does suggest the presence of carbon with weak peaks near the G, D, and 2D bands. Due to the relative intensities of the D and G bands, the carbon is most likely amorphous.
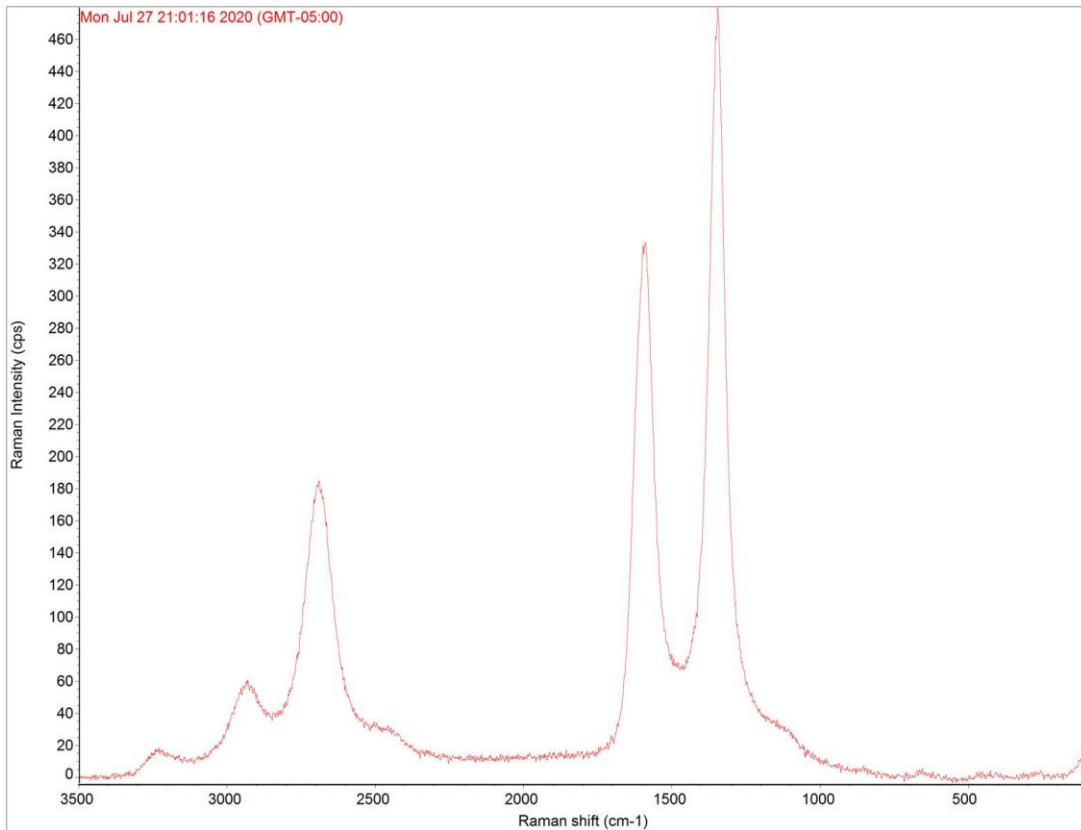
Figure 4.8. Raman spectra of amorphous carbon areas in Samples 1-4.

Figure 4.8 above shows the results of the Raman spectra taken from a suspected amorphous carbon region in Sample 2. Due to the inherent similarity of all the spectra taken in these regions from all four samples, only this spectra is shown.

Strong peaks located at the G and D bands suggest the presence of amorphous carbon. The I_D/I_G ratio is 1.43 Also, the presence of the 2D peak also suggests the presence of multilayer graphene with an I_{2D}/I_G ratio of 0.55.

4.2.1.1 Conclusion

Overall, all four samples showed to have nearly identical results in terms of resultant spectra in the identifiable regions on the surface. Also, the results were successful in producing ~5 layer graphene, but with very low uniformity. Most of the area can be seen to be bare Cu/Ni with small locals of multilayer graphene.

Sample 4, which had the highest amount of Cu/Ni of all the samples, demonstrated to also have the highest amount of amorphous carbon. This can be attributed to a higher content of Ni than the other 3 samples.

The overall conclusion of these samples is that the amount of Cu/Ni does not appear to have an effect on the presence and amount of multilayer graphene but does affect the amount of amorphous carbon present.

4.2.2 Samples 5 & 6

Samples 5 and 6 were the results of initial tests that were conducted using the Cu/Ni alloy. Sample 5 showed the successful result of using a W base with Cu/Ni alloy, while Sample 6 was the results of an unsuccessful result due to an oxygen leak. The subsequent oxygen leak resulted in the destruction of the sample and the production of tungsten oxide flakes.
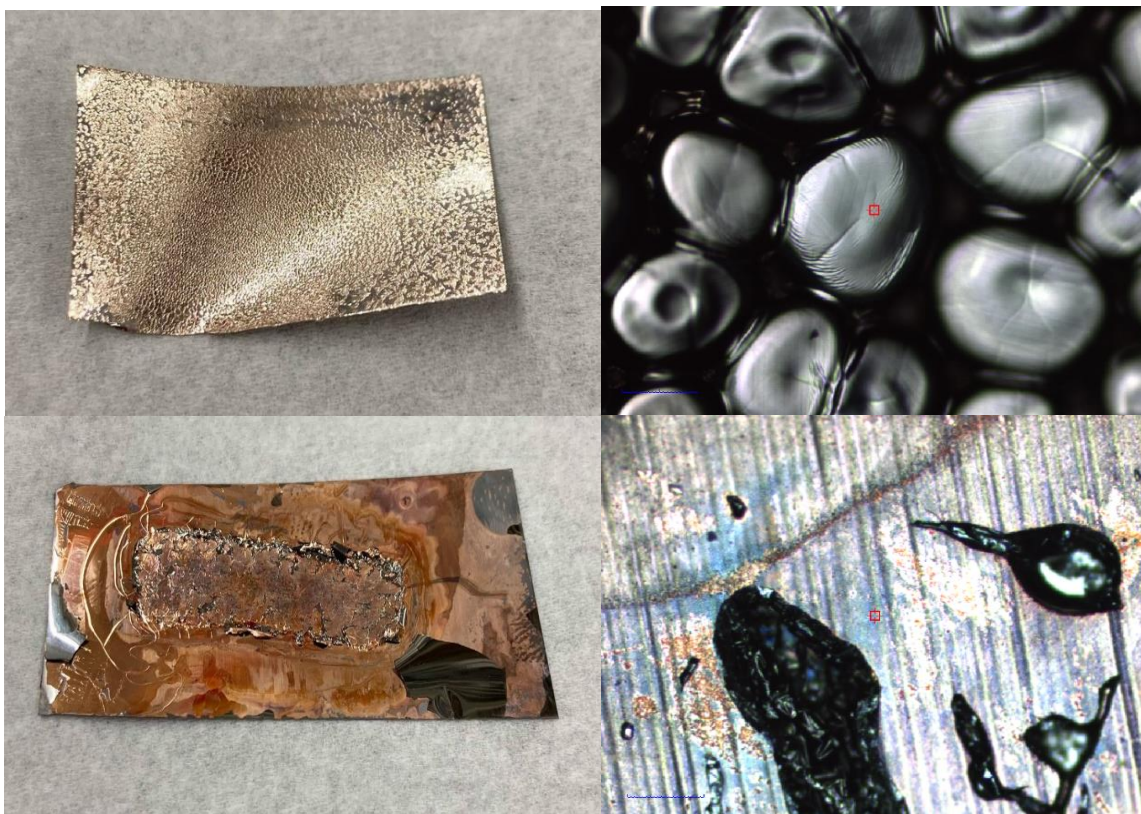
Figure 4.9. Image of Sample 5 (top left) and Sample 6 (bottom left) and at 10x magnifications (top right and bottom right). Scale bar indicates 120μm.

After initial trials proved to be unable to produce any graphene, the use of a copper-nickel alloy was utilized as nickel provides the substrate with a higher carbon concentration capacity than what can be achieved by using pure copper. This increased capacity can help to promote the growth of graphene as the initial trials suspected cause of failure was a low concentration of carbon atoms deposited during the growth phase. Figure 4.9 above are images of Sample 5 and Sample 6 after graphene growth.

After the graphene growth process, the sample was examined using Raman microscopy to determine the elemental composition and carbon arrangement on the surface. During the analysis of Samples 5 and 6, only one identifiable region could be found on Sample 5, while Sample 6 had three identifiable regions. Each of these regions were examined and compared to verify the consistency and accuracy of characterizing the

region. The results of the Raman analysis can be seen below.
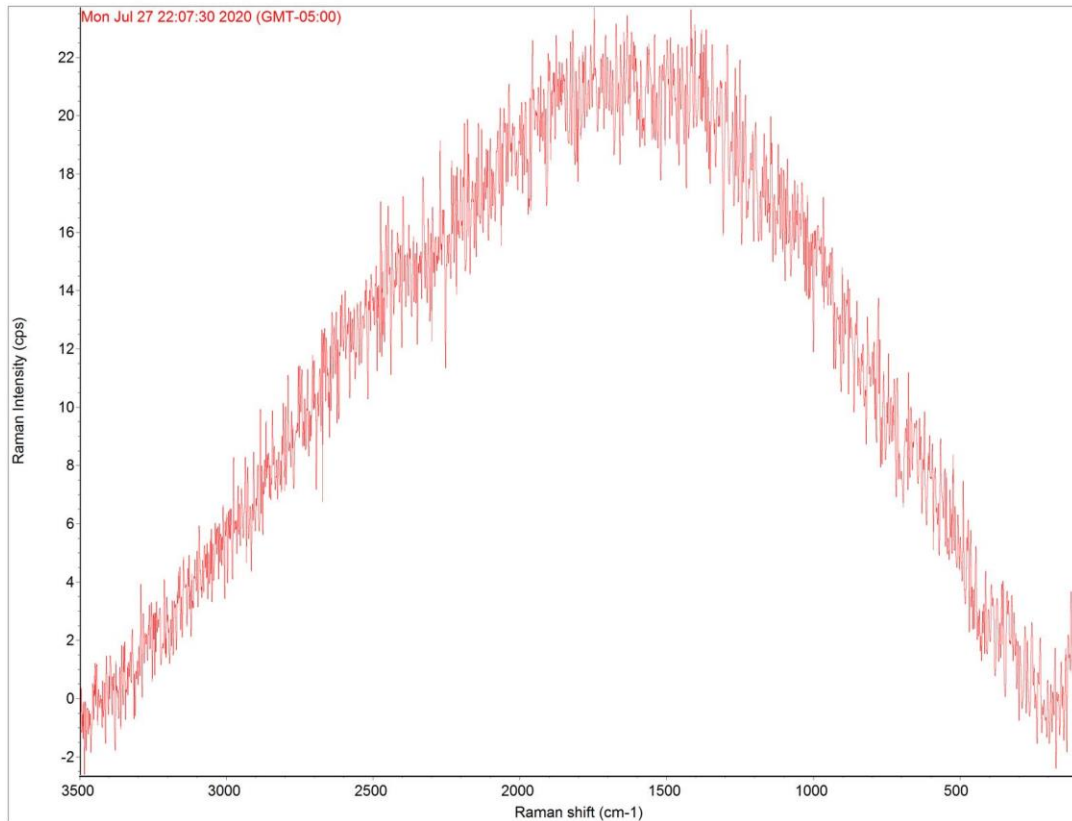
Figure 4.10. Raman spectra of Sample 5.

The spectra in Figure 4.10 has no discernable peaks and can be attributed to only the presence of the Cu/Ni alloy and potentially W. Due to the consistency between the measurements, only one spectra is shown.
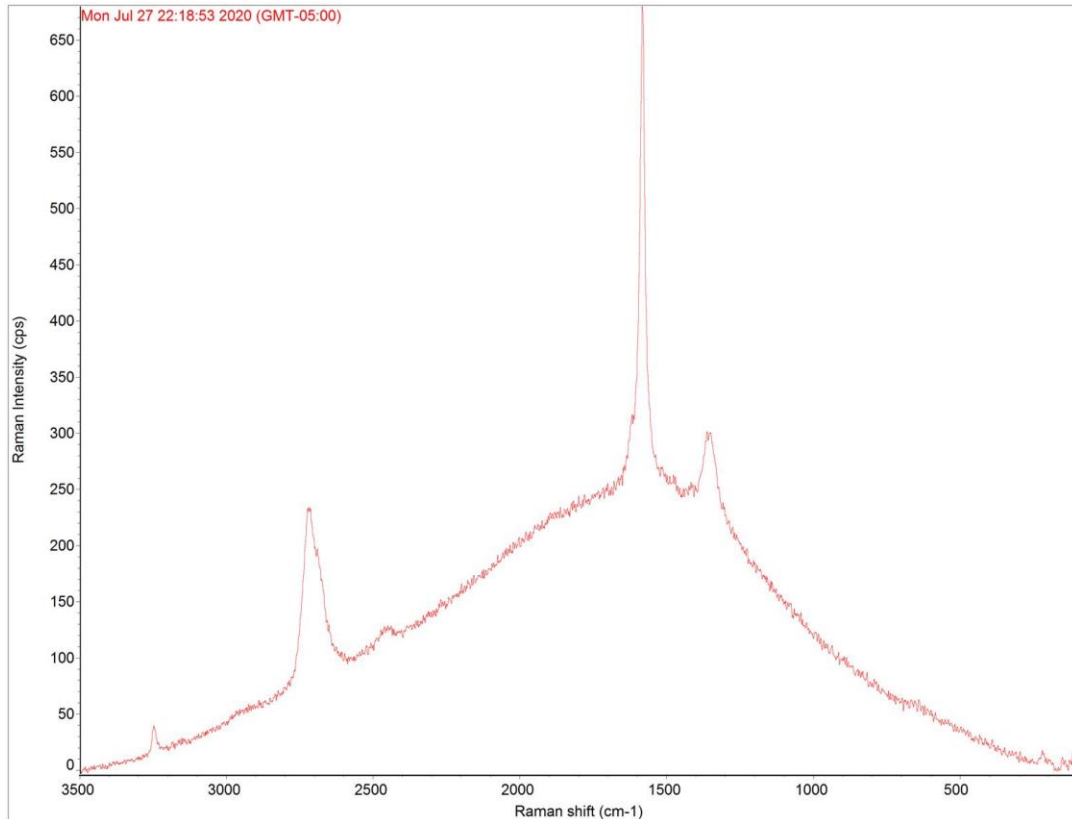
Figure 4.11. Raman spectra of W areas on Sample 6.

Figure 4.11 above shows the results of the Raman spectra taken from suspected W regions in Sample 6. Due to the inherent similarity of all the spectra taken in this region, only this spectra is shown.

This spectra strongly suggests the presence of multilayer graphene given the location of the peaks and ratio of I_{2D}/I_G is 0.39. The broad curve under the peaks indicate the presence of the W base. The I_D/I_G ratio is 0.43, indicating a certain degree of disorder.

41
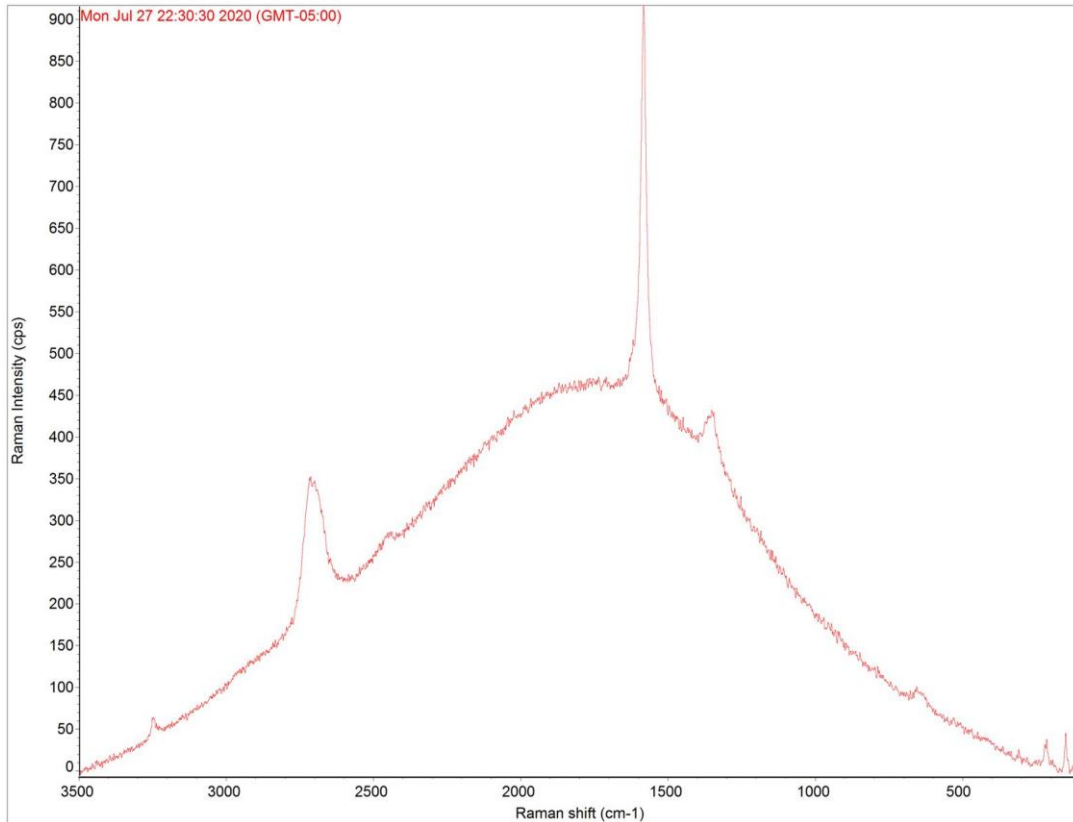
Figure 4.12. Raman spectra of Cu/Ni areas on Sample 6.

Figure 4.12 above shows the results of the Raman spectra taken from suspected Cu/Ni regions in Sample 6. Due to the inherent similarity of all the spectra taken in this region, only this spectra is shown.

This spectra strongly suggests the presence of multilayer graphene given the location of the peaks and ratio of I_{2D}/I_G is 0.38. The broad curve under the peaks indicate the presence of Cu/Ni. The I_D/I_G ratio is 0.46, indicating a certain degree of disorder within the carbon.
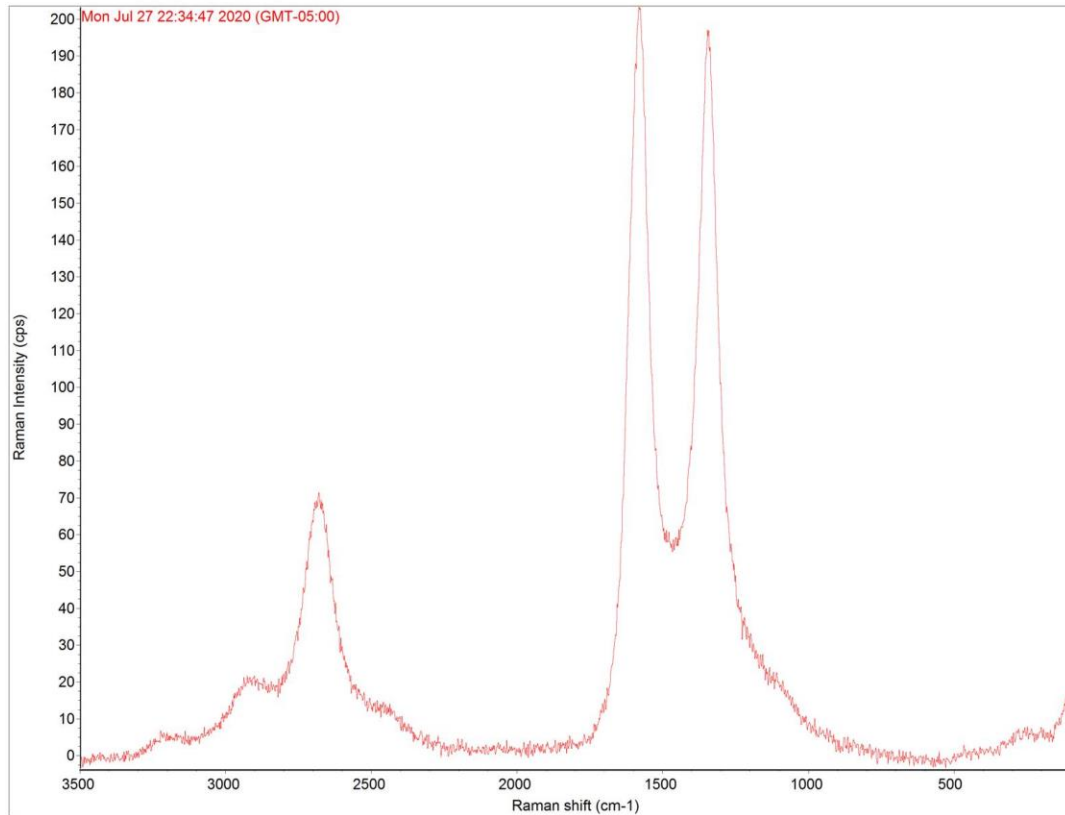
Figure 4.13. Raman spectra of amorphous carbon areas on Sample 6.

Figure 4.13 above shows the results of the Raman spectra taken from an amorphous carbon region in Sample 6. Due to the inherent similarity of all the spectra taken in these regions from both samples, only this spectra is shown.

Strong peaks located at the G and D bands suggest the presence of amorphous carbon. Also, the presence of the 2D peak also suggests the presence of multilayer graphene. The ratio of I_{2D}/I_G is 0.31. The broad curve under the peaks indicate the presence of Cu/Ni. The I_D/I_G ratio is 0.87, indicating a certain degree of disorder within the carbon.

4.2.2.1 Conclusion

Sample 5 showed no evidence of graphene, or even carbon present on the sample surface. The spectra found only a broad peak which indicates the Cu/Ni substrate. Sample 6, while was subject to an oxygen leak, did show to have multilayer graphene present on most of the surface. The is unusual due to the failure of the experiment. While most of the surface did show to have multilayer graphene, there was no uniformity on the surface due to the failure of the experiment.

4.2.3 Sample 7 & 8

Samples 7 and 8 were produced using a self-made alloy which should improve the uniformity in the new samples. These results were taken using Raman spectroscopy and compared to previous samples.
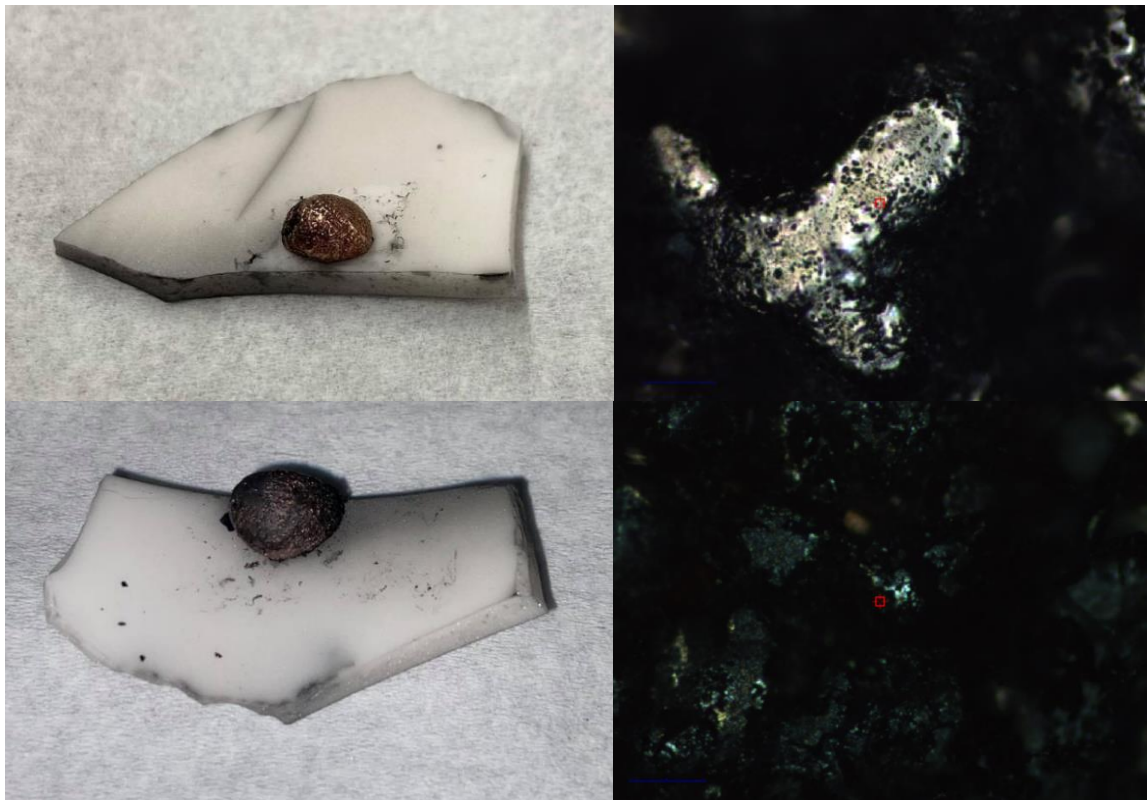
Figure 4.14. Image of Sample 7 (top left) and Sample 8 (bottom left) and at 10x magnifications (top right and bottom right). Scale bar indicates 120μm.

To potentially improve the uniformity of the multi-layer graphene, the Cu/Ni alloy was self-produced using high quality Cu and Ni. The previously used Cu/Ni alloy was made at the University of Texas at Austin and was suspected to have some impurities. Being able to self-produce the Cu/Ni alloy also allows for the ability to control the Ni content of the alloy. In this case, the self-made alloy was 15:1 Cu/Ni, reduced from the previous content of 10:1 Cu/Ni.

After the graphene growth process, the samples were examined using Raman microscopy to determine the elemental composition and carbon arrangement on the surface. During the analysis of Samples 7 and 8, three identifiable regions were found. Each of these regions were examined and compared to verify the consistency and accuracy of characterizing the region. The results of the Raman analysis can be seen below.
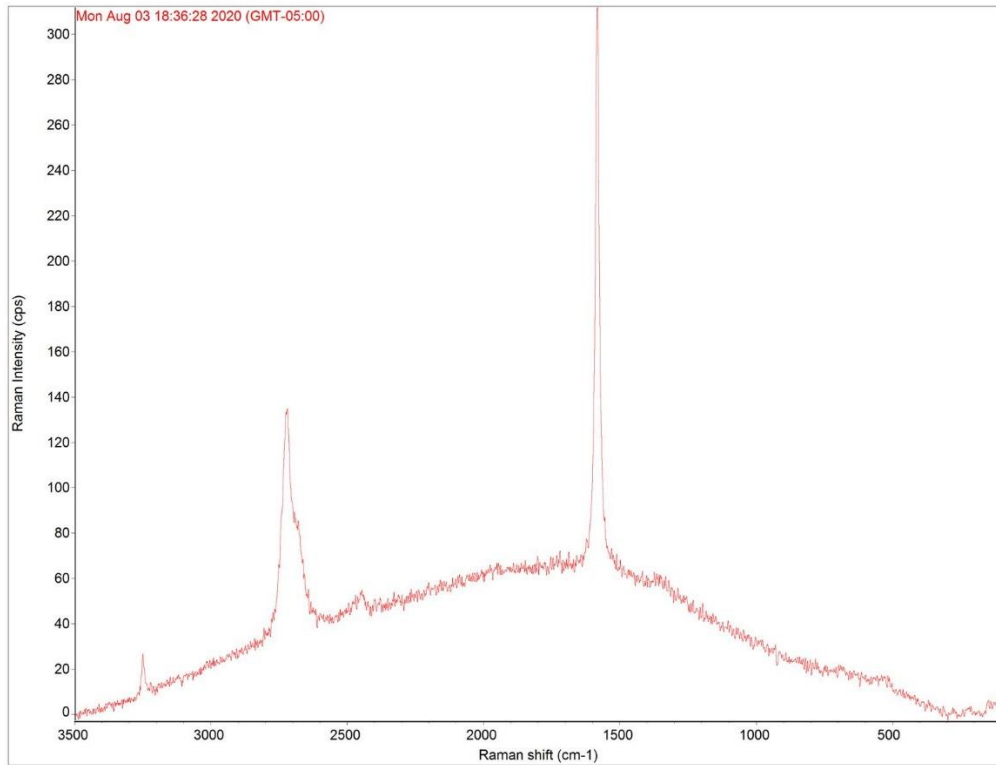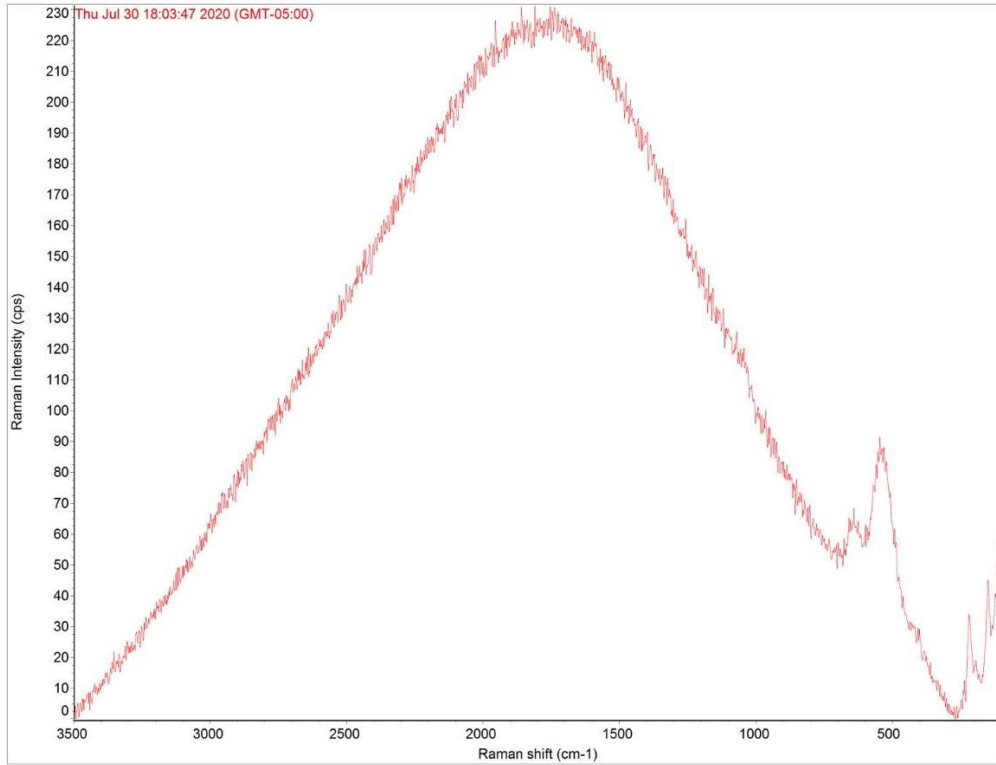
Figure 4.15. Raman spectra of Cu/Ni areas on Sample 7 and 8

46

Figure 4.15 above shows the results of the Raman spectra taken from suspected Cu/Ni regions in Samples 7 and 8. Due to the inherent similarity of all the spectra taken in this region, only these spectra are shown.

The top graph, from Sample 7, has no discernable peaks for carbon. The broad peak indicates the Cu/Ni substrate. However, the bottom graph, from Sample 8, indicates not only the broad peak from the Cu/Ni substrate, this spectra strongly suggests the presence of multilayer graphene given the location of the peaks and ratio of I_{2D}/I_G is approximately 0.39. There is no discernable peak for the D band, suggesting little to no disorder in the carbon.

No Cu/Ni region on Sample 7 showed any indication of the presence of graphene, but Sample 8 did show some regions which contain this multi-layer graphene.
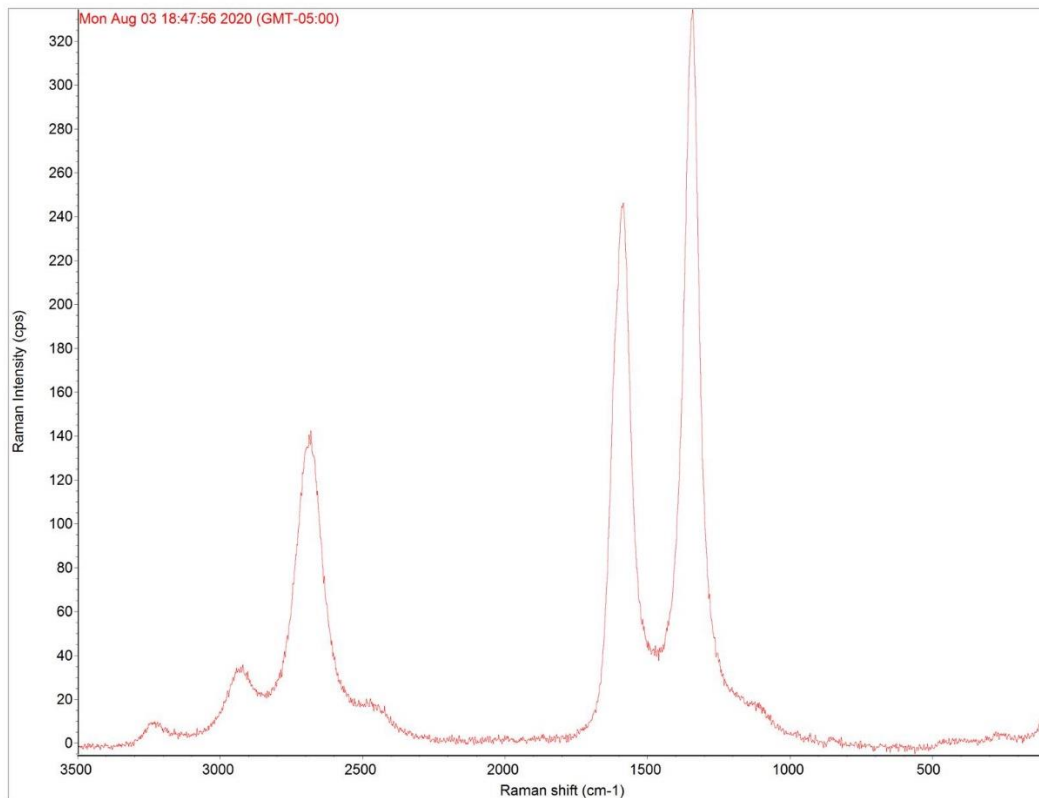

Figure 4.16. Raman spectra of amorphous carbon areas on Sample 7 and 8

Figure 4.16 above shows the results of the Raman spectra taken from an amorphous carbon region in Samples 7 and 8. Due to the inherent similarity of all the spectra taken in these regions from both samples, only this spectra is shown.

Strong peaks located at the G and D bands suggest the presence of amorphous carbon. Also, the presence of the 2D peak also suggests the presence of multilayer graphene with an I_{2D}/I_G of 0.55. The I_D/I_G ratio is 1.39, indicating a large amount of disorder in the carbon.
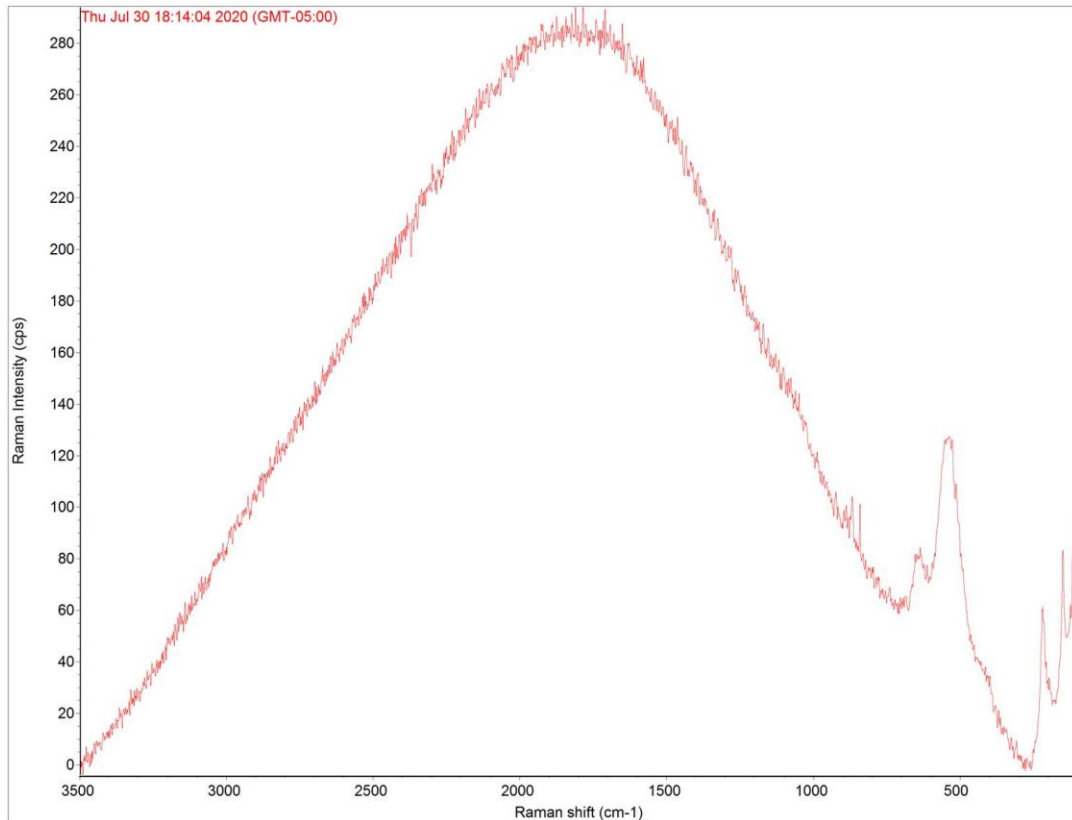
Figure 4.17. Raman spectra of Ni areas on Sample 7

Figure 4.17 above shows the results of the Raman spectra taken from an Ni region on Sample 7. Due to the inherent similarity of all the spectra taken in these regions, only this spectra is shown.

There is no indication of a carbon material present in any of these areas and only suggests that Ni or a combination of Cu/Ni is present.
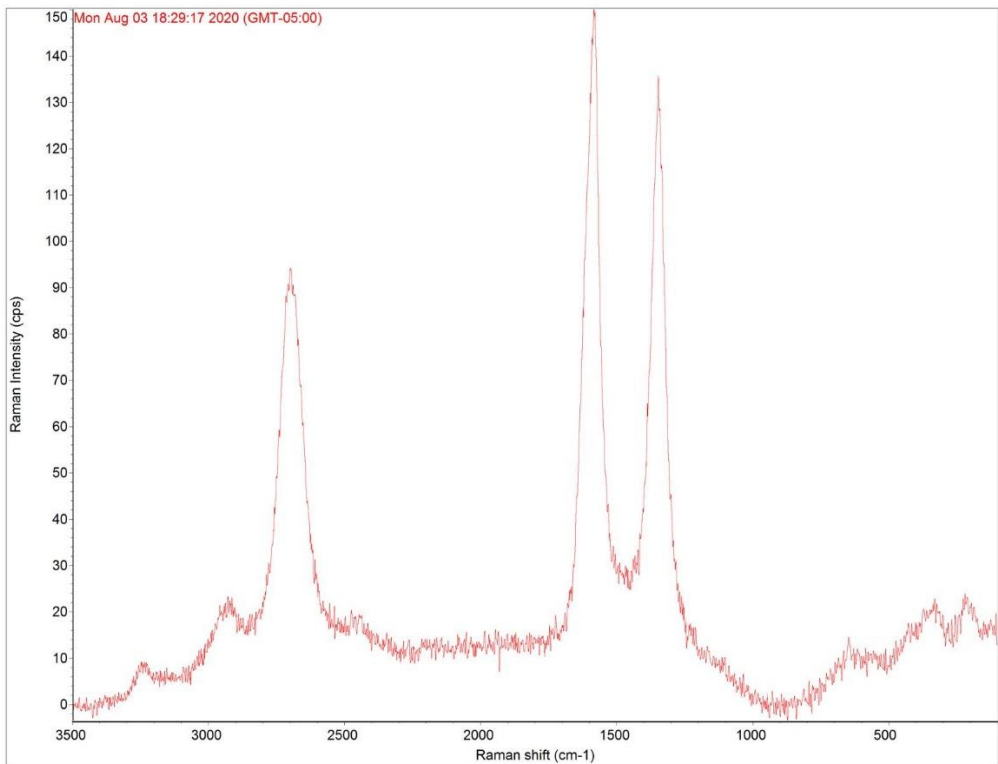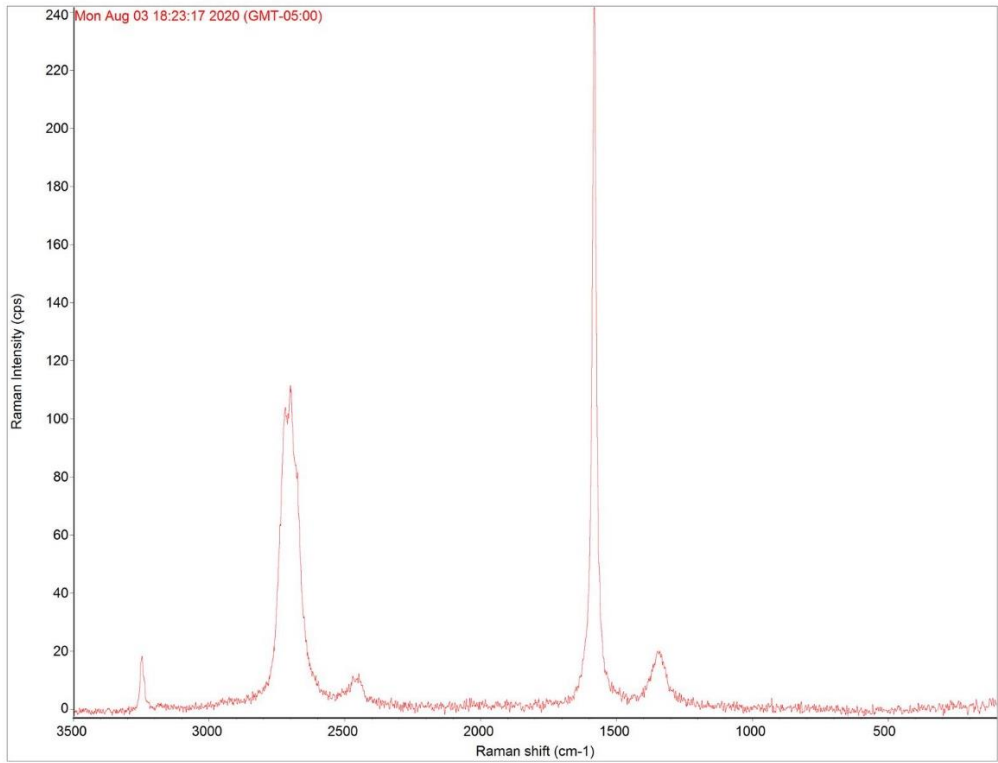
Figure 4.18. Raman spectra of graphene areas on Sample 8

Figure 4.18 above shows the results of the Raman spectra taken from graphene areas on Sample 8. Due to the inherent similarity of all the spectra taken in these regions, only these spectra are shown.

In the top graph, as mentioned previously, these peaks strongly suggest the presence of multilayer graphene due to the relative peak heights and shape of the 2D band. Also, the bottom graph indicates that some of these regions which appear to contain graphene also contain amorphous carbon. The top spectra has an I_{2D}/I_G ratio of 0.41 and an I_D/I_G ratio of 0.083, indicating a small degree of disorder. The bottom spectra has an I_{2D}/I_G ratio of 0.59 and an I_D/I_G ratio of 0.86, indicating a high degree of disorder in the carbon.

4.2.3.1 Conclusion

As mentioned previously, Samples 7 and 8 were created with the attempt of improving the uniformity of the multilayer graphene. Unfortunately, Sample 7 did not seem to contain any areas of graphene, although some areas of the amorphous carbon did seem to also contain graphene. Sample 8, however, was able to produce graphene including areas of the Cu/Ni alloy.

The suspected cause for why Sample 7 was unsuccessful while Sample 8 was successful was that Sample 7 did not seem to be able to properly integrate the Ni into the Cu to produce the Cu/Ni alloy. Sample 8 did not have any area in which bare Ni could be seen, also indicating a more proper distribution of Ni.

As compared to Samples 1-4, Sample 8 did appear to be more uniform with multi-layer graphene, but also seemed to have a much higher concentration of amorphous carbon than even what can be seen in Sample 4.

4.2.4 Samples 9-12

Samples 9-12 were examined using Raman microscopy to determine if there were any areas which had concentrated Ni (as seen in Sample 7) and identify the black regions seen in Figure 4.19 below.
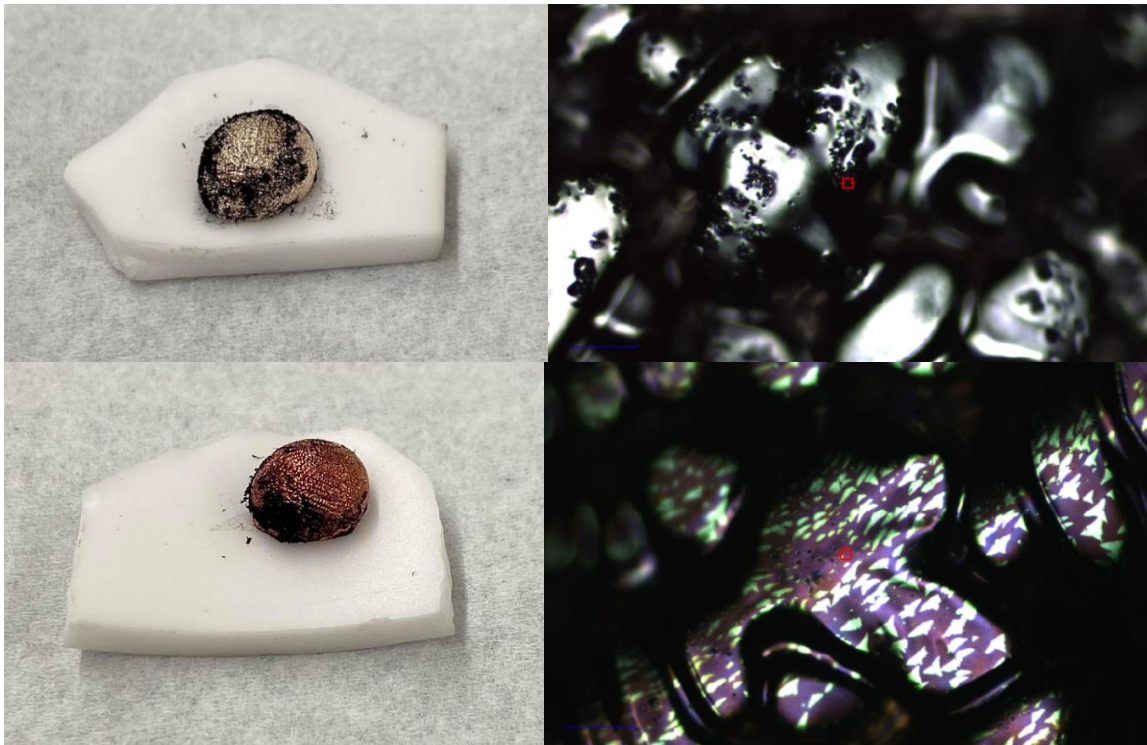
Figure 4.19. Image of Sample 9 (top left) and Sample 12 (bottom left) and at 10x magnifications (top right and bottom right). Scale bar indicates 120μm.

Given the apparent issue of the Ni not properly distributing within the Cu, Samples 9-12 were examined to verify the Ni distribution and to check the black regions on the alloy after the heating process. These regions are suspected to be carbon material from contamination of the Cu or Ni metal or from the Al_2O_3 base.

After the heating process, the samples were examined using Raman microscopy to determine the elemental. During the analysis of Samples 9-12, three identifiable regions were found on Samples 9-11, and four regions on Sample 12. Each of these regions were examined and compared to verify the consistency and accuracy of characterizing the

region. The results of the Raman analysis can be seen below.
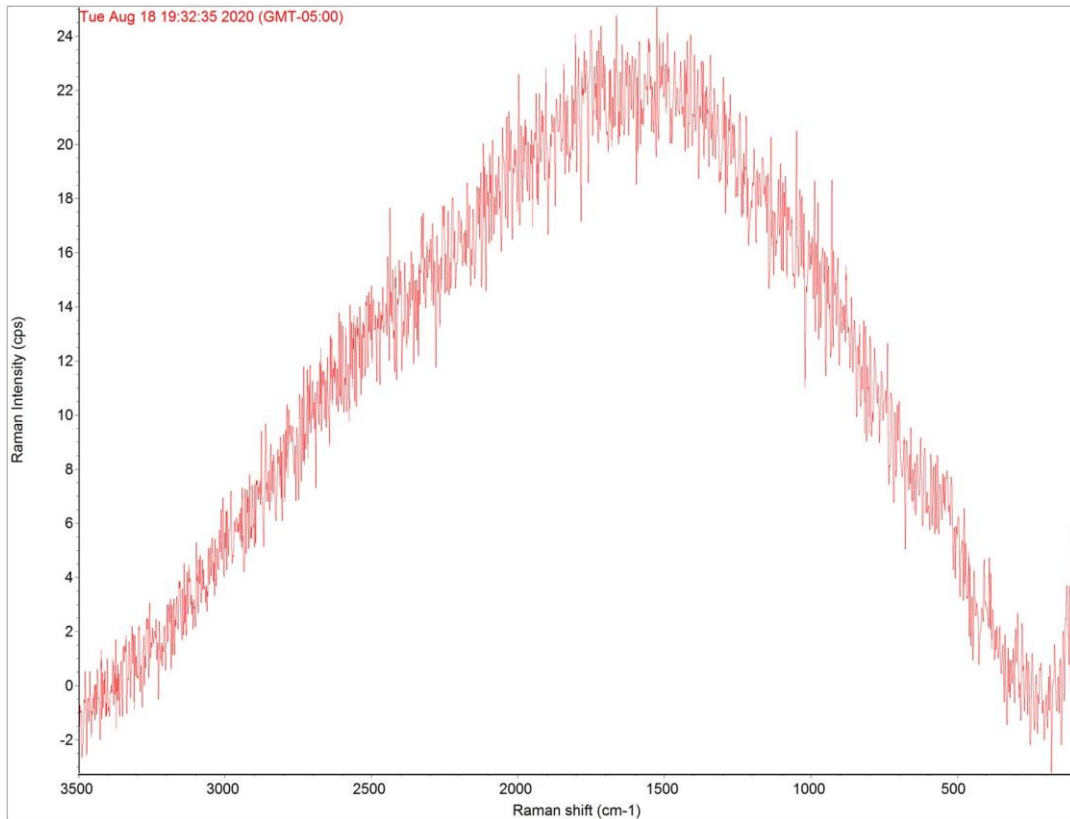
Figure 4.20. Raman spectra of Cu/Ni areas on Sample 9.

The spectra in Figure 4.20 has no discernable peaks and can be attributed to only the presence of the Cu/Ni. Due to the consistency between the measurements of all four samples, only one spectra is shown.
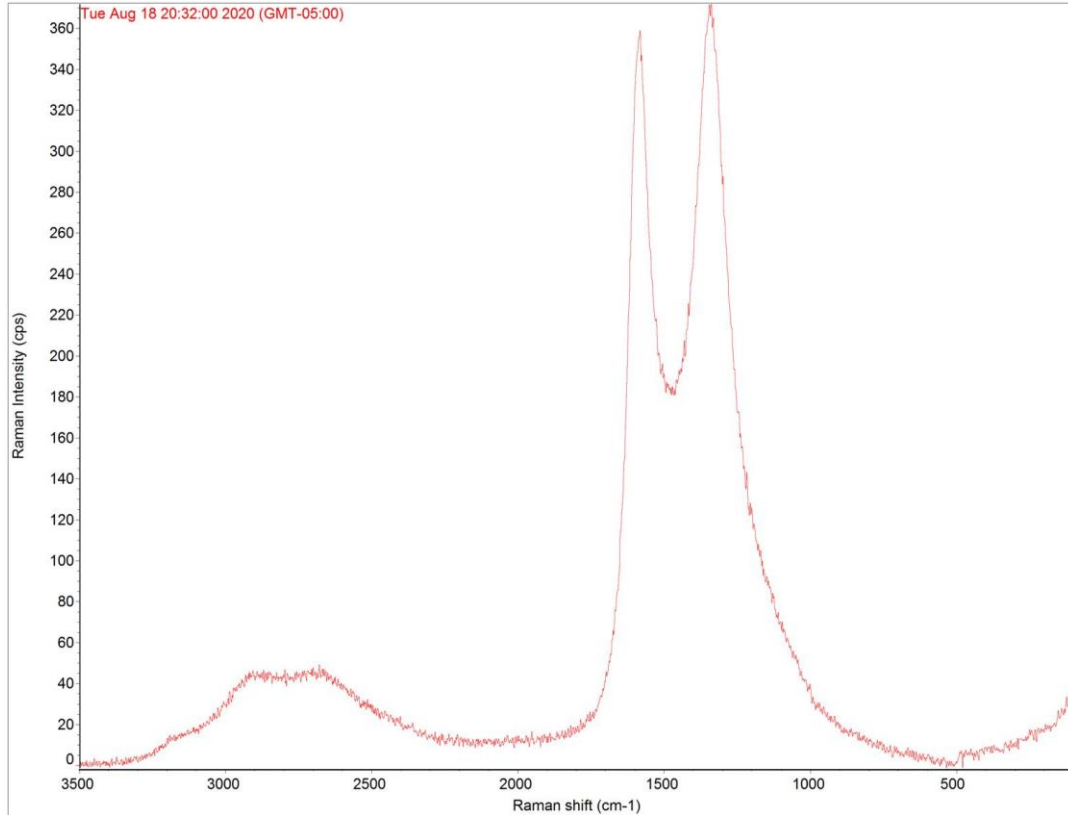
Figure 4.21. Raman spectra of amorphous carbon areas on Sample 11.

Figure 4.21 above shows the results of the Raman spectra taken from a suspected amorphous carbon region in Sample 11. Due to the inherent similarity of all the spectra taken in these regions from all samples, only this spectra is shown.

Strong peaks located at the G and D bands suggest the presence of amorphous carbon. Also, the lack of the presence of the 2D band suggests that no graphene is on the sample surface, which is to be expected. The I_D/I_G ratio is 1.06.
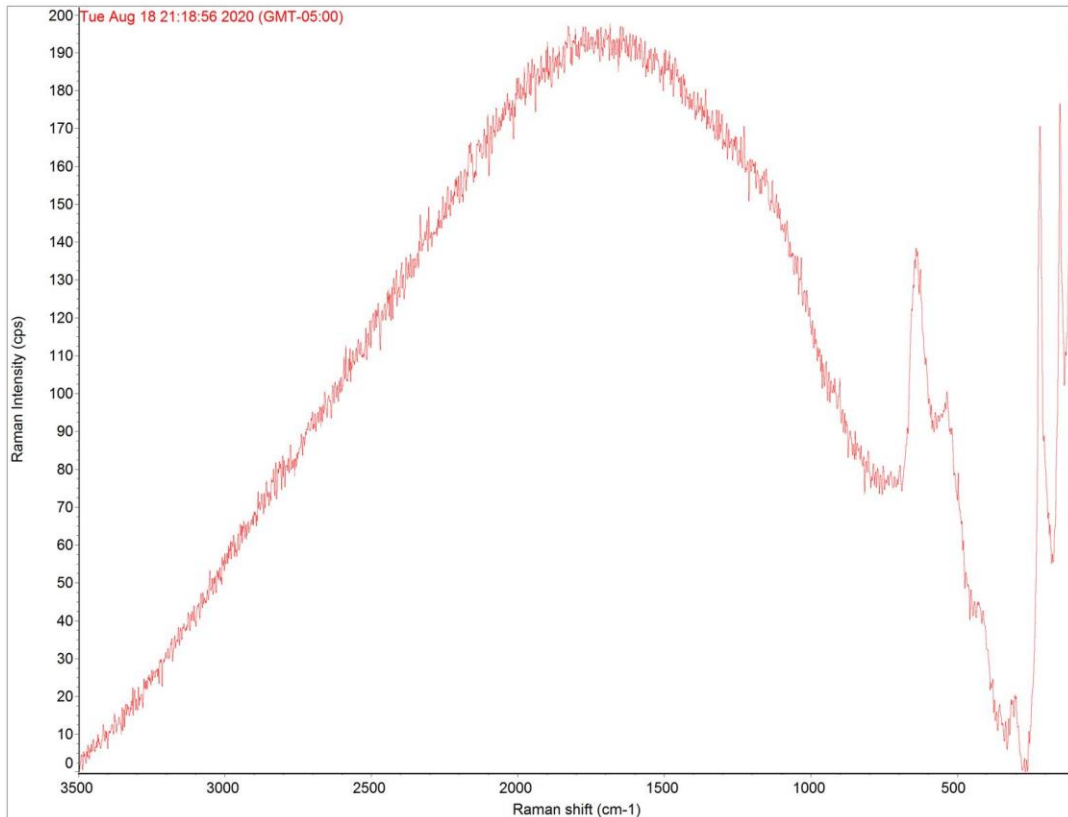
Figure 4.22. Raman spectra of Cu oxide areas on Sample 12.

Figure 4.22 above shows the results of the Raman spectra taken from suspected Cu oxide regions in Sample 12. Due to the inherent similarity of all the spectra taken in these regions from all, only this spectra is shown. The spectra in Figure 4.22 has no discernable peaks for carbon and can be attributed to only the presence of Cu or Cu oxide.

4.2.4.1 Conclusion

Samples 9-12 were produced with the attempt of examining the quality of the Ni distribution in Cu. For all four samples, no area was identified of pure Ni, suggesting a good distribution of Ni as compared to Sample 7. Also, the black areas indicated the presence of amorphous carbon with no presence of graphene, which is to be expected.

4.2.5 Samples 13 & 14

Samples 13 and 14 were examined using Raman spectroscopy to determine the cleanliness of the Al_2O_3 base. Sample 13 is the Al_2O_3 base prior to the cleaning process and Sample 14 is the result of the cleaning process.
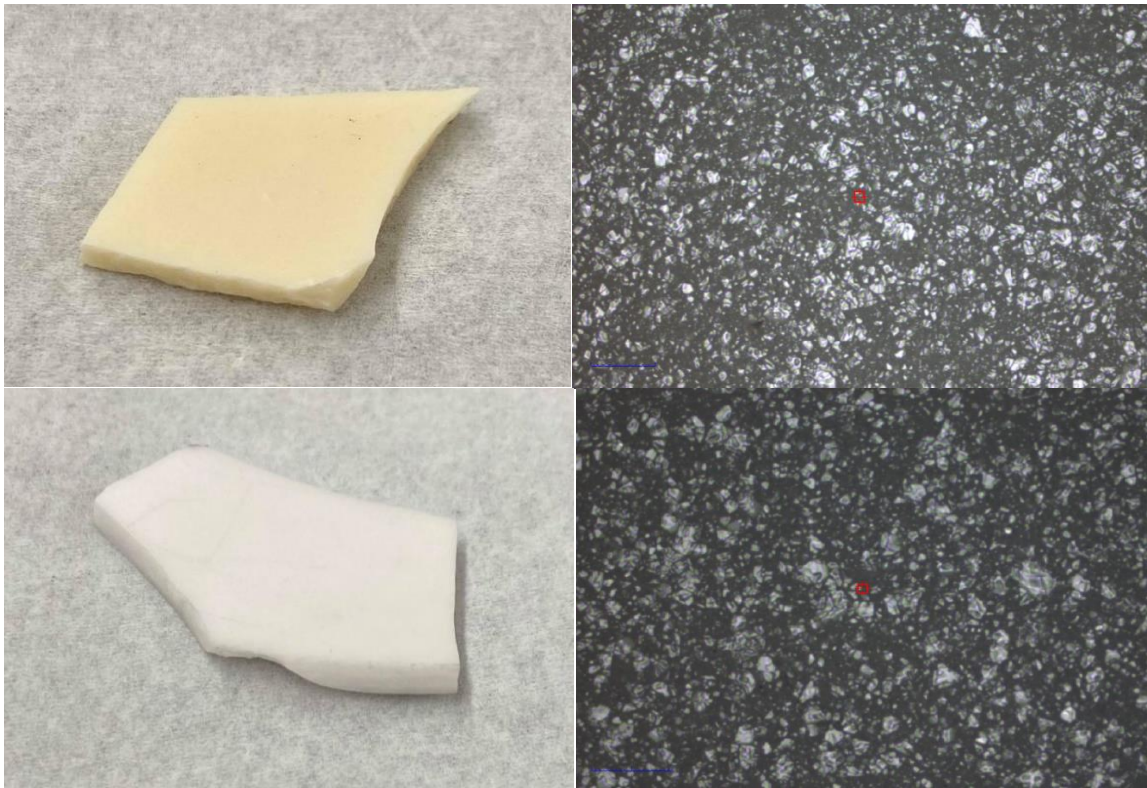

Figure 4.23. Image of Sample 13 (top left) and Sample 14 (bottom left) and at 10x magnifications (top right and bottom right). Scale bar indicates 120µm.

Based on the results of the Raman spectroscopy of Samples 9-12, black regions were present and identified as amorphous carbon. The source of this carbon is likely contamination from the Cu, Ni, or Al_2O_3 base. To eliminate the potential contamination from the Al_2O_3 substrates, care was taken by using an ultrasonic clean for ten minutes using isopropanol, then heated to 1100°C for one hour.

After the cleaning process, the samples were examined using Raman microscopy to determine the elemental composition and potential carbon areas. During the analysis of

Samples 13 and 14, two identifiable regions can be seen. Each of these regions were

examined and compared to verify the consistency and accuracy of characterizing the

region. The results of the Raman analysis can be seen below.
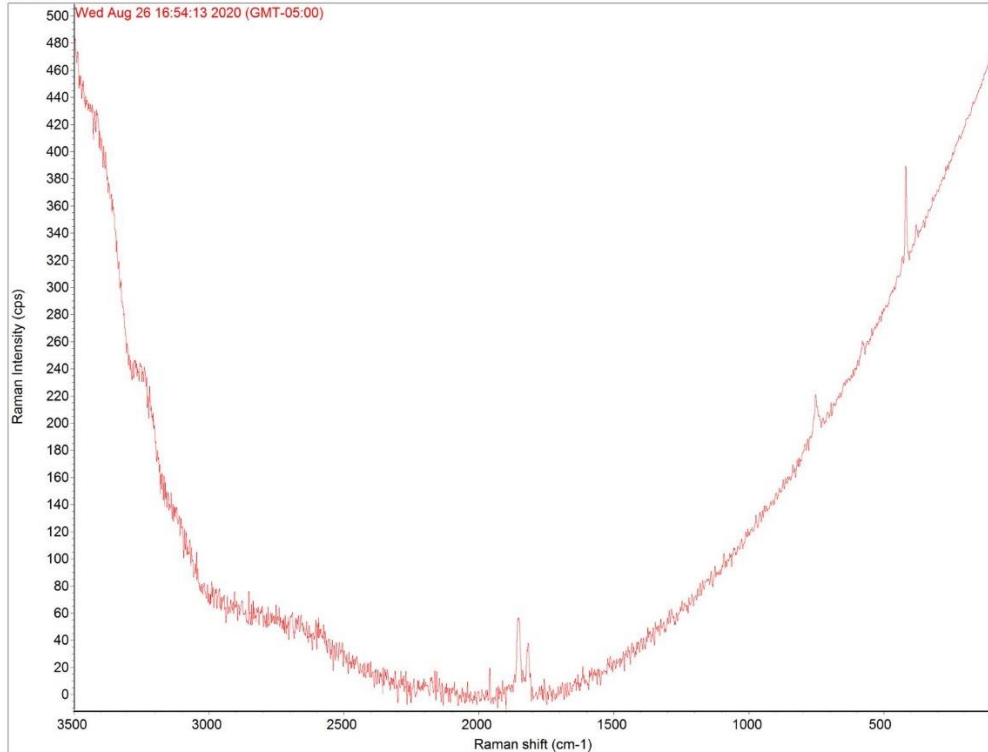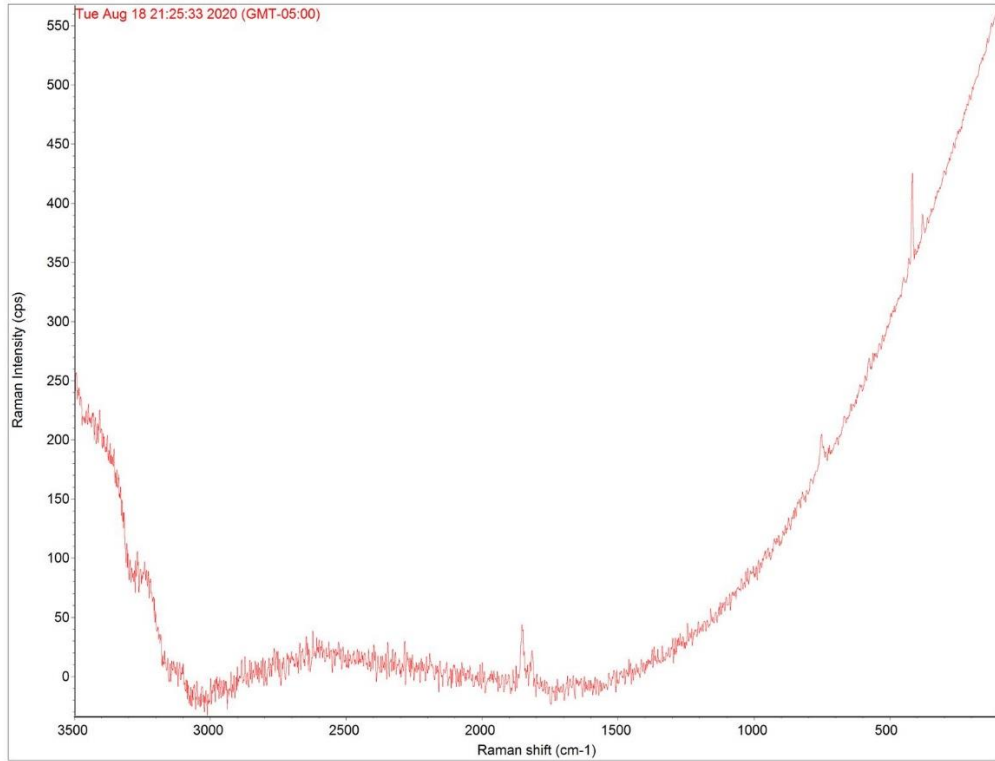
Figure 4.24. Raman spectra of Sample 13 (top) and Sample 14 (bottom)

Figure 4.24 above shows the results of the Raman spectra taken from Sample 13

and 14. Due to the inherent similarity of all the spectra taken in both identifiable regions

from both samples, only these spectra are shown. No carbon can be identified due to the

lack of the bands typically present of carbon materials.

4.2.5.1 Conclusion

The results of the Raman spectra do not indicate the presence of any carbon

before or after the cleaning process. However, the cleaning process does cause an

obvious change in the color of the base, indicating that the ultrasonic and heating

procedure does clean the material.

4.2.6 Sample 15-17

Samples 15-17 were produced to test the results of the improved cleaning process

of the Cu, Ni, and Al_2O_3 as well as the effect of the methane flow on the graphene growth

and uniformity. Sample 15 used 100sccm, Sample 16 used 50 sccm, and Sample 17 used

25 sccm.
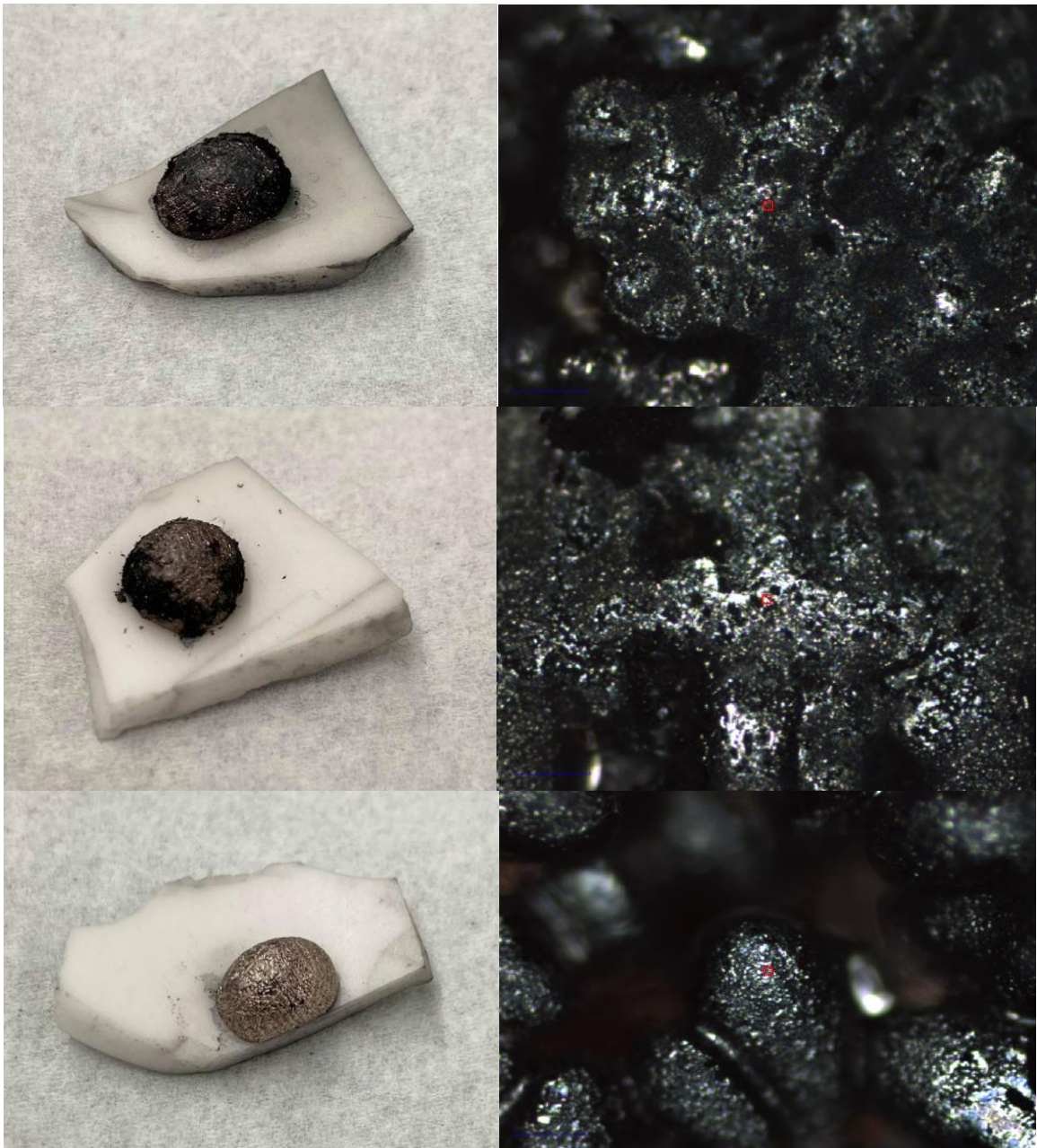
Figure 4.25. Image of Sample 15 (top left), Sample 16 (middle left), and Sample 17 (bottom left) at 10x magnifications. Scale bar indicates 120μm.

Based on the results of Samples 7 and 8, Sample 8 had a large concentration of amorphous carbon. To potentially mitigate this issue, Samples 15-17 were produced to compare the results of the methane flow rate as the flow rate will affect the amount of carbon produced on the samples. Also, the improved cleaning process should increase the quality and uniformity of the graphene by reducing contaminates.

After the graphene growth process, the samples were examined using Raman microscopy to determine the elemental composition and carbon arrangement on the surface. During the analysis of Samples 15-17, four identifiable regions were found in Samples 15 and 16, and three regions in Sample 17. Each of these regions were examined and compared to verify the consistency and accuracy of characterizing the region. The results of the Raman analysis can be seen below.
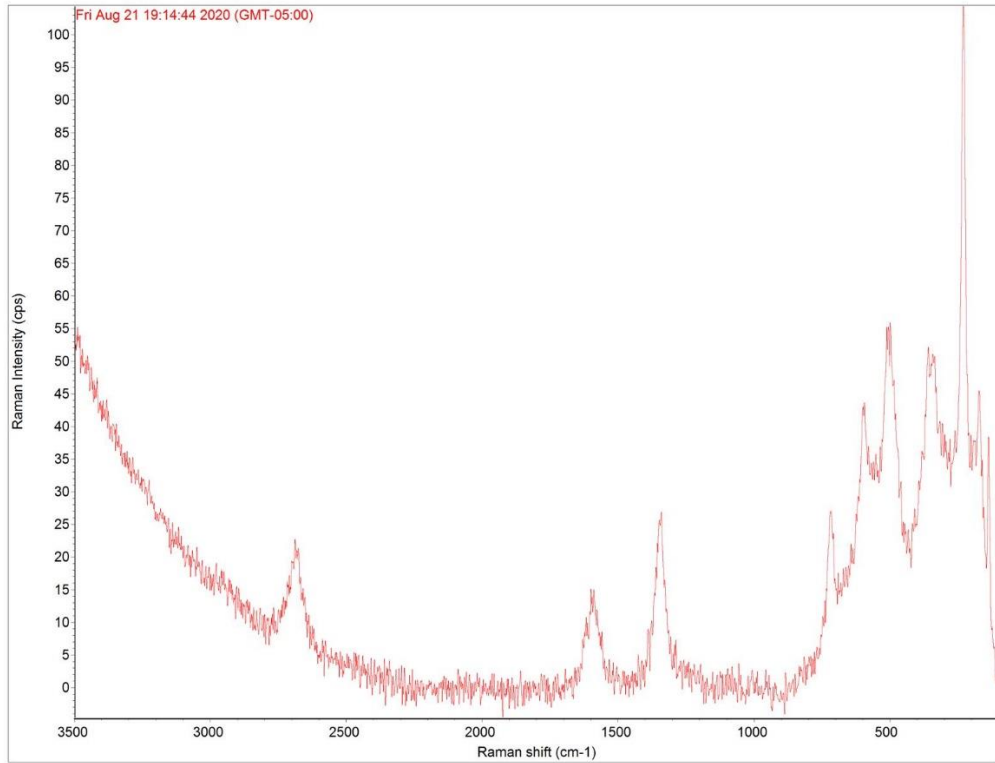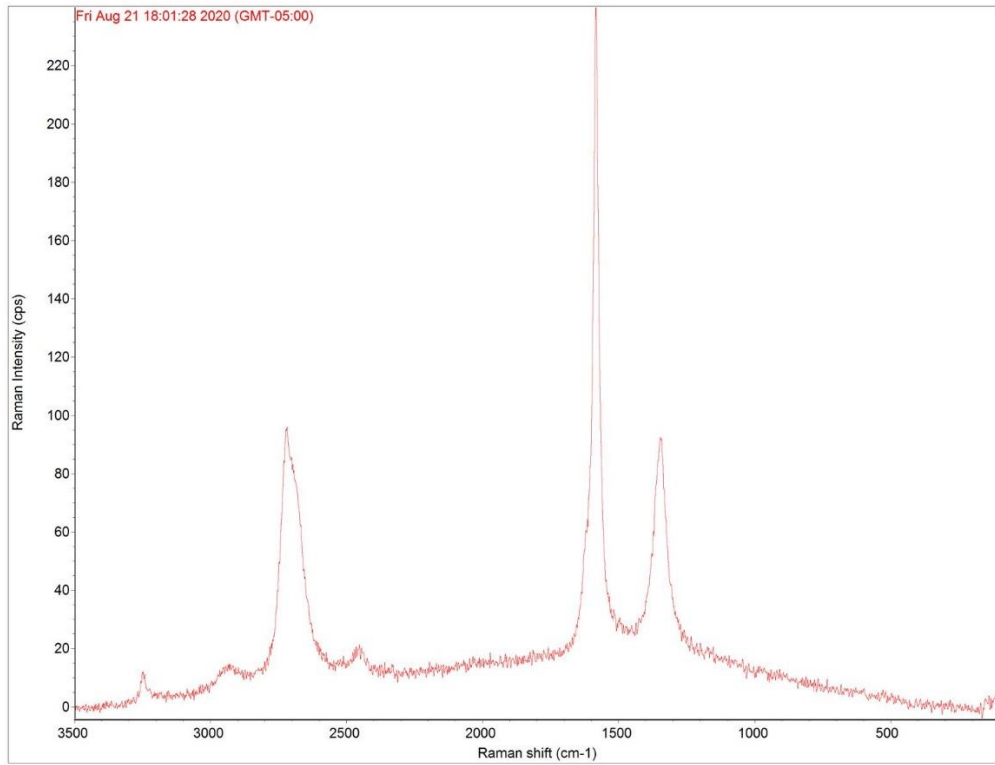
Figure 4.26. Raman spectra of Sample 16 (top) and Sample 17 (bottom) on Cu/Ni areas

Figure 4.26 above shows the results of the Raman spectra taken from suspected Cu/Ni regions in Samples 16 and 17. Due to the inherent similarity of all the spectra taken in these regions from all three samples, only these spectra are shown.

Samples 15, 16 and 17 had very discernable peaks from the G, D, and 2D bands indicating the presence of multilayer graphene. Also, the 2D band indicates the presence of graphene. The I_{2D}/I_G ratio of the top spectra is 0.42, which indicates multilayer graphene. The I_{2D}/I_G ratio of the bottom spectra is 1.69, indicating bilayer graphene. The I_D/I_G ratio of the top spectra is 0.38. The I_D/I_G ratio of the bottom spectra is 1.85.
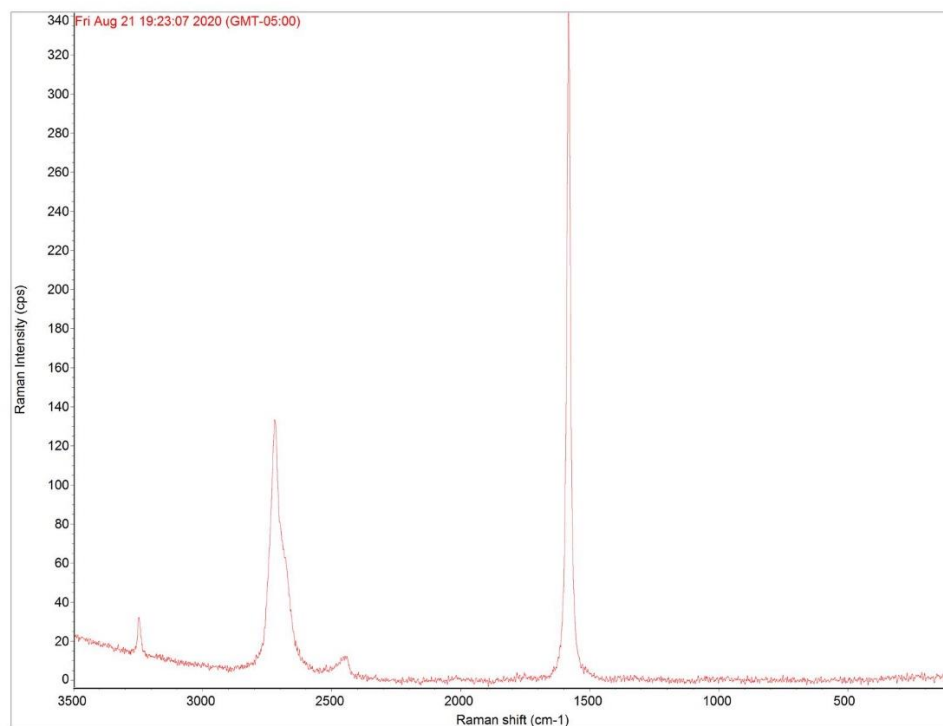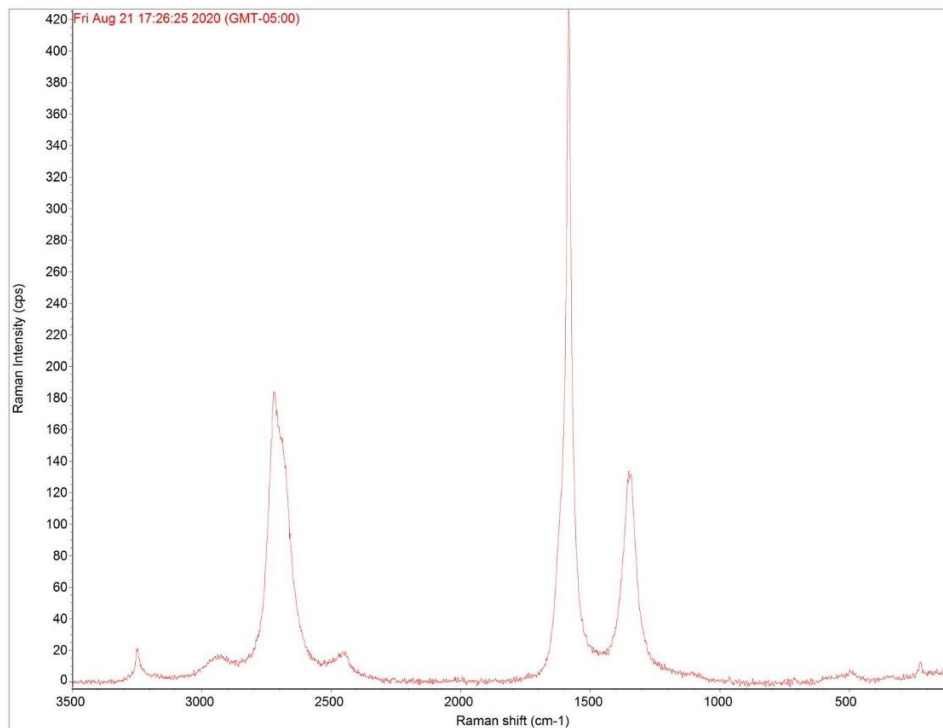
Figure 4.27. Raman spectra of Sample 15 (top) and Sample 17 (bottom) on graphene areas

Figure 4.27 above shows the results of the Raman spectra taken from suspected graphene regions on Samples 15 and 17. Due to the inherent similarity of all the spectra taken in these regions from all three samples, only these spectra are shown.

Samples 15, 16, and 17 had very discernable peaks from the G, D, and 2D bands indicating the presence of multilayer graphene. However, Sample 17 did not have the presence of the D peak, suggesting a low number of defects present in the graphene regions. The I_{2D}/I_G ratio of the top spectra is 0.44 and 0.40 for the bottom spectra, suggesting multilayer graphene. The I_D/I_G ratio of the top spectra is 0.31, indicating disorder in the graphene. The bottom spectra has not discernable D band, thus there is little to no disorder in the graphene.
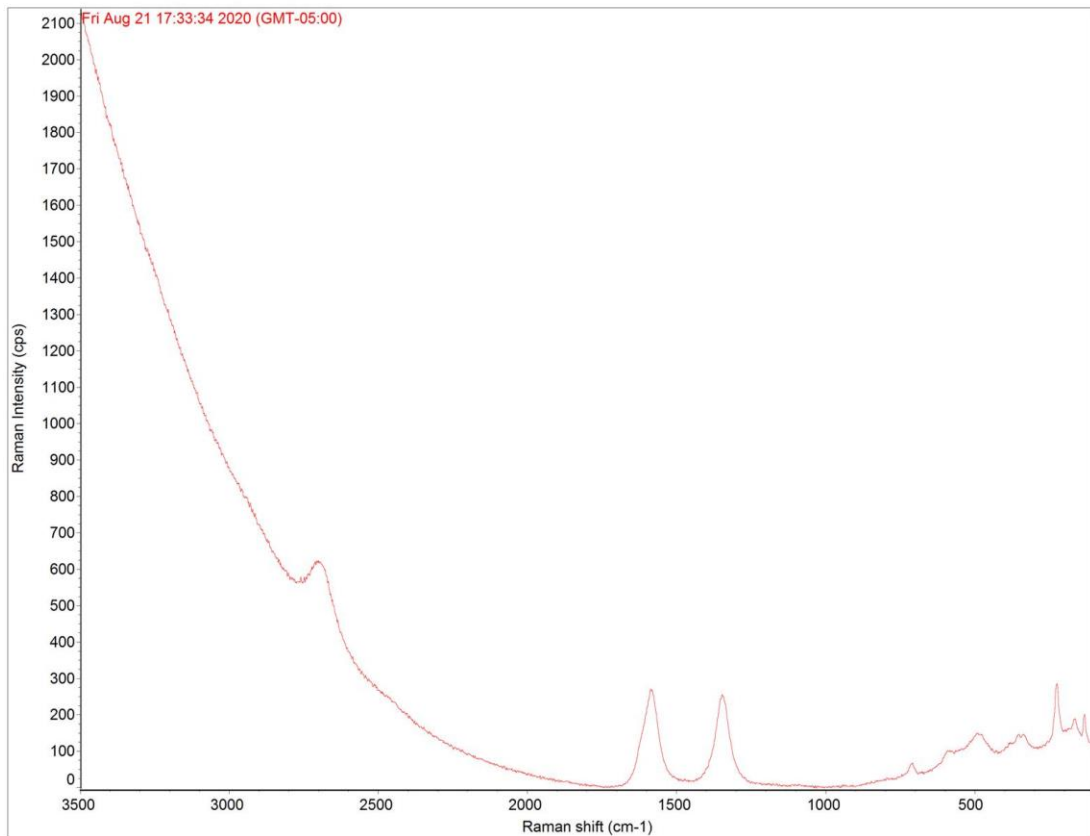
Figure 4.28. Raman spectra of Sample 15 (top) dark graphene areas

Figure 4.28 above shows the results of the Raman spectra taken from suspected dark graphene regions in Sample 15. Due to the inherent similarity of all the spectra taken in these regions from Samples 15 and 16, only this spectra is shown.

There are very discernable peaks from the G, D, and 2D bands indicating the presence graphene. The I_{2D}/I_G ratio is 2.1, indicating monolayer graphene. The I_D/I_G ratio is 0.85, indicating a certain degree of disorder in the graphene.
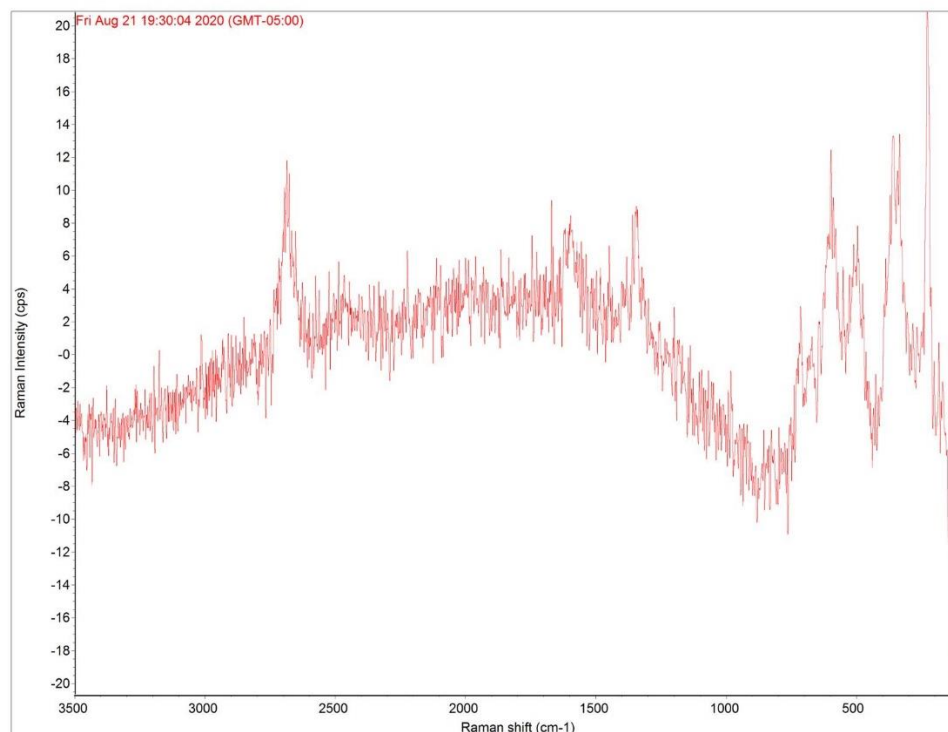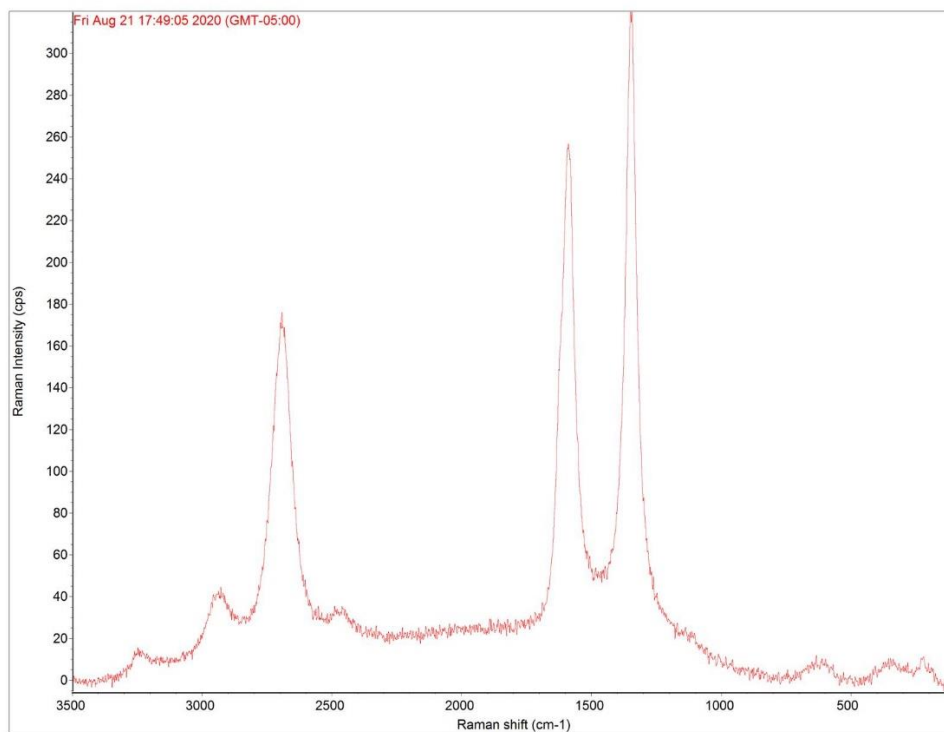
Figure 4.29. Raman spectra of Sample 15 (top) and Sample 17 (bottom) on amorphous carbon areas.

Figure 4.29 above shows the results of the Raman spectra taken from suspected amorphous carbon regions in Samples 15 and 17. Due to the inherent similarity of all the spectra taken in these regions from Samples 15 and 17, only this spectra is shown.

There are very discernable peaks from the G, D, and 2D bands indicating the presence graphene. The I_{2D}/I_G ratio of the top spectra is 0.67, suggesting multilayer graphene. The I_D/I_G ratio is 1.25, indicating a large degree of disorder in the graphene. The spectra from Sample 17 indicates a weak signal from the G, D, and 2D peaks, however, the peaks are not clear enough to determine the I_{2D}/I_G or I_D/I_G ratios.

4.2.6.1 Conclusion

Overall, graphene is present over most of the entirety of the three samples, which is a better result than Samples 7 and 8. However, all three samples show a low level of uniformity. Out of the three samples, Sample 15 showed to have the highest content of amorphous carbon while also containing the most amount of visible graphene, likely due to the high methane flow rate as compared to Samples 16 and 17.

4.2.7 Sample 18

Sample 18 utilized the pre-made Cu/Ni alloy to compare the results to the self-made alloy using the new and improved techniques of cleaning and Ni distribution.
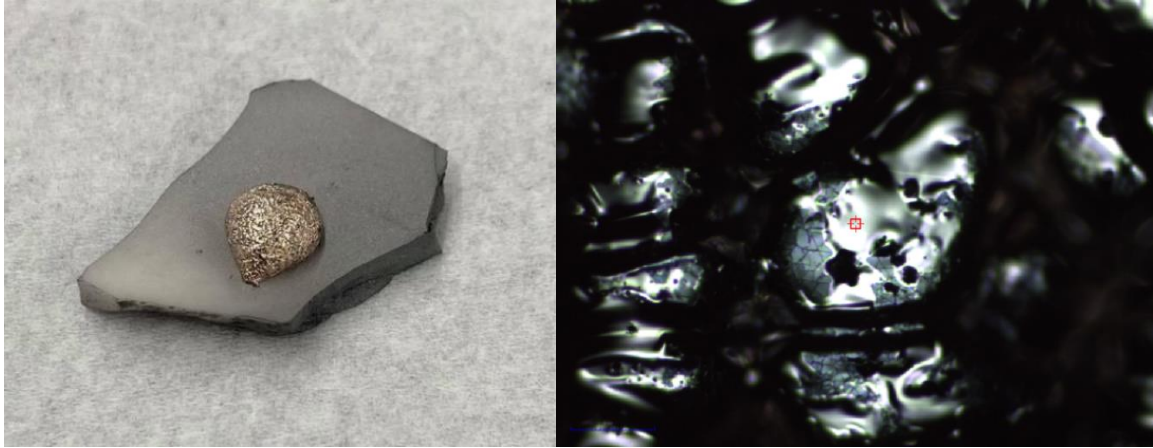
Figure 4.30. Image of Sample 13 (top left) and Sample 14 (bottom left) and at 10x magnifications (top right and bottom right). Scale bar indicates 120μm.

The new and improved techniques have demonstrated a great increase in the ability to produce more uniform multilayer graphene with the Raman analysis showing graphene over the majority of the sample surface. Sample 18 focuses on the difference between the quality of graphene produced using the pre-made alloy and the self-made alloy. This comparison allows for a more accurate representation of the quality of the self-made alloy and its ability to produce uniform multi-layer graphene.

After the graphene growth process, the sample was examined using Raman microscopy to determine the elemental composition and carbon arrangement on the surface. During the analysis, three identifiable regions were found. Each of these regions were examined and compared to verify the consistency and accuracy of characterizing the region. The results of the Raman analysis can be seen below.
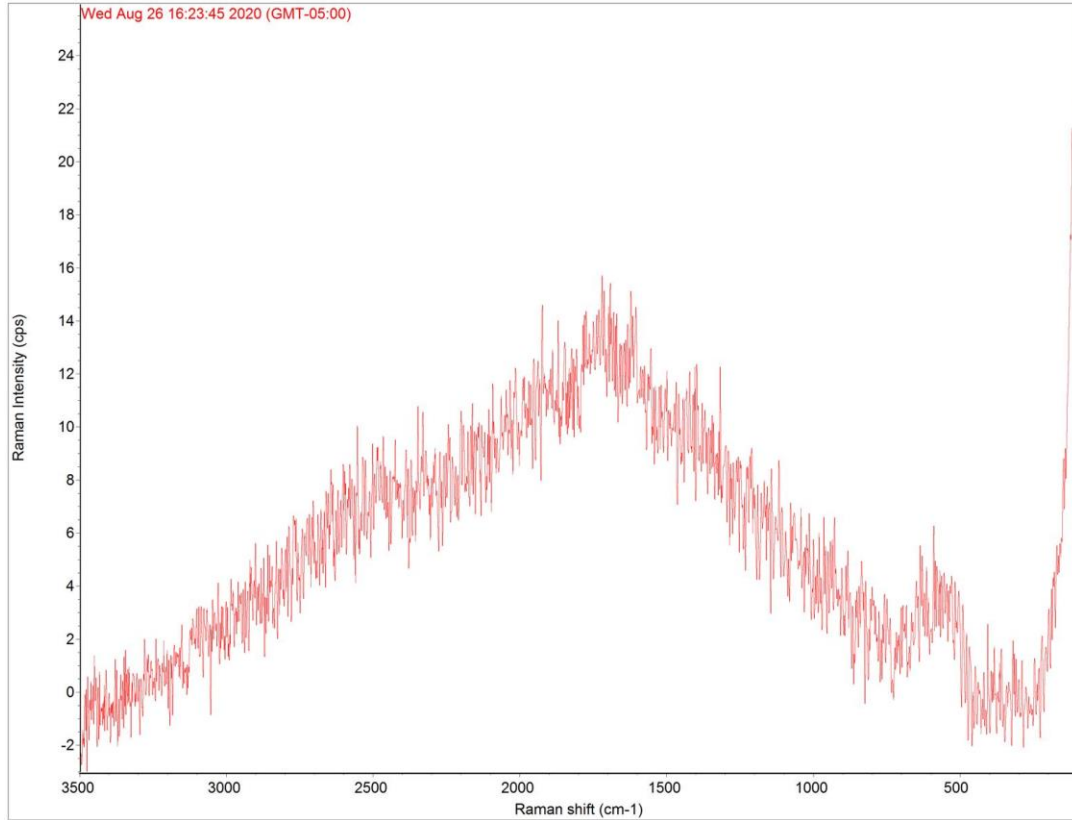
Figure 4.31. Raman spectra of Sample 18 on Cu/Ni area.

Figure 4.31 above shows the results of the Raman spectra taken from suspected Cu/Ni regions in Sample 18. Due to the inherent similarity of all the spectra taken in these regions, only this spectra is shown. The spectra in Figure 4.31 has no discernable peaks for carbon and can be attributed to only the presence of the Cu/Ni substrate.
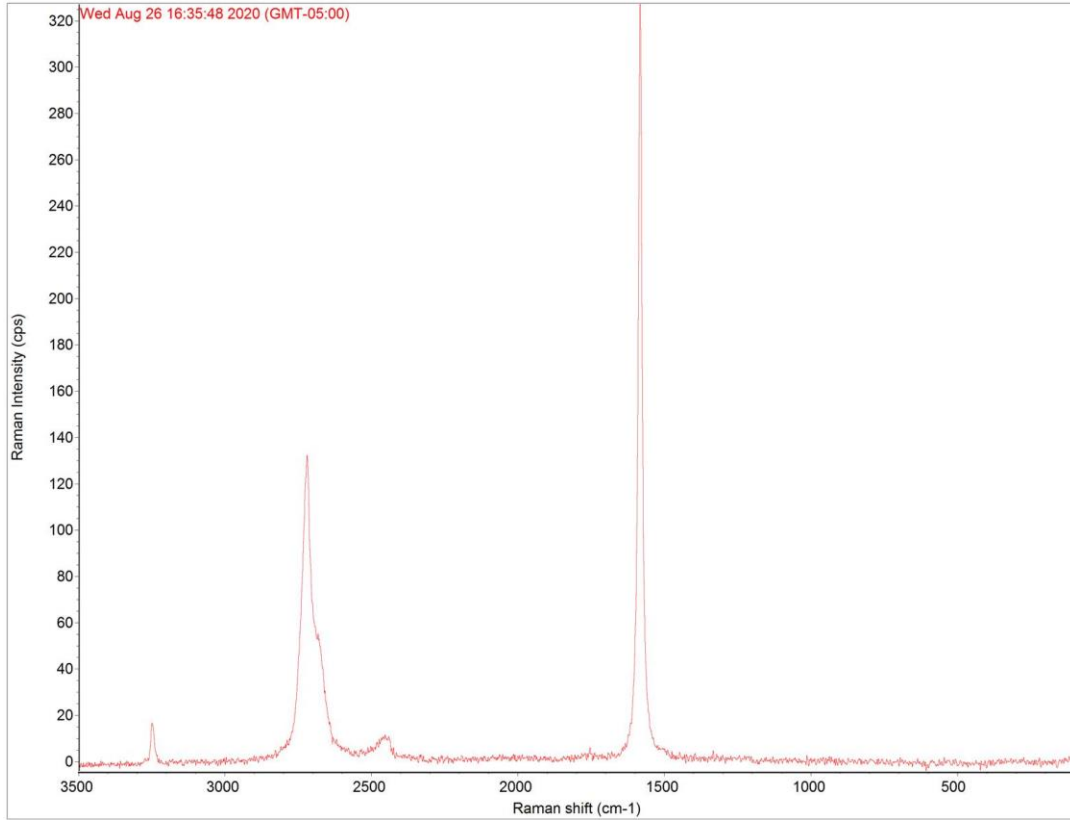
Figure 4.32. Raman spectra of Sample 18 on graphene area.

Figure 4.32 above shows the results of the Raman spectra taken from suspected graphene regions in Sample 18. Due to the inherent similarity of all the spectra taken in this region, only this spectra is shown.

Sample 18 had very discernable peaks from the G and 2D bands indicating the presence of graphene. The I_{2D}/I_G ratio is 0.4, indicating multilayer graphene. There is no discernable D band suggesting that there is little to no disorder in the graphene.
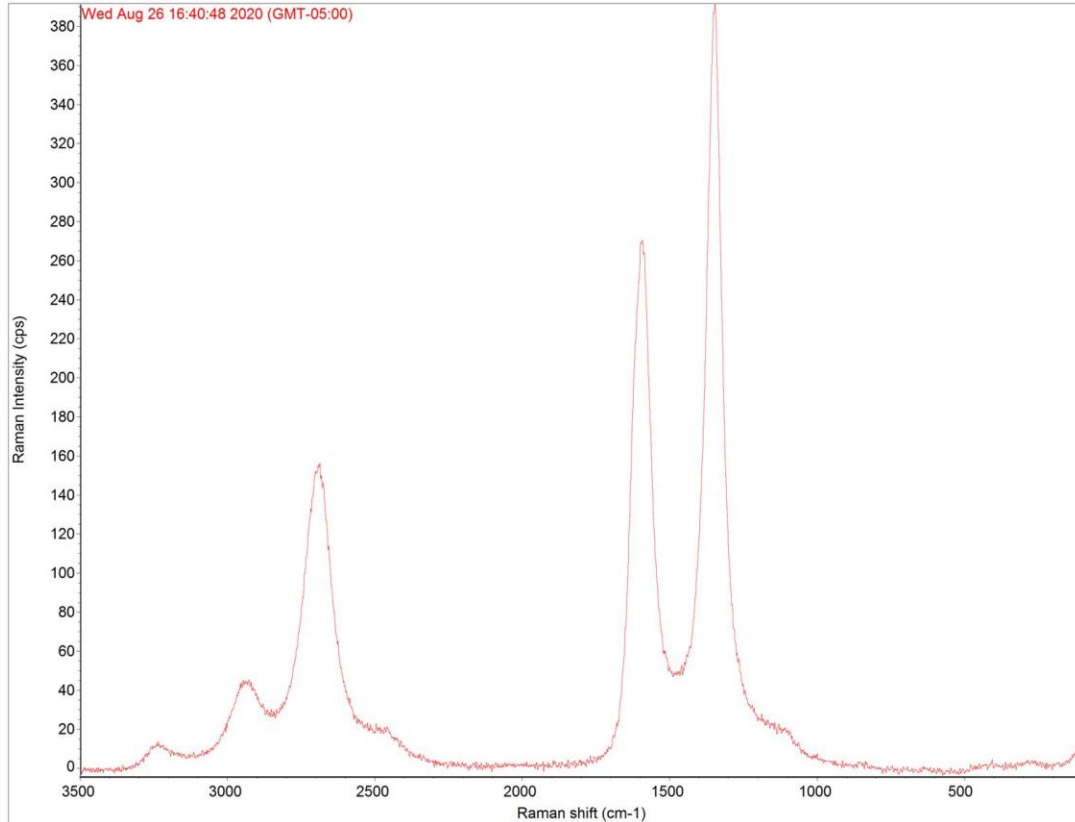
Figure 4.33. Raman spectra of Sample 18 on amorphous carbon area.

Figure 4.33 above shows the results of the Raman spectra taken from suspected amorphous carbon regions in Sample 18. Due to the inherent similarity of all the spectra taken in these regions, only this spectra is shown.

There are very discernable peaks from the G, D, and 2D bands indicating the presence graphene. The I_{2D}/I_G ratio is 0.57, indicating multilayer graphene. The I_D/I_G ratio is 1.48, indicating a high amount of disorder in the carbon.

4.2.7.1 Conclusion

Sample 18 was produced to compare how the pre-made alloy could produce uniform multilayer graphene to the self-made alloy. This pre-made alloy was capable of producing multilayer graphene, but in a much smaller area, and not very uniform. Thus,

the self-made alloy produces better results as compared to the pre-made alloy. However, this pre-made alloy does produce less amorphous carbon.

4.2.8 Samples 19 & 20

Samples 19 and 20 were produced to evaluate the ability of alloys produced using a two hour bake time, compared to the previous one hour, as well as the effect of the methane flow rate. As such, both samples were produced using a two hour bake time during the alloy production phase. Sample 19 used 100sccm and Sample 20 used 50sccm of methane.


Figure 4.34. Image of Sample 19 (top left) and Sample 20 (bottom left) and at 10x magnifications (top right and bottom right). Scale bar indicates 120μm.

A potential constraint in the ability to produce graphene is the proper distribution of Ni within the Cu. A more well distributed sample will be able to produce a higher

quality sample in terms of Cu/Ni uniformity. To test this and the effect of the flow rates, Samples 19 and 20 were produced using a two-hour bake time to more properly distribute the Ni within the Cu.

After the graphene growth process, the sample was examined using Raman microscopy to determine the elemental composition and carbon arrangement on the surface. During the analysis, three identifiable regions were found in both samples. Each of these regions were examined and compared to verify the consistency and accuracy of characterizing the region. The results of the Raman analysis can be seen below.
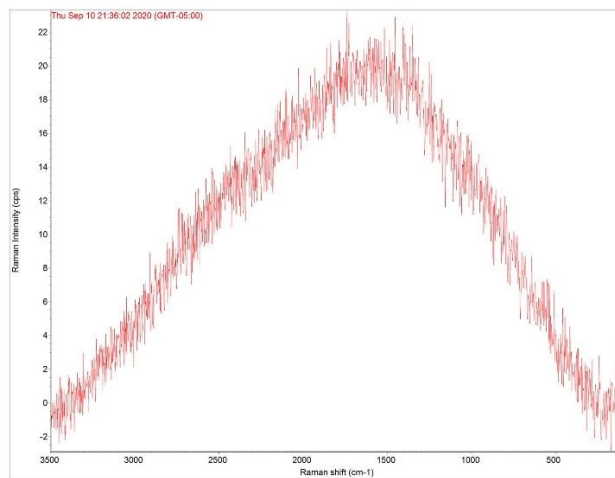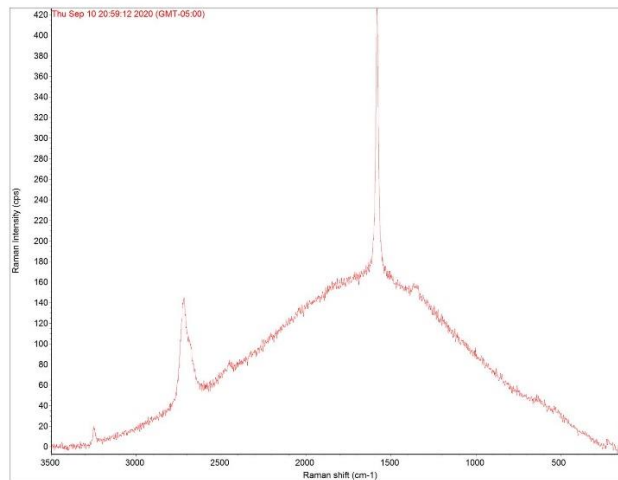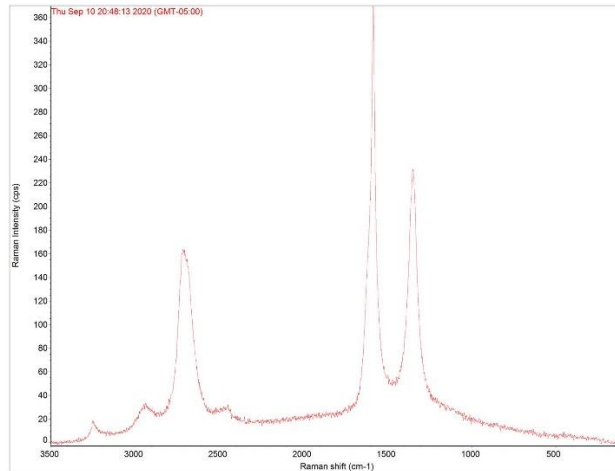
Figure 4.35. Raman spectra of Sample 19 (top and middle) and Sample 20 (bottom) on Cu/Ni areas.

Figure 4.35 above shows the results of the Raman spectra taken from suspected Cu/Ni regions in Samples 19 and 20. Due to the inherent similarity of all the spectra taken in this region, only these spectra are shown.

Overall, most of the Cu/Ni areas indicate the presence of graphene. The I_{2D}/I_G ratio of the top spectra is 0.43, indicting multilayer graphene. The I_D/I_G ratio of the top spectra is 0.62, indicating a certain degree of disorder in the graphene. The I_{2D}/I_G ratio of the middle spectra is 0.33, indicting multilayer graphene. There is not a clear indication of the D peak within the middle spectra. The bottom spectra does not indicate the presence of the 2D, G, or D bands, suggesting that there is no presence of graphene.
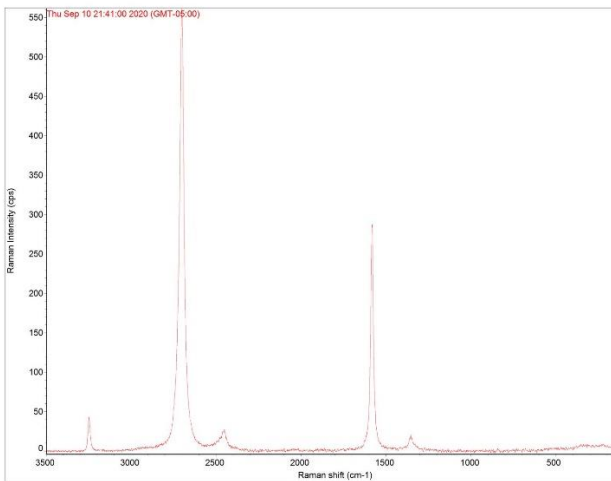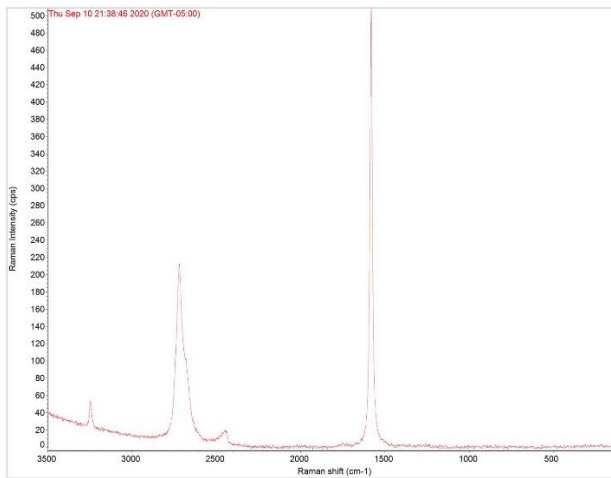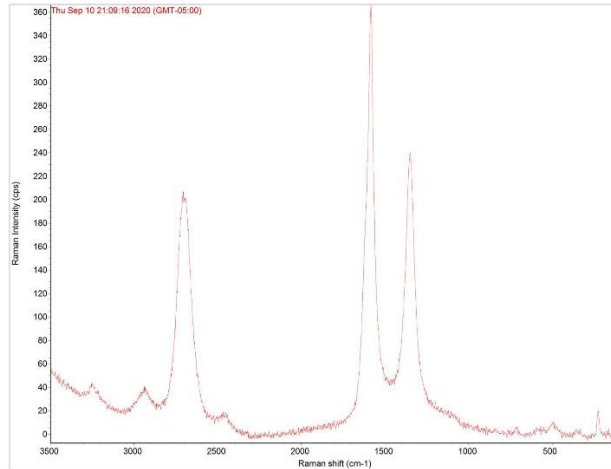
Figure 4.36. Raman spectra of Sample 19 (top) and Sample 20 (middle and bottom) on graphene areas.

Figure 4.36 above shows the results of the Raman spectra taken from suspected graphene regions in Samples 19 and 20. Due to the inherent similarity of all the spectra taken in this region, only these spectra are shown.

The strong peaks of the carbon G and 2D bands indicate the presence of graphene. The difference between these spectra are variations in the content of disorder in the graphene, given by the intensity of the D band. The I_{2D}/I_G ratio of the top spectra is 0.55, indicting multilayer graphene. The I_D/I_G ratio of the top spectra is 0.66, indicating a certain degree of disorder in the graphene. The I_{2D}/I_G ratio of the middle spectra is 0.41, indicting multilayer graphene. There is no discernable D band, suggesting that there is little to no disorder in the graphene. The I_{2D}/I_G ratio of the bottom spectra is 1.93, indicting bilayer graphene. The I_D/I_G ratio of the bottom spectra is 0.07, indicating a certain degree of disorder in the graphene.
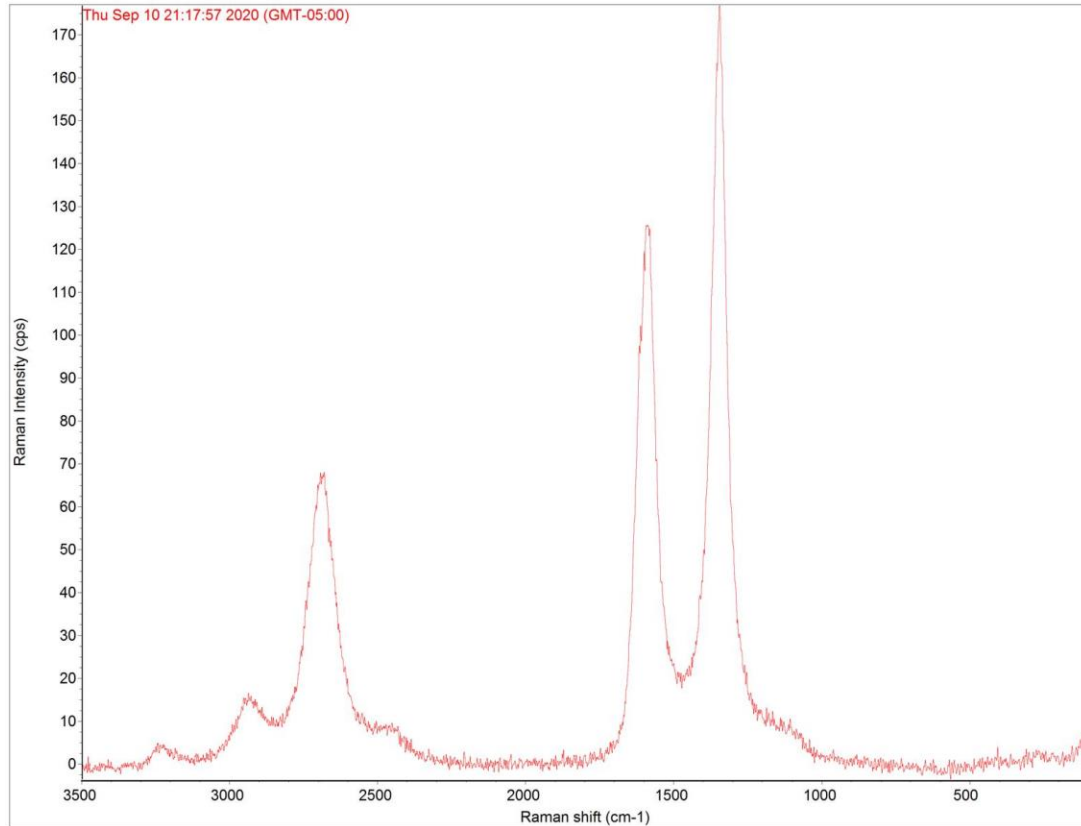
Figure 4.37. Raman spectra of Sample 19 on amorphous carbon area.

Figure 4.37 above shows the results of the Raman spectra taken from suspected amorphous carbon regions in Sample 19. Due to the inherent similarity of all the spectra taken in this region, only this spectra is shown.

The strong peaks of the carbon G and 2D bands indicate the presence of graphene. The I_{2D}/I_G ratio of the spectra is 0.55, indicting multilayer graphene. The I_D/I_G ratio of the spectra is 1.42, indicating a certain degree of disorder in the graphene.

4.2.8.1 Conclusion

The bare Cu/Ni regions seem to indicate the presence of multilayer graphene over most of the surface with varying degree of disorder from the D band. Also, the optical verification shows that Samples 19 and 20 have a much smaller region of bare Cu/Ni

areas, as most areas are dominated by graphene or amorphous carbon.

The graphene areas inspected have demonstrated to be mostly multilayer, with some areas of bilayers. Also, there is a varying degree of disorder indicated by the D band. Finally, the amorphous carbon areas show to have multilayer graphene, with high D band intensity indicating high disorder.

Overall, the graphene and amorphous carbon seem to dominate the sample surface, more so than previous samples. This is attributable to the improvement in the graphene growth process. Namely, the cleaning of the materials and Ni distribution in the self-made alloy.

4.2.9 Samples 21-23

During the initial experimentation, using pure Cu did not produce any samples with graphene. After the improved cleaning and system optimizations, pure Cu was used to produce samples using molten Cu. Samples 21-23 used varied methane flow rates to compare the relative graphene quality and uniformity to the Cu/Ni samples and the carbon cover samples. The flow rates for Samples 21-23 were 100sccm, 50sccm, and 25sccm respectively.

Figure 4.38. Image of Sample 21 (top left), Sample 22 (middle left), and Sample 23 (bottom left) at 10x magnifications (top right, middle right, and bottom right). Scale bar indicates 120μm.

The improvement of the production of uniform multi-layer graphene using Cu/Ni and pure Cu has brought the question of which samples would produce more uniform and high quality graphene. Samples 19 and 20, being the best samples of Cu/Ni trials, are compared to Samples 21-23 and then to Samples 24-26, which use the carbon cover.

After the graphene growth process, the sample was examined using Raman microscopy to determine the elemental composition and carbon arrangement on the surface. During the analysis, three identifiable regions were found in all three samples. Each of these regions were examined and compared to verify the consistency and accuracy of characterizing the region. The results of the Raman analysis can be seen below.
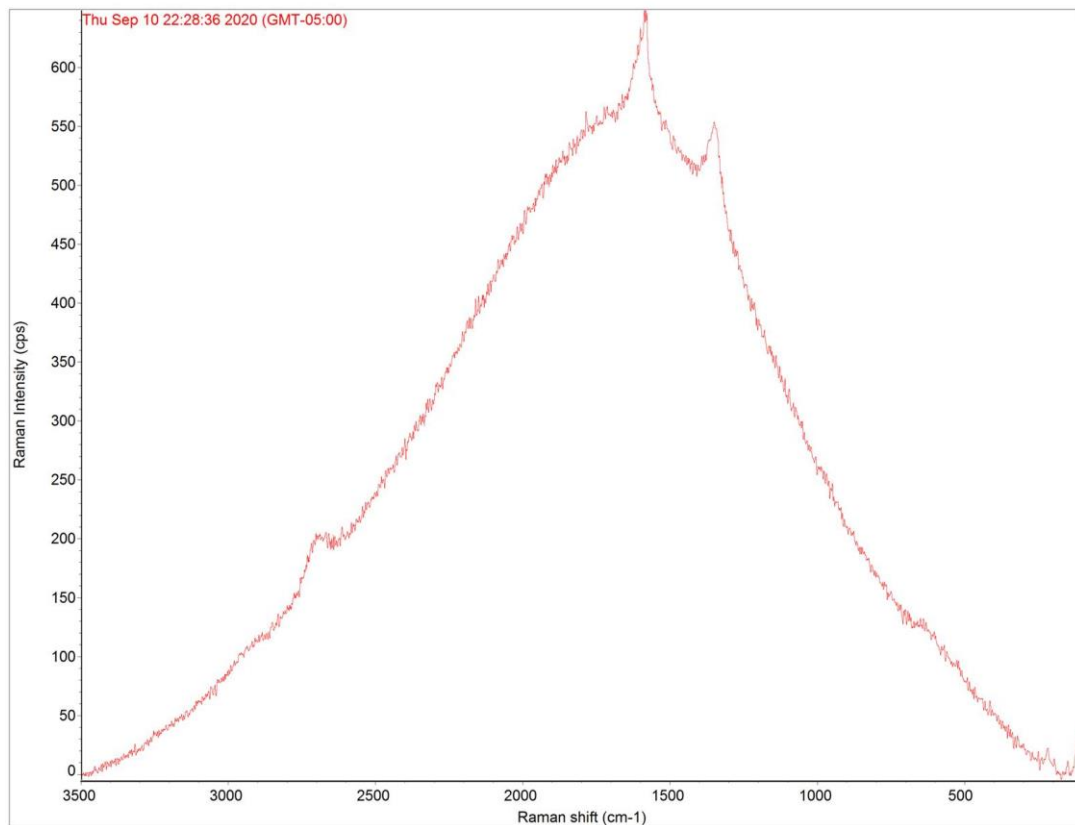
Figure 4.39. Raman spectra of Sample 22 on Cu areas.

Figure 4.39 above shows the results of the Raman spectra taken from Cu regions in Sample 22. Due to the inherent similarity of all the spectra taken in this region, only these spectra are shown.

Overall, the Cu areas indicate the presence of graphene in all three samples. The

broad peak under indicates the Cu substrate. The I_{2D}/I_G ratio of the spectra is 0.31,

indicting multilayer graphene. The I_D/I_G ratio of the spectra is 0.85, indicating a certain

degree of disorder in the graphene.
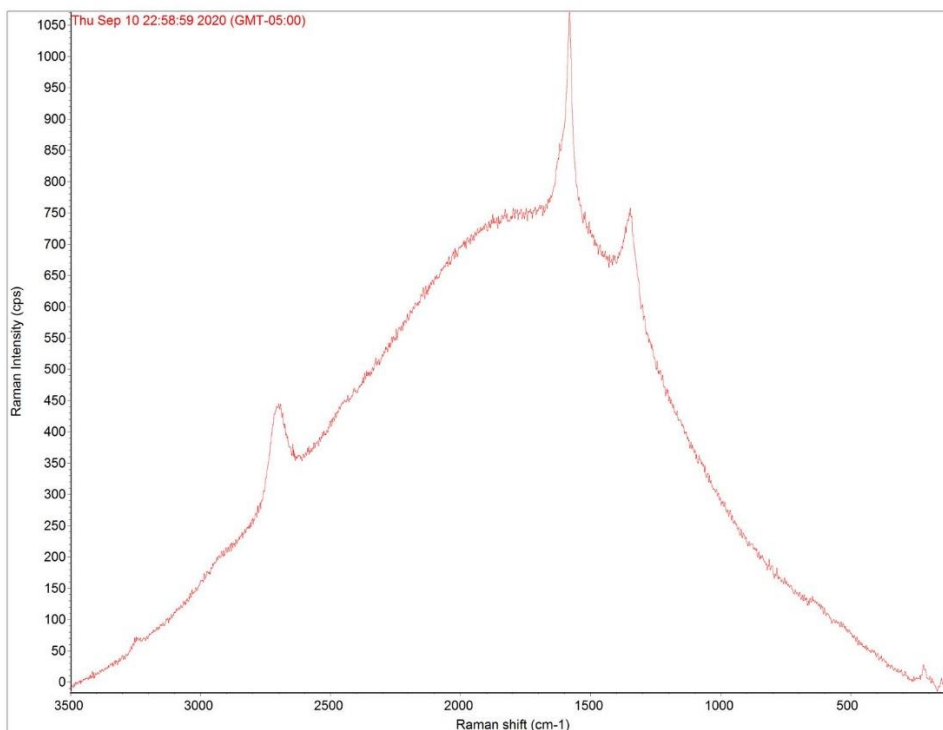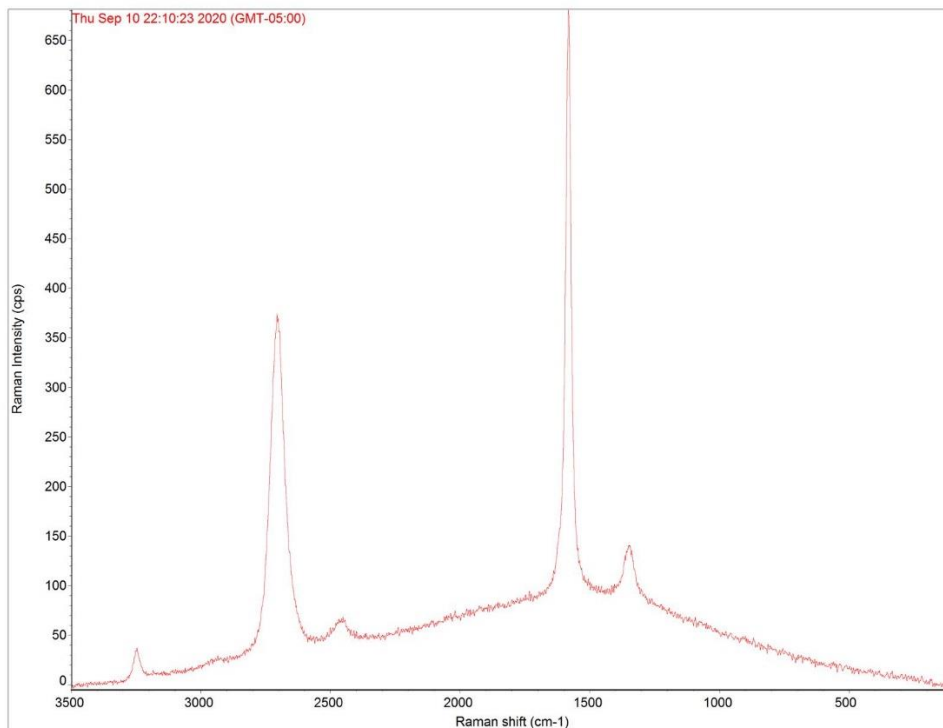
Figure 4.40. Raman spectra of Sample 21 (top) and Sample 23 (bottom) on graphene areas.

Figure 4.40 above shows the results of the Raman spectra taken from suspected graphene regions in Samples 21 and 23. Due to the inherent similarity of all the spectra taken in this region, only these spectra are shown.

The broad peak in the bottom graph indicates the Cu substrate. The other peaks indicate the presence of graphene. The I_{2D}/I_G ratio of the top spectra is 0.55, indicting multilayer graphene. The I_D/I_G ratio of the top spectra is 0.21, indicating a certain degree of disorder in the graphene. The I_{2D}/I_G ratio of the bottom spectra is 0.42, indicating multilayer graphene. The I_D/I_G ratio of the bottom spectra is 0.70, indicating a certain degree of disorder in the graphene.
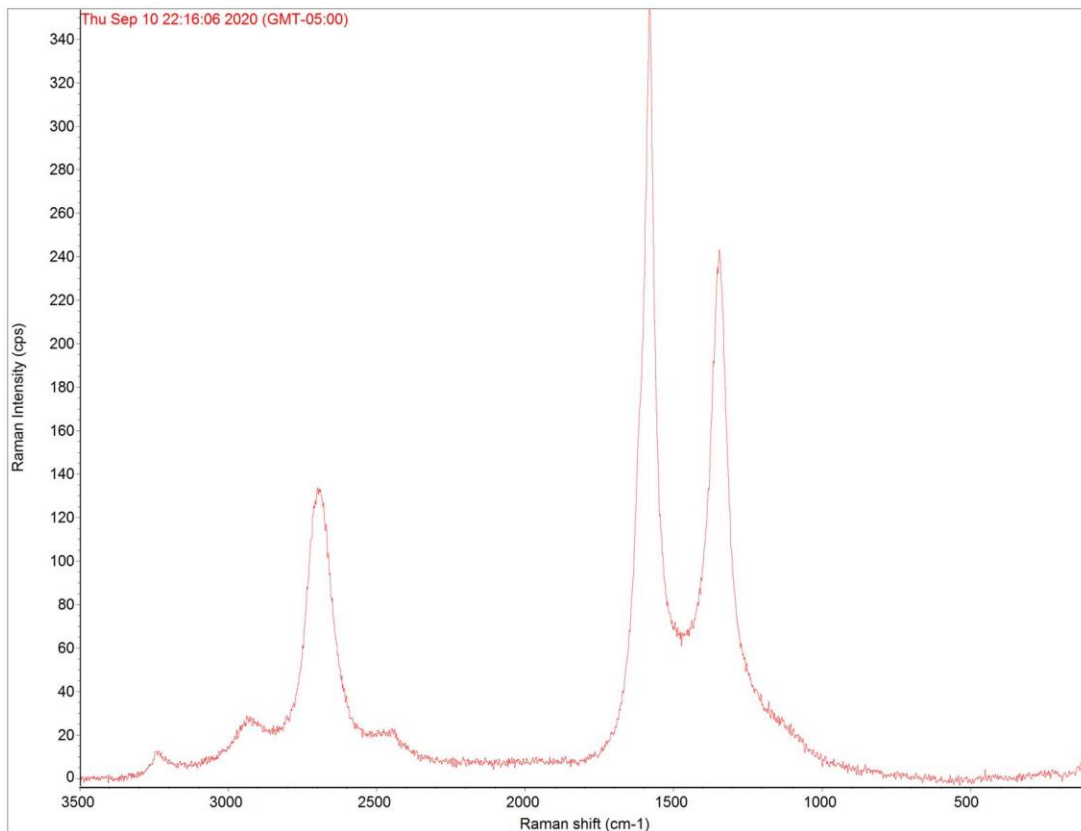
Figure 4.41. Raman spectra of Sample 21 on amorphous carbon areas.

Figure 4.41 above shows the results of the Raman spectra taken from suspected

amorphous carbon regions in Sample 21. Due to the inherent similarity of all the spectra taken in this region, only these spectra are shown.

Unlike the previous regions, the broad Cu curve is not noticeable in these amorphous carbon regions, likely due to the thickness of the carbon. The I_{2D}/I_G ratio of the spectra is 0.37, indicting multilayer graphene. The I_D/I_G ratio of the spectra is 0.69, indicating a certain degree of disorder in the graphene.

4.2.9.1 Conclusion

Overall, the graphene was present on the vast majority of the sample. However, the uniformity was low. As compared to the Cu/Ni Samples 19 and 20, Samples 21-23 also had a lower amount of amorphous carbon.

4.2.10 Sample 24-26

Samples 24-26 were produced to compare the quality and uniformity with Samples 19-23. These samples utilized the carbon cover to create a temperature gradient. This gradient should promote the uniformity and number of layers present as mentioned previously. Samples 24-26 also varied the flow rate of methane from 100sccm, 50sccm, and 25sccm respectively.
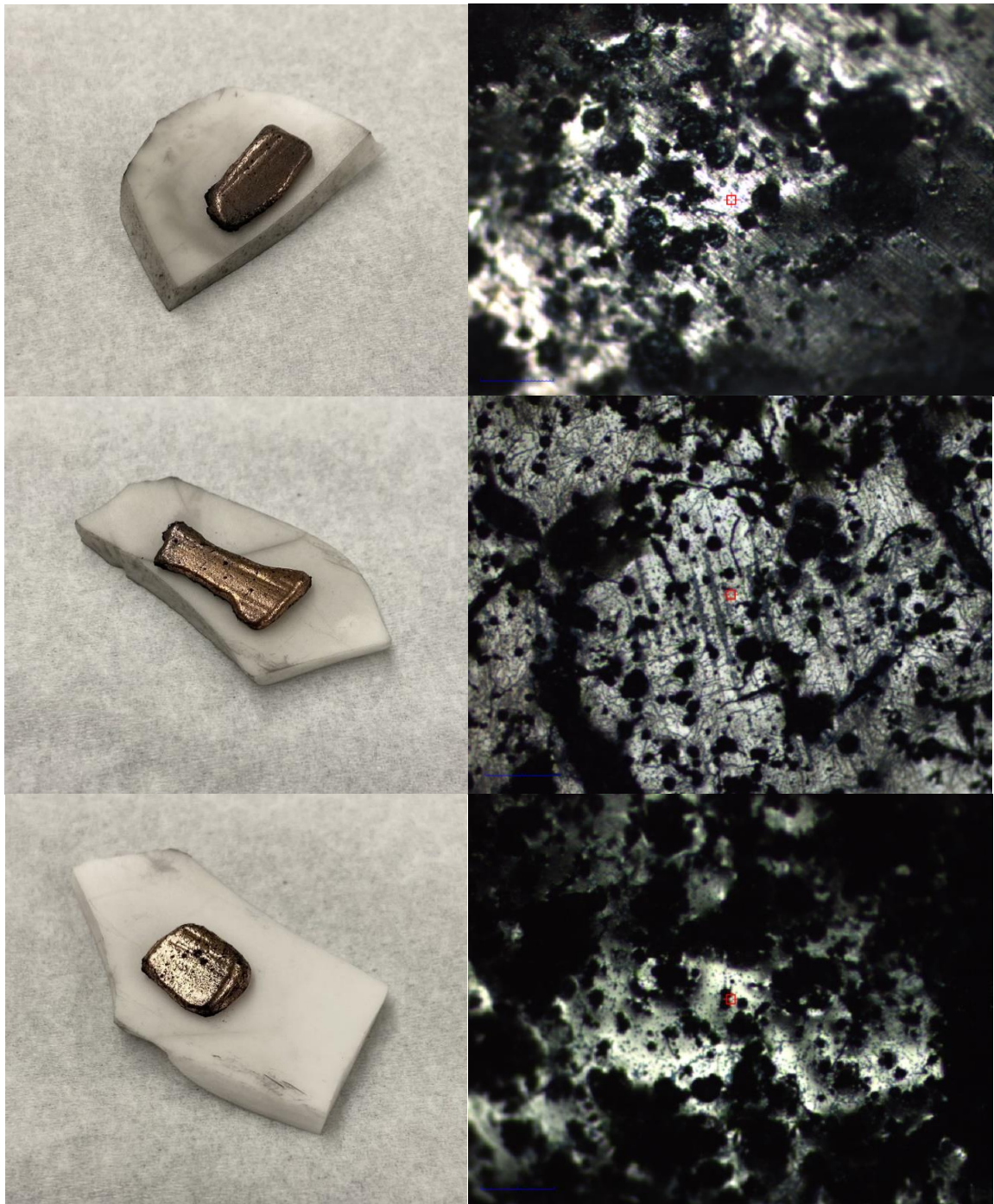
Figure 4.42. Image of Sample 24 (top left), Sample 25 (middle left), and Sample 26 (bottom left) at 10x magnifications (top right, middle right, and bottom right). Scale bar indicates 120μm.

With an objective of this research to improve the uniformity of multi-layer graphene, the use of the carbon cover theoretically should allow for the sample surface to form a larger number of layers with higher uniformity.

After the graphene growth process, the sample was examined using Raman microscopy to determine the elemental composition and carbon arrangement on the surface. During the analysis, three identifiable regions were found in all three samples. Each of these regions were examined and compared to verify the consistency and accuracy of characterizing the region. The results of the Raman analysis can be seen below.
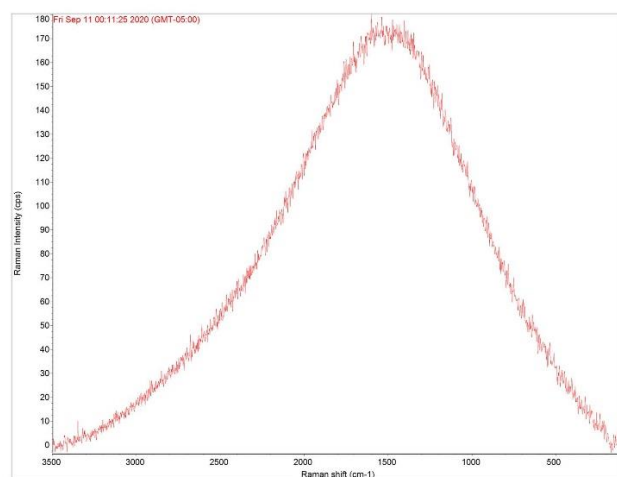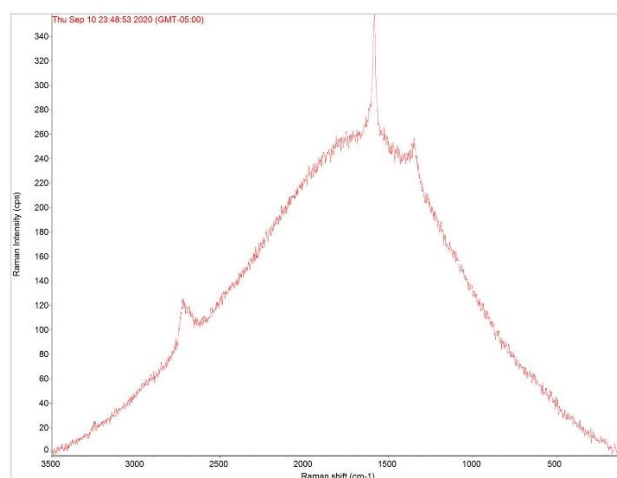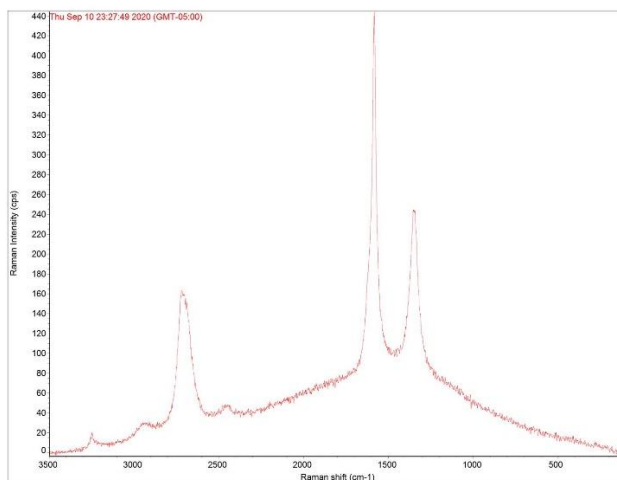
Figure 4.43. Raman spectra of Sample 24 (top), Sample 25 (middle) and Sample 26 (bottom) on Cu areas.

Figure 4.43 above shows the results of the Raman spectra taken from suspected Cu regions in Samples 23-26. Due to the inherent similarity of all the spectra taken in this region, only these spectra are shown.

The top and middle graphs indicate the presence of graphene. The broad peak under indicates the Cu substrate. The other peaks indicate the presence of graphene. The I_{2D}/I_G ratio of the top spectra is 0.36, indicting multilayer graphene. The I_D/I_G ratio of the top spectra is 0.54, indicating a certain degree of disorder in the graphene. The I_{2D}/I_G ratio of the middle spectra is 0.33, indicating multilayer graphene. The I_D/I_G ratio of the middle spectra is 0.68, indicating a certain degree of disorder in the graphene. The lack of peaks at the 2D, G, and D bands for carbon suggest the lack of graphene in the Cu areas of Sample 26.
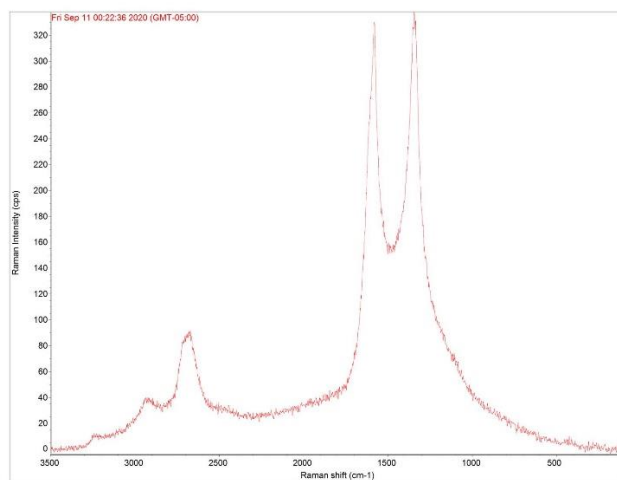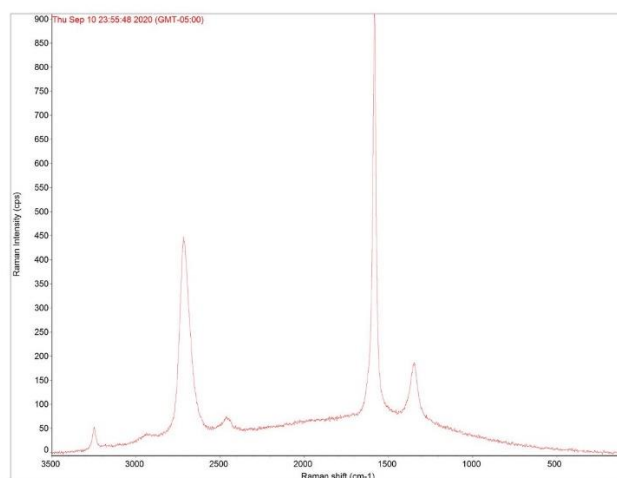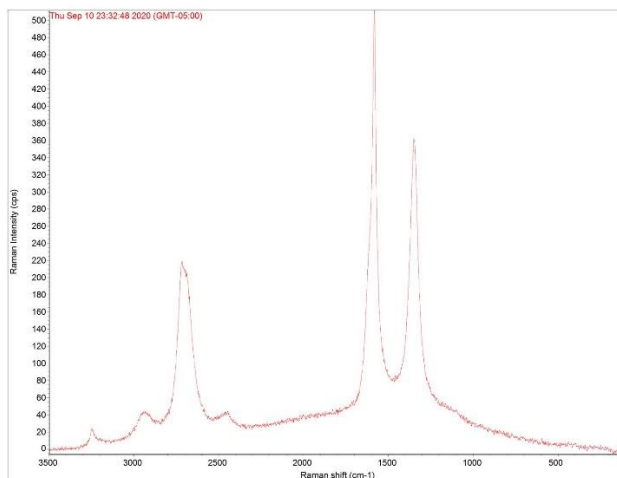
Figure 4.44. Raman spectra of Sample 24 (top), Sample 25 (middle) and Sample 26 (bottom) on graphene areas.

Figure 4.44 above shows the results of the Raman spectra taken from suspected graphene regions in Samples 23-26. Due to the inherent similarity of all the spectra taken in this region, only these spectra are shown.

All spectra indicate the presence of graphene. The broad peak under indicates the Cu substrate. The other peaks indicate the presence of graphene. The I_{2D}/I_G ratio of the top spectra is 0.43, indicating multilayer graphene. The I_D/I_G ratio of the top spectra is 0.71, indicating a certain degree of disorder in the graphene. The I_{2D}/I_G ratio of the middle spectra is 0.49, indicating multilayer graphene. The I_D/I_G ratio of the middle spectra is 0.19, indicating a certain degree of disorder in the graphene. The I_{2D}/I_G ratio of the bottom spectra is 0.26, indicating multilayer graphene. The I_D/I_G ratio of the bottom spectra is 1.03, indicating a certain degree of disorder in the graphene.
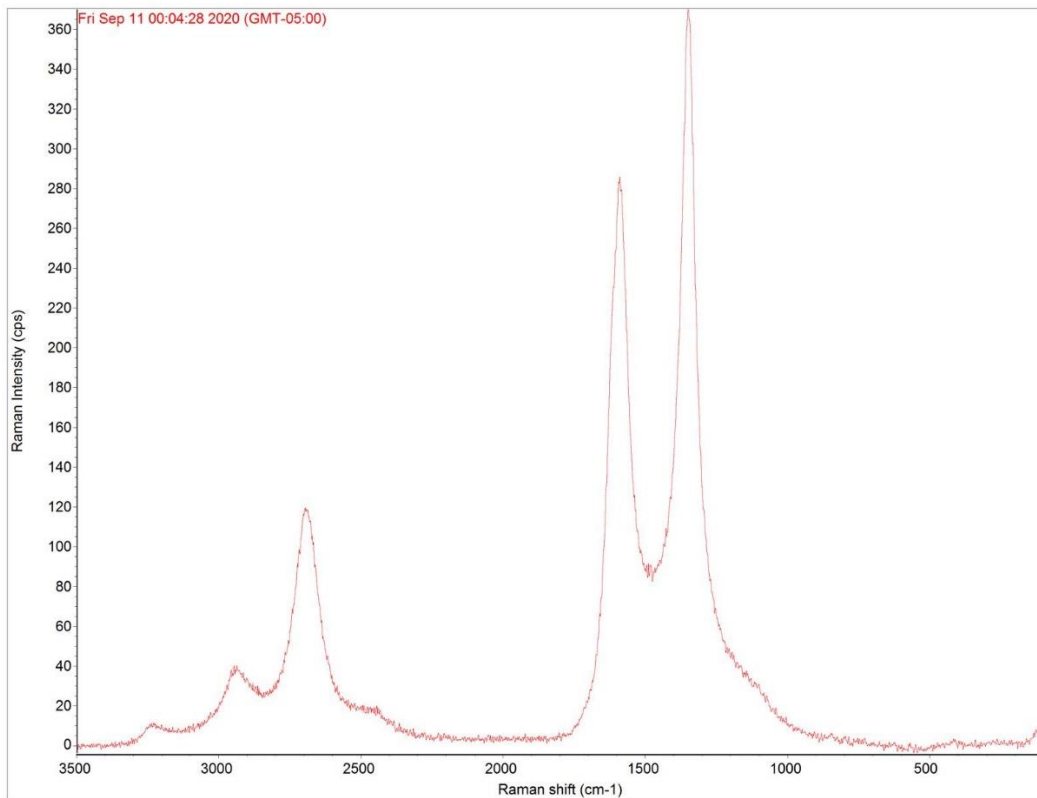
Figure 4.45. Raman spectra of Sample 25 on amorphous carbon areas.

Figure 4.45 above shows the results of the Raman spectra taken from suspected amorphous carbon regions in Sample 25. Due to the inherent similarity of all the spectra taken in this region, only these spectra are shown.

Unlike the previous regions, the broad Cu curve is not noticeable in these amorphous carbon regions. The presence of the G, 2D, and D peaks indicate the presence of graphene. The I_{2D}/I_G ratio of the top spectra is 0.42, indicating multilayer graphene. The I_D/I_G ratio of the top spectra is 1.30, indicating a certain degree of disorder in the graphene.

4.2.10.1 Conclusion

Compared to Samples 21-23, the use of the carbon cover seemed to have a negative effect on the uniformity of the graphene while the amount of amorphous carbon seemed to be unaffected. In terms of quality, Samples 21-23 was better in quality and uniformity.

4.2.11 Raman Spectroscopy – Overview of Samples 19-26

As mentioned previously, Samples 19-26 were developed to examine the quality and uniformity of three different sample types, Cu/Ni, pure Cu, and pure Cu with the carbon cover. After the trials were completed, all samples were examined with Raman spectroscopy, a highly valuable tool in determining elemental composition as well as the quality of graphene produced. Extensive studies have been conducted which make Raman spectroscopy a valuable tool in determining the number of layers present, which is one of the main points of this work.
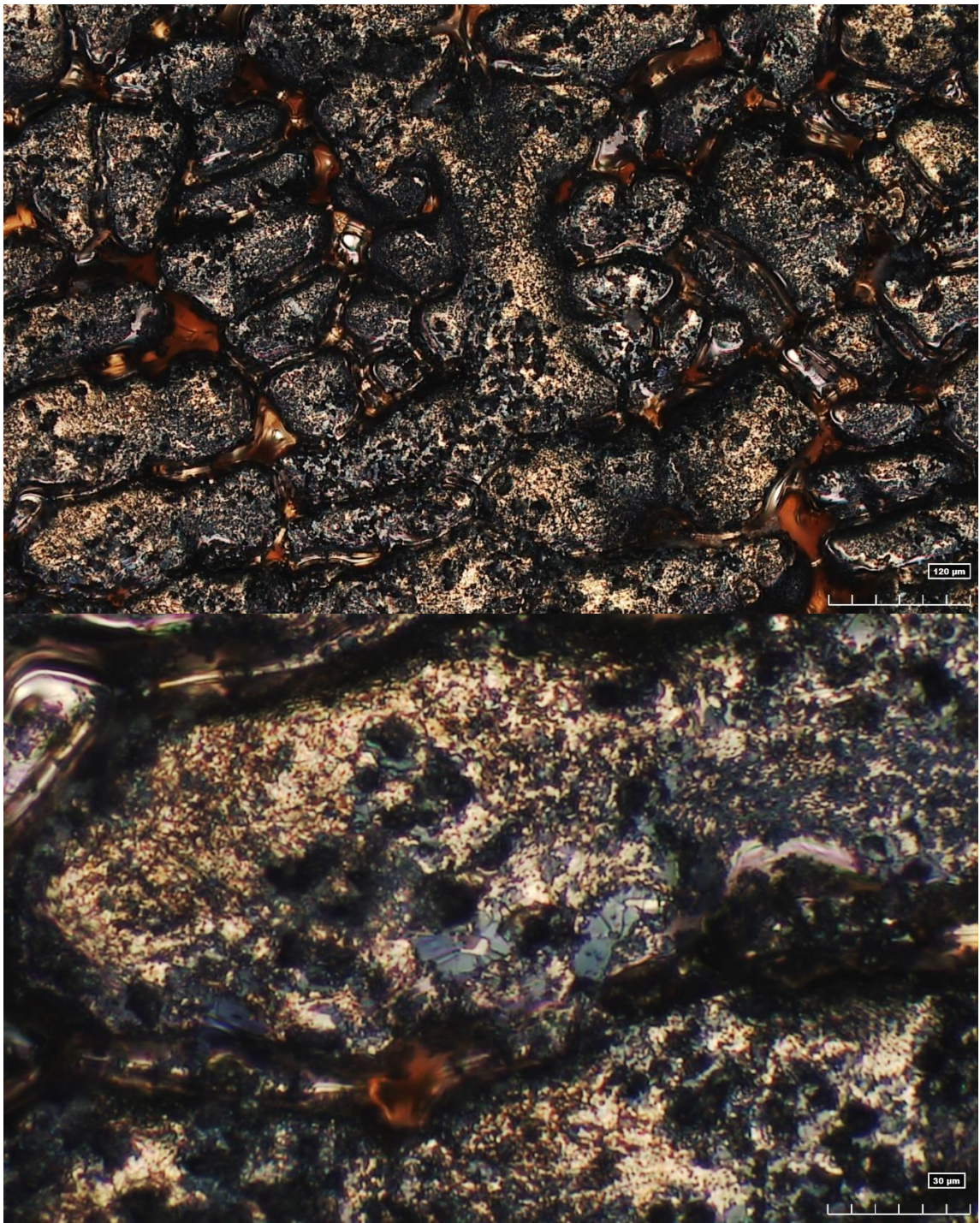
Figure 4.46. Optical images of Sample 19.
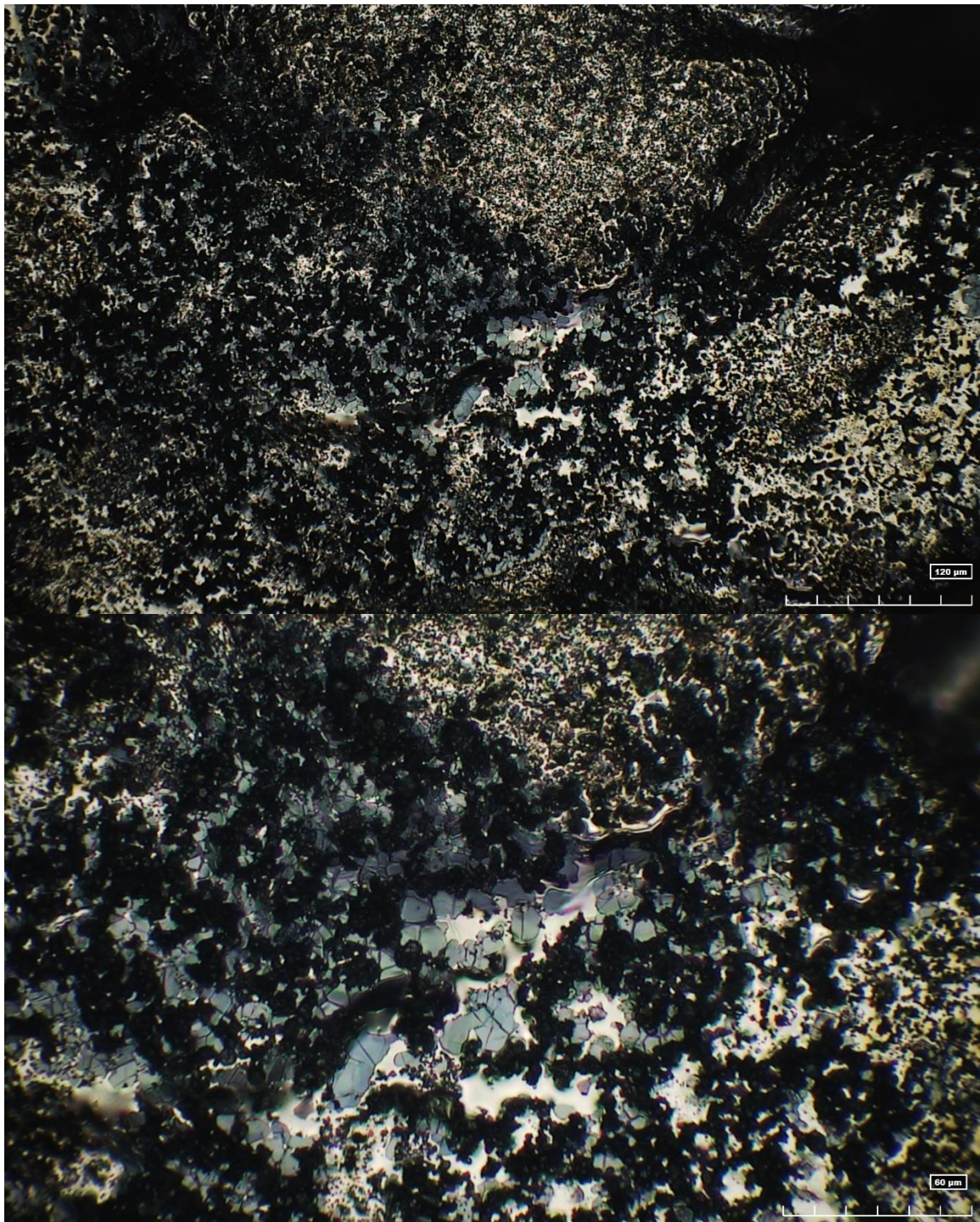
Figure 4.47. Optical Images of Sample 20.

Overall, based on the Raman analysis, Samples 19 and 20 showed the best results

in terms of uniformity. As compared to previous samples, Samples 19 and 20 had the

greatest area of graphene and amorphous carbon, which also contained multilayer

graphene. Unlike the pure Cu samples and carbon cover samples, there was little area of visible Cu/Ni. However, out of all the samples, Samples 19 and 20 had the largest amount of amorphous carbon, likely due to the higher carbon saturation limit of Ni.

Figure 4.48. Optical Images of Sample 21.
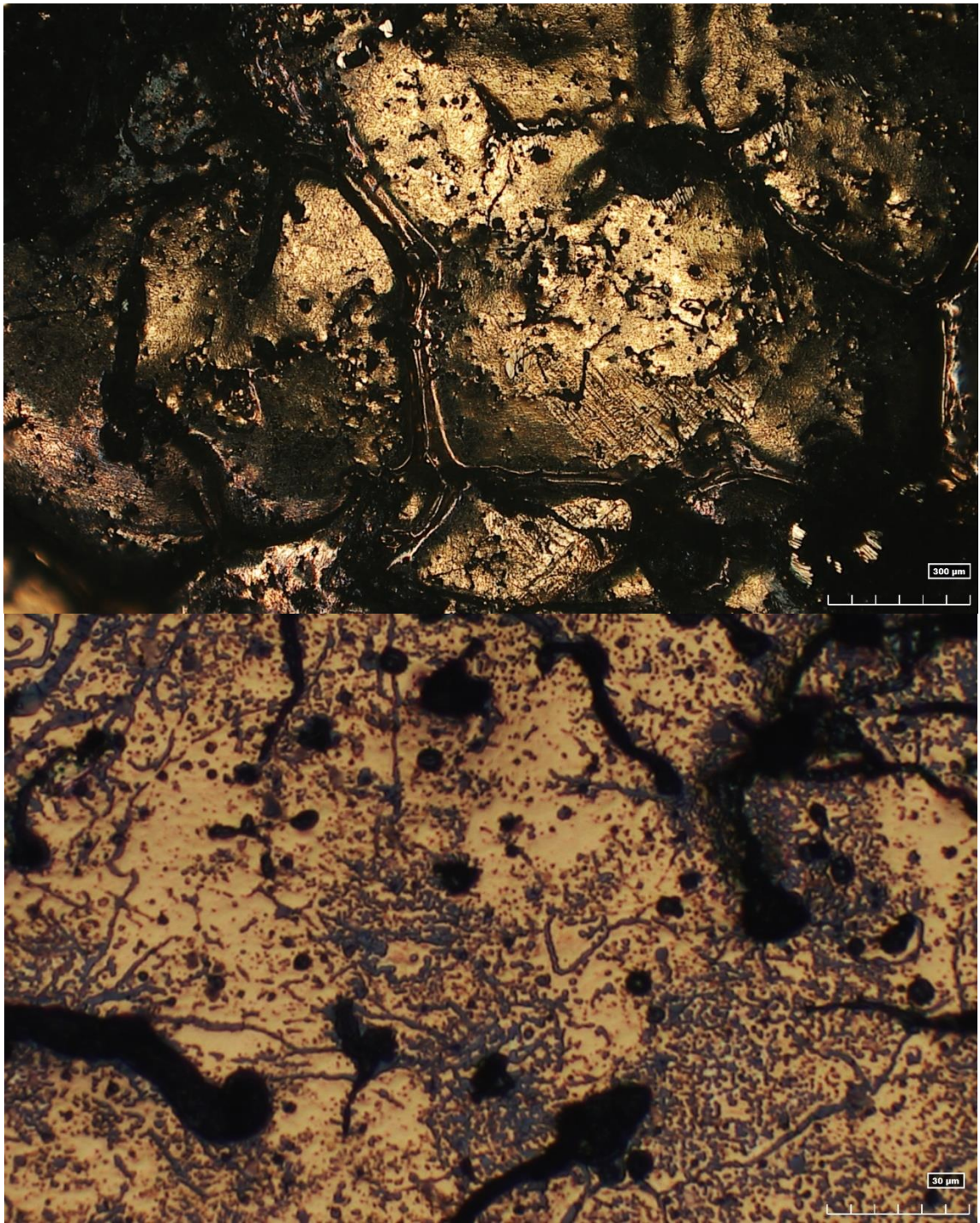
Figure 4.49. Optical Images of Sample 22.
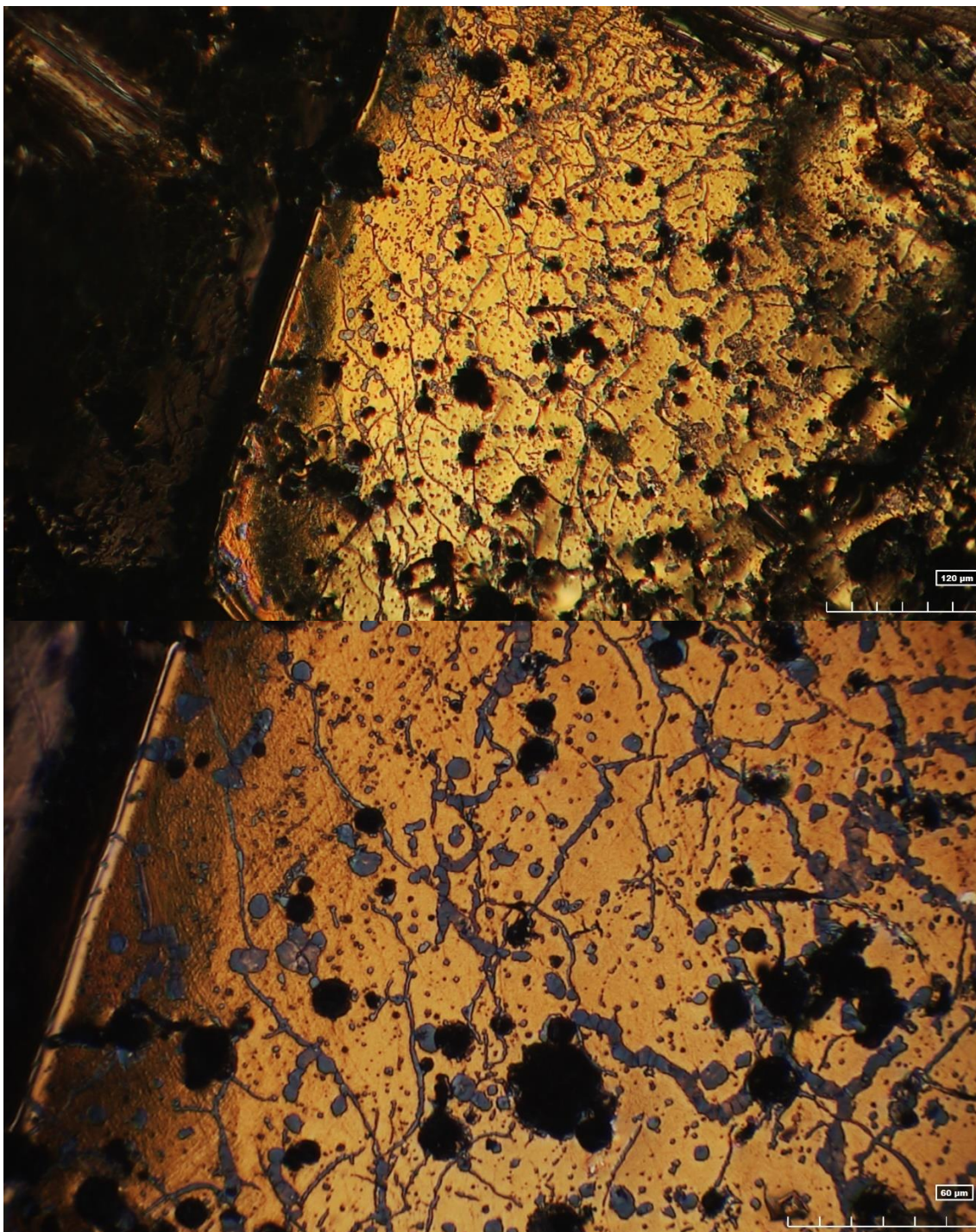
Figure 4.50. Optical Images of Sample 23.

Next, Samples 21, 22, and 23 were produced to compare with the Cu/Ni samples and the carbon cover samples as a control group. The spectra taken from these samples showed that multilayer graphene was present in all areas measured, including the

apparent Cu areas. However, the uniformity of the graphene was low as compared to Samples 19 and 20. These samples also show to have less amorphous carbon than the Cu/Ni samples.
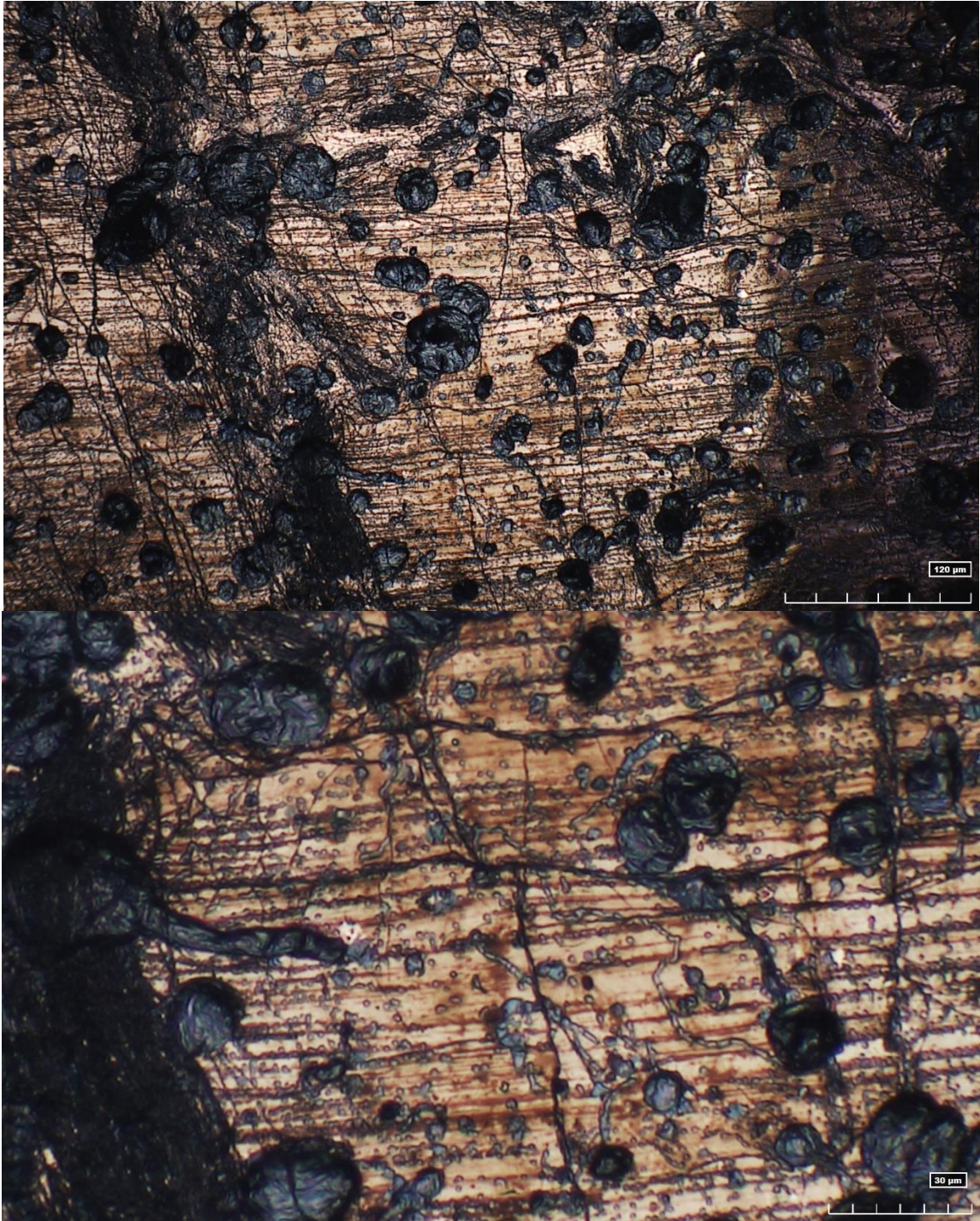
Figure 4.51. Optical Images of Sample 24.
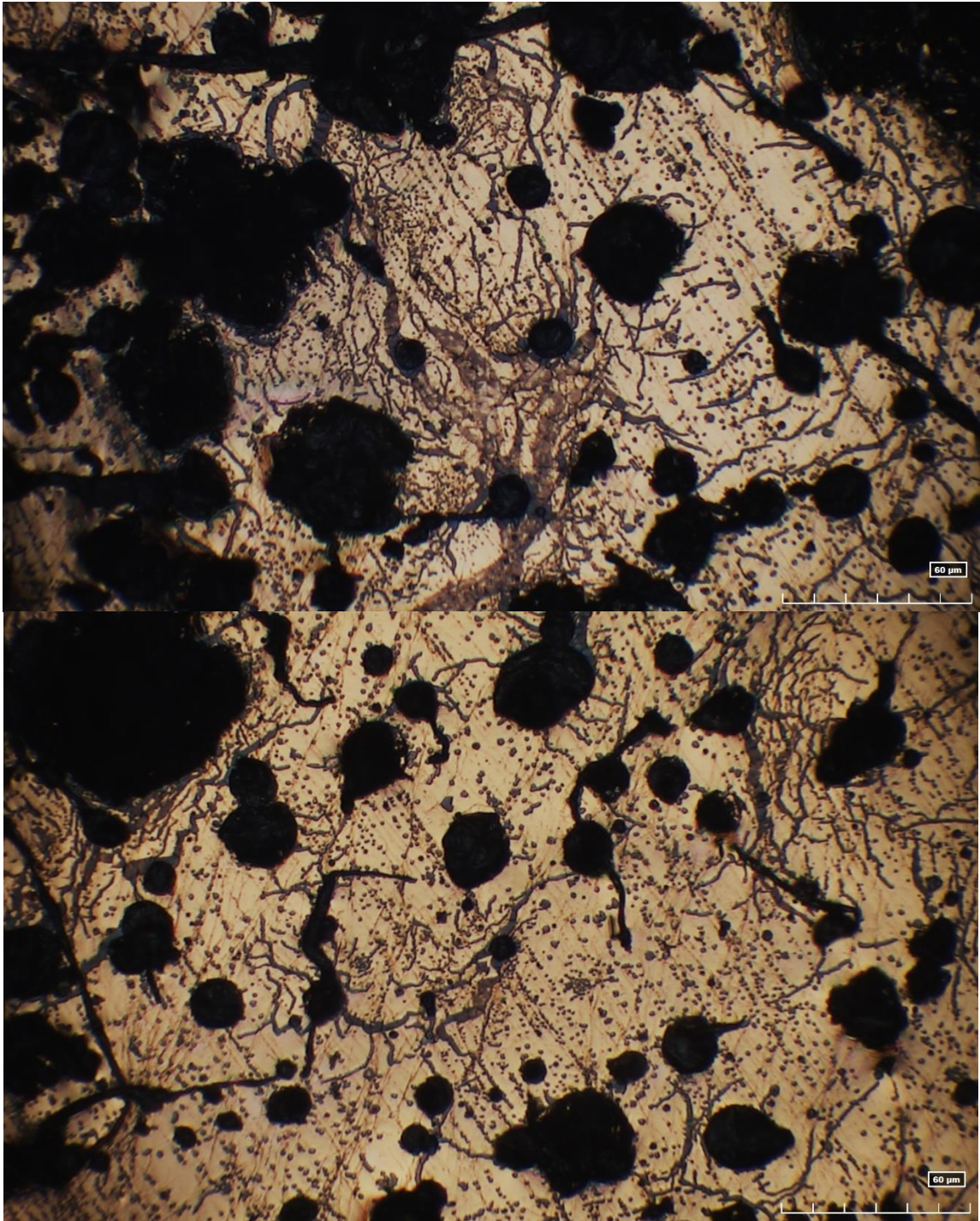
Figure 4.52. Optical Images of Sample 25.
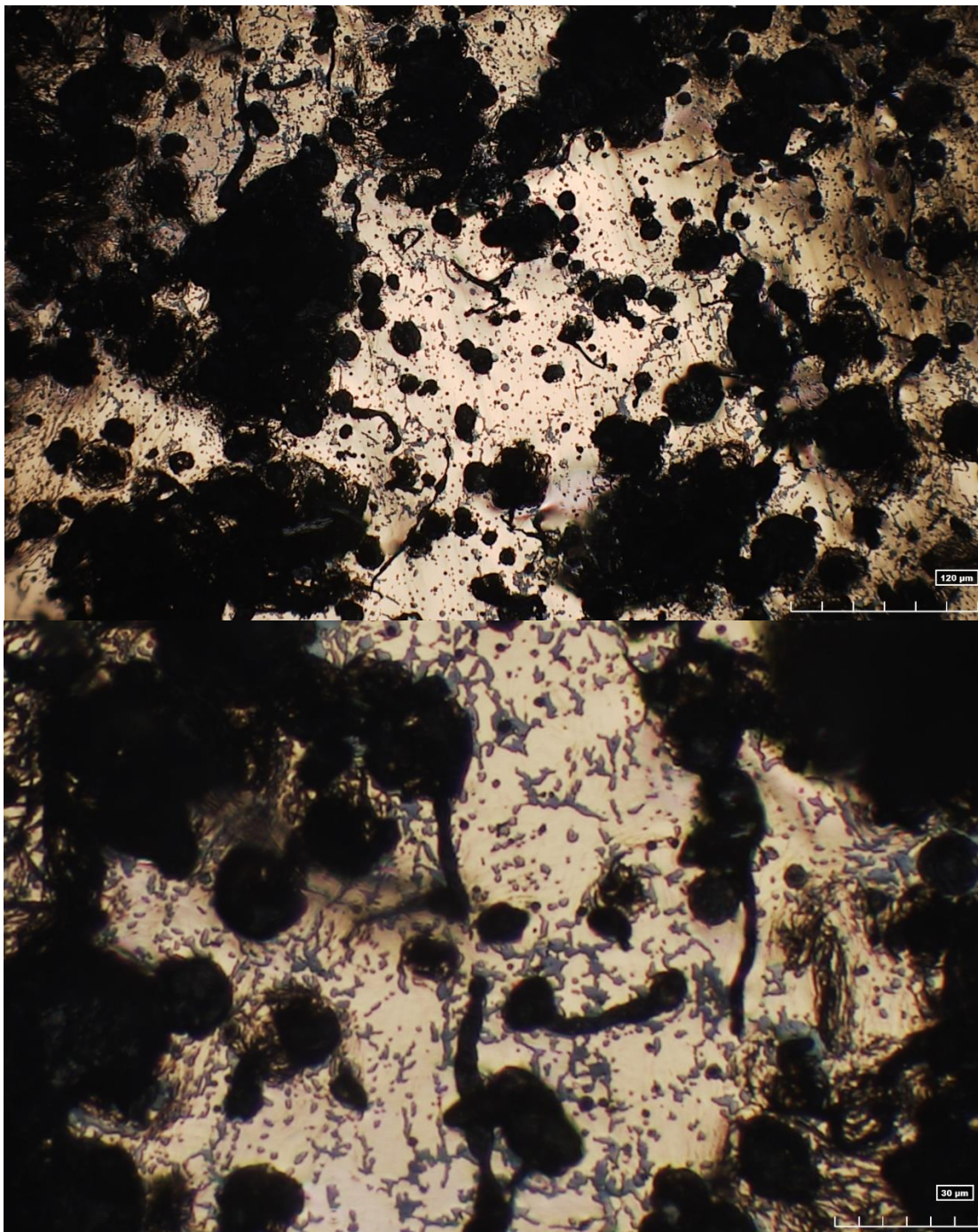
Figure 4.53. Optical Images of Sample 26.

Finally, Samples 24, 25, and 26 were produced and examined to investigate the

effect that the carbon cover had on the quality and uniformity of the graphene.

Unfortunately, the results of this experiment showed very low uniformity and a high

amount of amorphous carbon.

4.3 XPS Analysis

XPS is a crucial technique which can provide surface characterization for a number of different types of materials. In particular, carbon materials tend to be especially sensitive to XPS by providing information of elemental and chemical information. The following section will cover the XPS data received from Samples 19-26.

To characterize the samples, the C 1s, Cu 3s, and O 1s peaks will be analyzed. The C 1s peak can be used to evaluate the quality of the graphene produced by determining the quantity of oxygen components to the C sp2 component. The Cu 3s peak is most suitable for peak decomposition to evaluate oxidation due to the low flat background surrounding the peak, and the O 1s peak provides information for the state of the oxygen in the sample.

This information can provide a better understanding of the quality of the graphene produced. This section will also compare the quality of the graphene produced in each sample to determine the effects that the Cu/Ni, pure copper, and carbon cover samples had on the quality of the graphene.
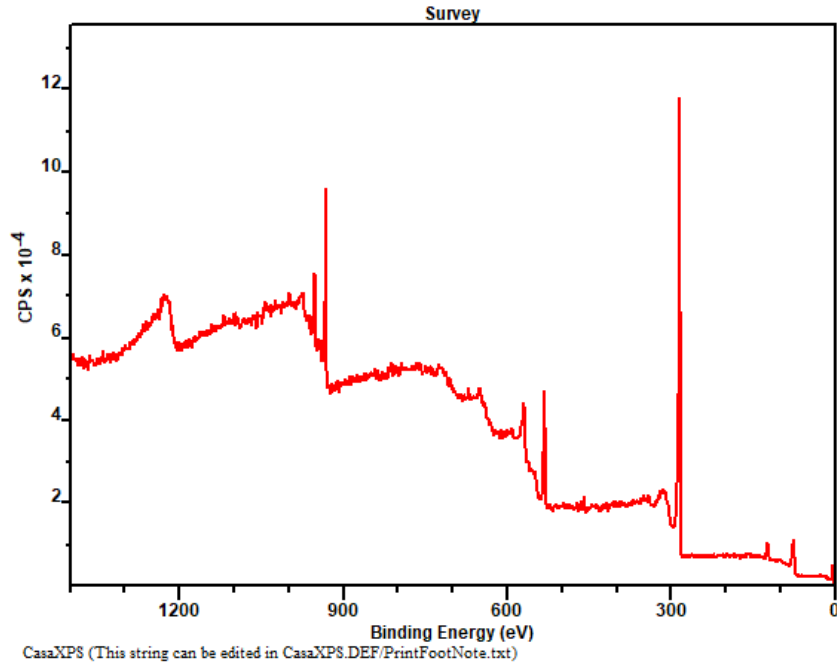
Figure 4.54. General scan for the graphene grown on the self-made Cu/Ni substrate for Sample 19.
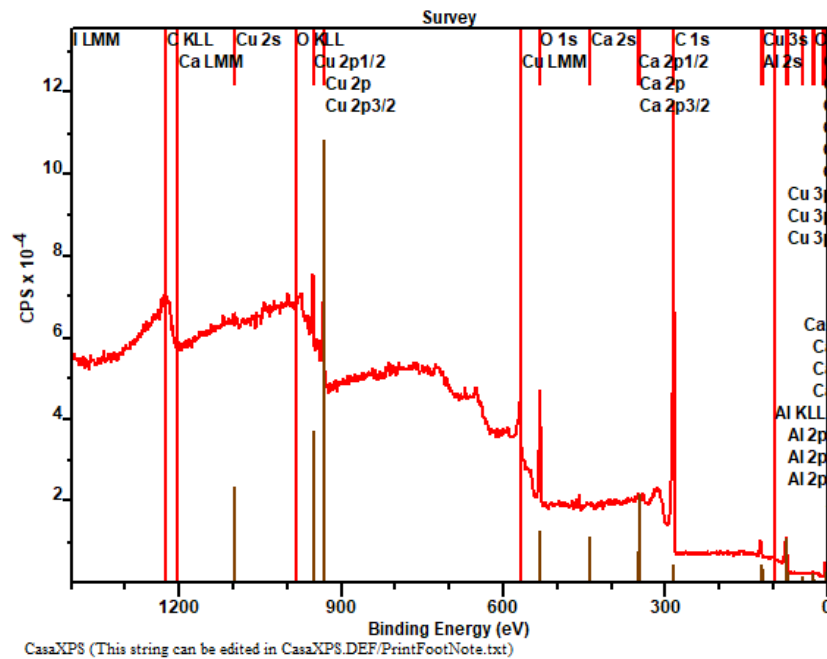
Figure 4.55. General scan for the graphene grown on the self-made Cu/Ni substrate for Sample 19 with labeled peak locations.

Figure 4.54 shows the general scan for the graphene grown on the self-made

Cu/Ni substrate for Sample 19. Figure 4.55 includes peak labels for the general scan. The identifiable peaks include C KLL, O KLL, Cu 2p ½, Cu 2p, Cu 2p 3/2, Cu LMM, O 1s, Ca 2p ½, Ca 2p, Ca 2p 3/2, C 1s, Cu 3s, and Cu 3p. For the purposes of this experiment, the peaks of interest are the C 1s, Cu 3s, and O 1s core level peaks.

The general scan of Sample 19 does not show any real indication of impurities present.
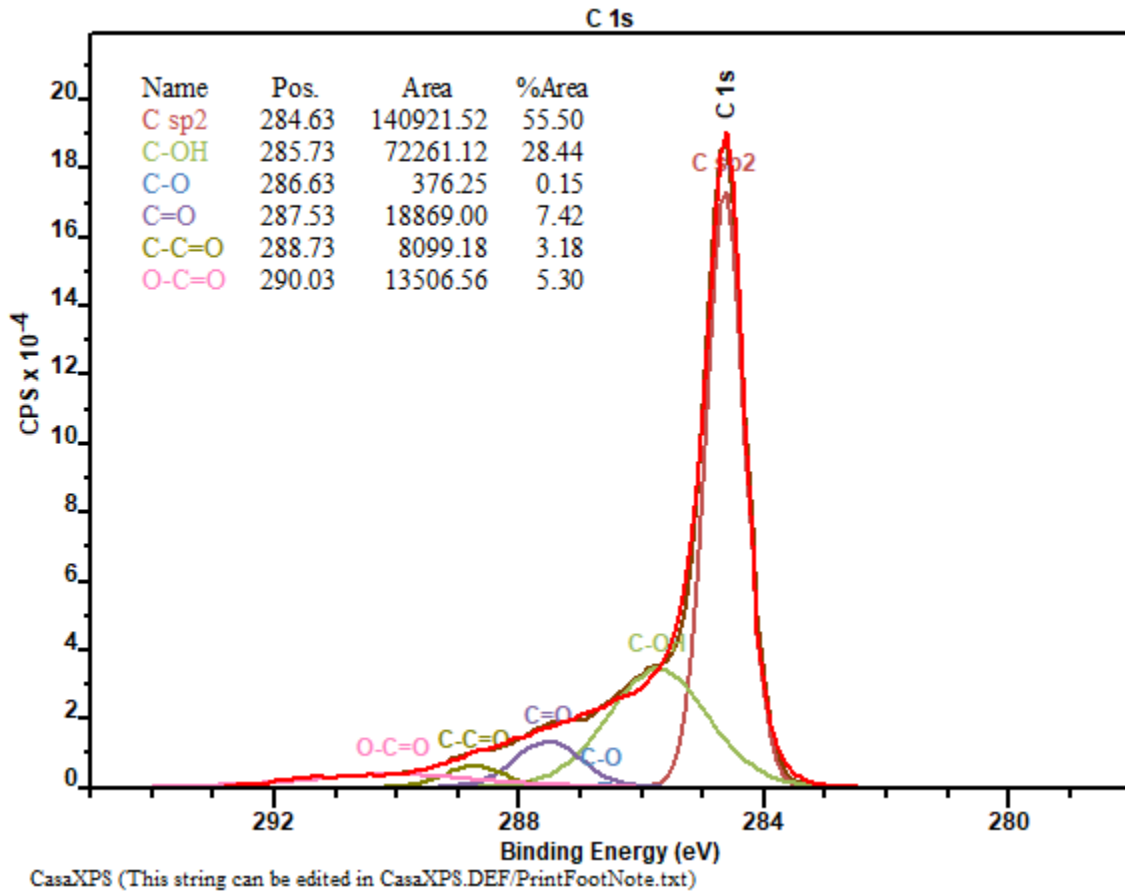
Figure 4.56. High-resolution scan for the C 1s core level peak of graphene on the self-made Cu/Ni substrate of Sample 19.

The oxygen-related components of the decomposed peak correspond to 44.50% of the total area of the C 1s peak, indicating a relatively high degree of oxidation, likely due to the persistent oxygen leaks during the research process. Of all samples tested using

XPS, Sample 19 showed to have the highest oxygen content in the C 1s peak.

Name	Pos.	Area	%Area
Cu=C	119.66	576.41	4.35
Cu-C	121.16	3219.96	24.26
Cu-Cu	122.56	6936.15	52.21
Cu-O	123.76	472.63	3.56
Cu-OH	124.86	2079.40	15.63

CasaXPS (This string can be edited in CasaXPS.DEF/PrintFootNote.txt)
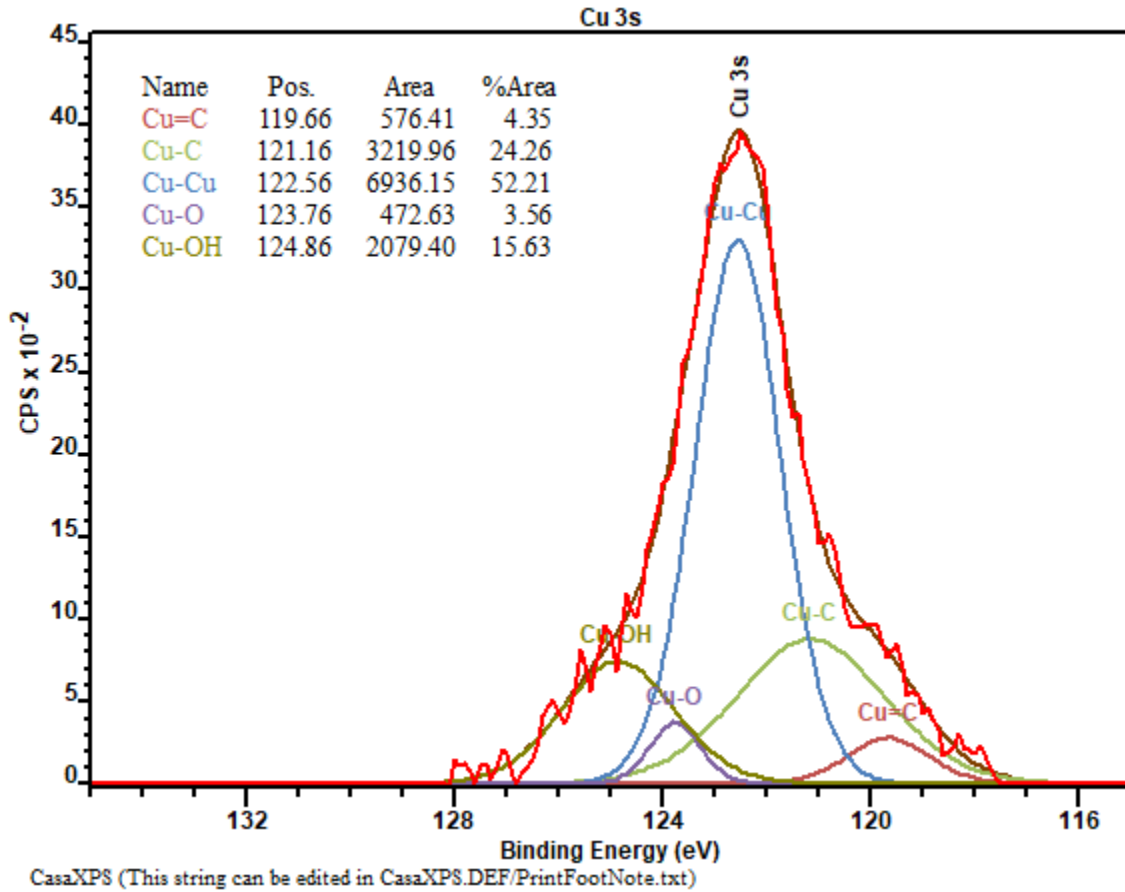
Figure 4.57. High-resolution scan for the Cu 3s core level peak of graphene on the self-made Cu/Ni substrate of Sample 19.

The oxygen-related components of the decomposed peak correspond to 19.19% of the total area of the Cu 3s peak, indicating a certain degree of oxidation.
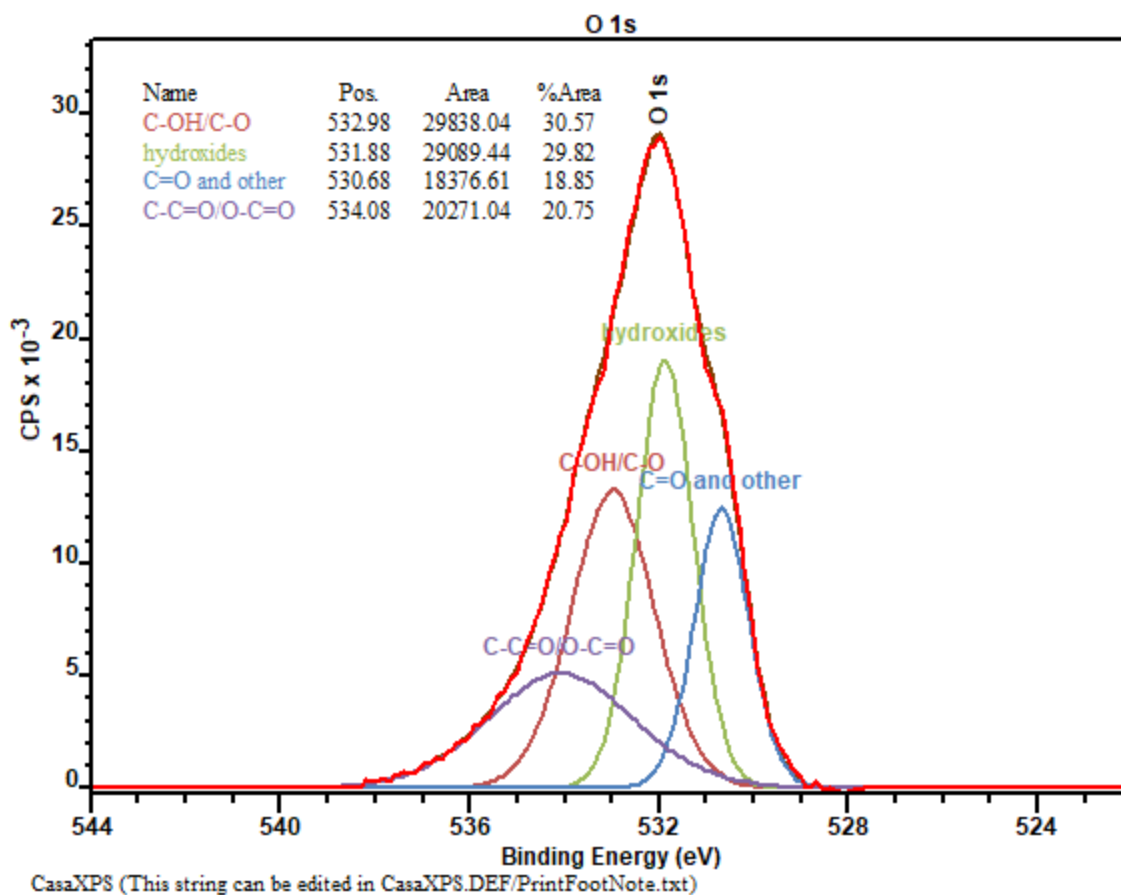
Figure 4.58. High-resolution scan for the O 1s core level peak of graphene on the self-made Cu/Ni substrate of Sample 19.

The decomposed peak components indicate that most of the oxygen present is in the form of C-OH/C-O.

4.3.2 Sample 20
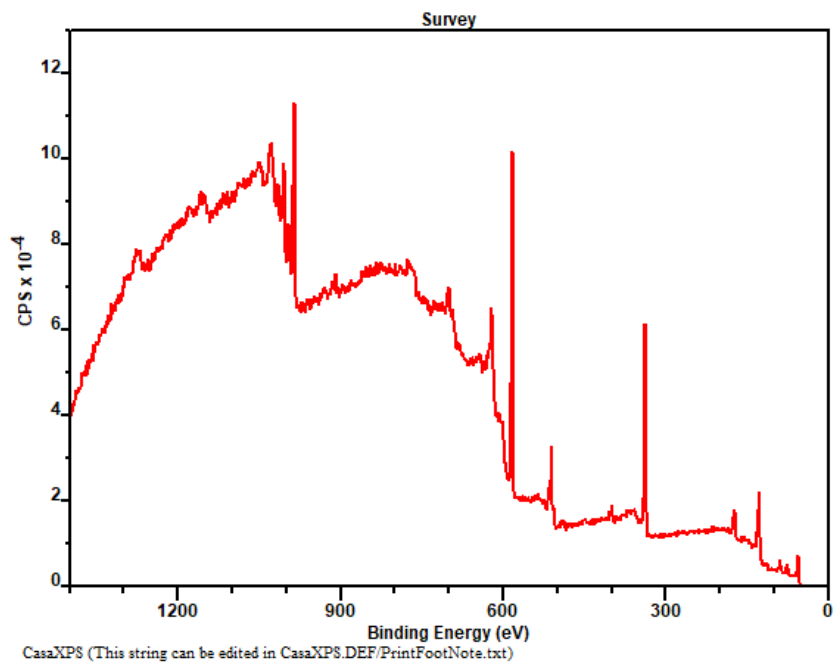
Figure 4.59. General scan for the graphene grown on the self-made Cu/Ni substrate for Sample 20.
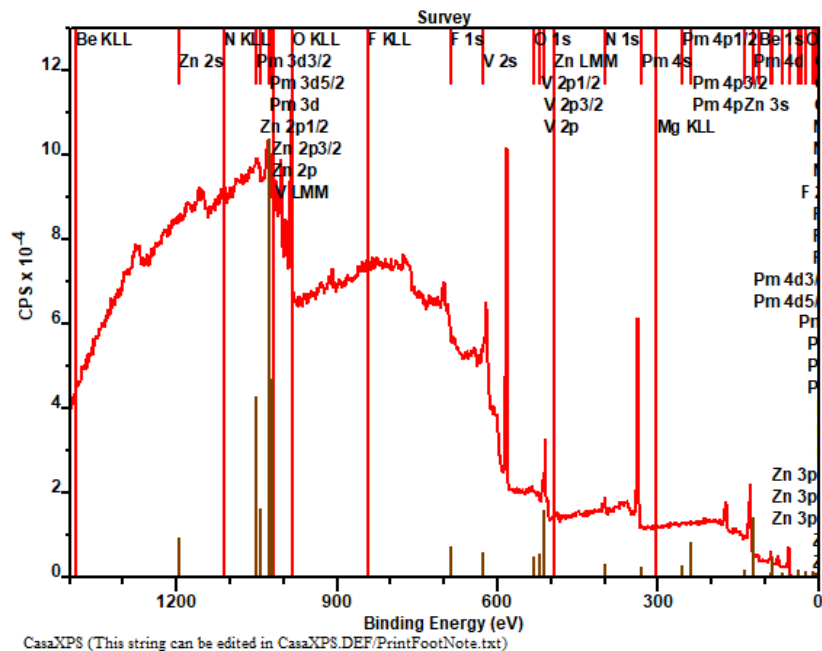
Figure 4.60. General scan for the graphene grown on the self-made Cu/Ni substrate for Sample 20 with labeled peak locations.

Figure 4.59 shows the general scan for the graphene grown on the self-made

Cu/Ni substrate for Sample 20. Figure 4.60 includes peak labels for the general scan. The identifiable peaks include O KLL, F 1s, O 1s, N 1s, C 1s, Cu 3s. For the purposes of this experiment, the peaks of interest are the C 1s, Cu 3s, and O 1s core level peaks.
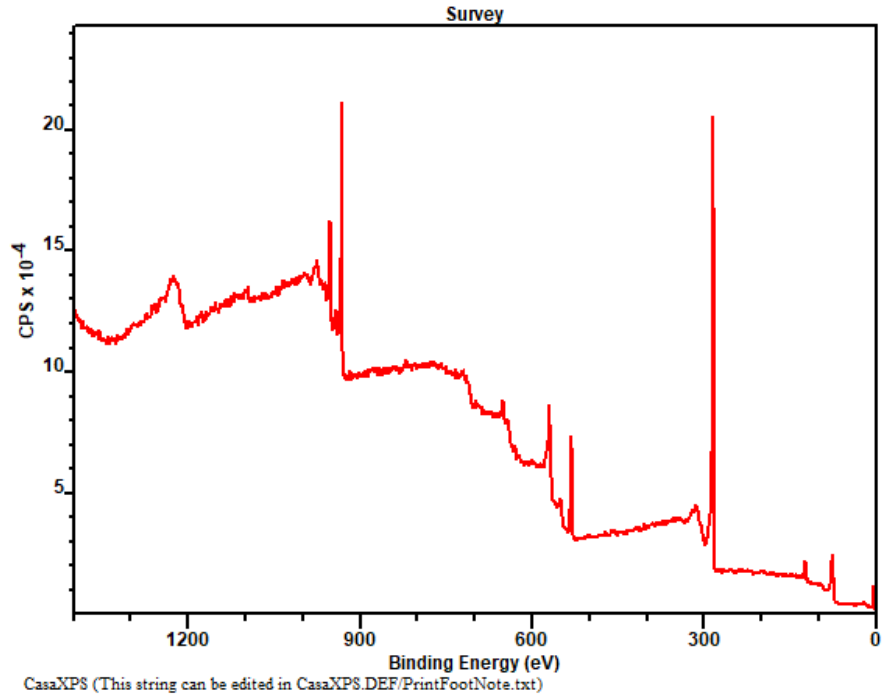
Figure 4.61. General scan for the graphene grown on the Cu substrate for Sample 21.
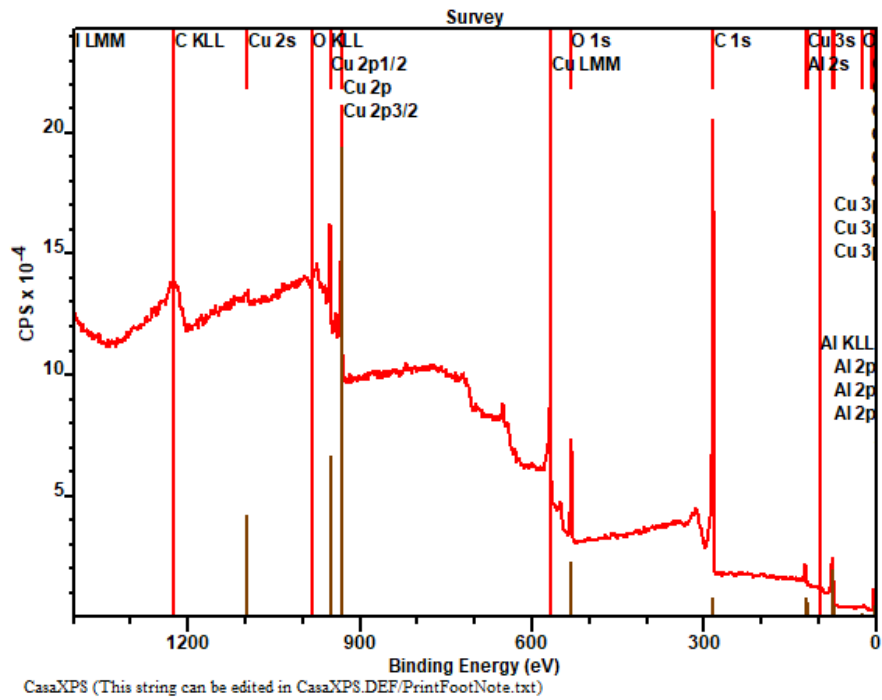
Figure 4.62. General scan for the graphene grown on the self-made Cu substrate for Sample 21 with labeled peak locations.

Figure 4.61 shows the general scan for the graphene grown on the Cu substrate for Sample 21. Figure 4.62 includes peak labels for the general scan. The identifiable peaks include C KLL, O KLL, Cu 2p ½, Cu 2p, Cu 2p 3/2, Cu LMM, O 1s, C 1s, and Cu 3s. For the purposes of this experiment, the peaks of interest are the C 1s, Cu 3s, and O 1s core level peaks.

C 1s

Name	Pos.	Area	%Area
C sp2	284.56	307672.03	78.79
C-OH	285.66	41172.98	10.54
C-O	286.56	16278.56	4.16
C=O	287.46	9597.73	2.45
C-C=O	288.66	10052.59	2.57
O-C=O	289.96	5802.37	1.48

CPS x 10^{-4}

Binding Energy (eV)

CasaXPS (This string can be edited in CasaXPS.DEF/PrintFootNote.txt)
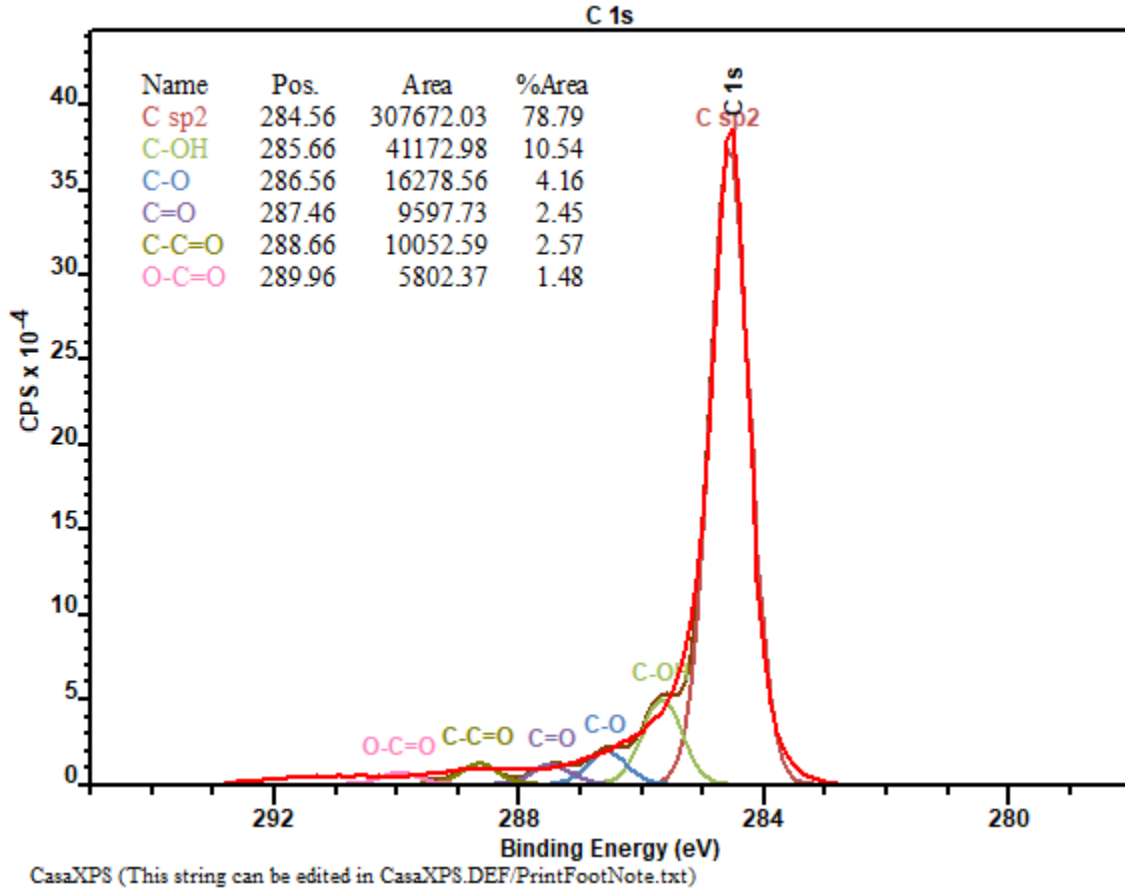
Figure 4.63. High-resolution scan for the C 1s core level peak of graphene on the Cu substrate of Sample 21.

The oxygen-related components of the decomposed peak correspond to 21.21% of the total area of the C 1s peak, indicating a certain degree of oxidation.
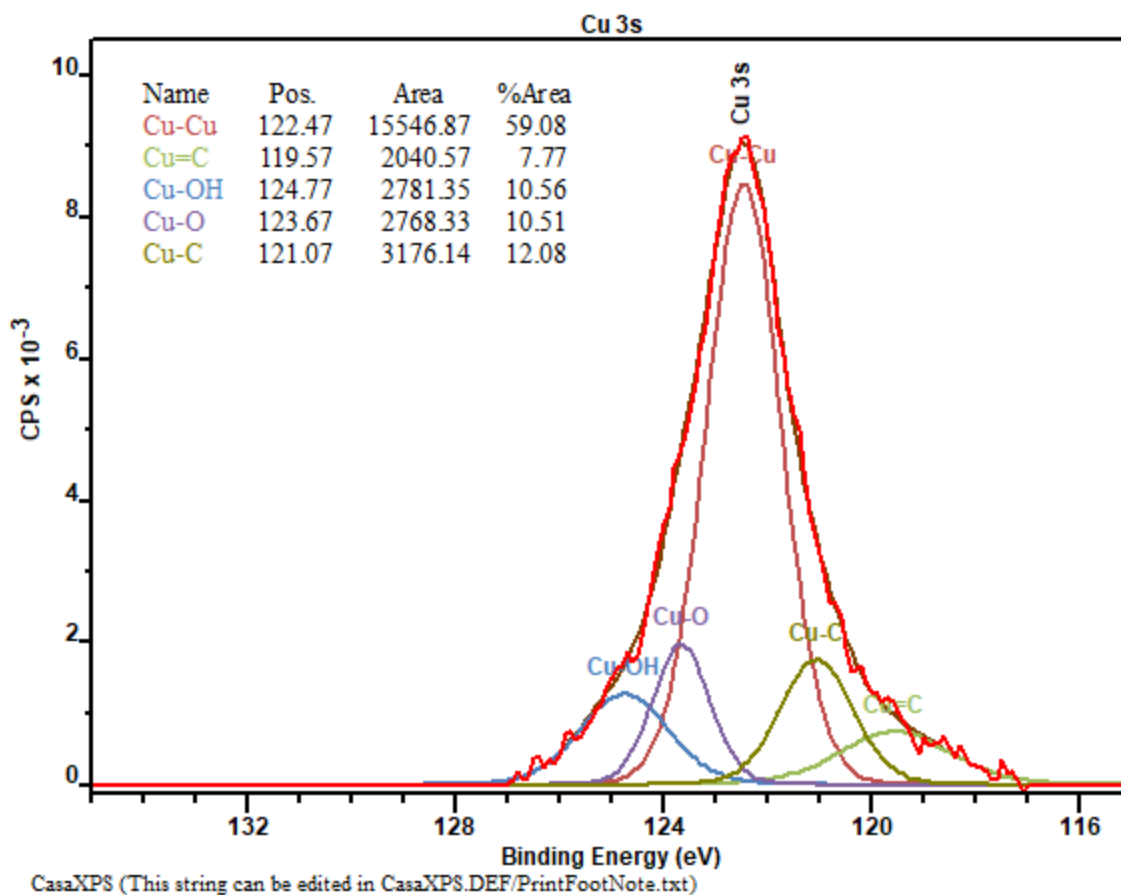
Figure 4.64. High-resolution scan for the Cu 3s core level peak of graphene on the Cu substrate of Sample 21.

The oxygen-related components of the decomposed peak correspond to 21.07% of the total area of the Cu 3s peak, indicating a certain degree of oxidation.
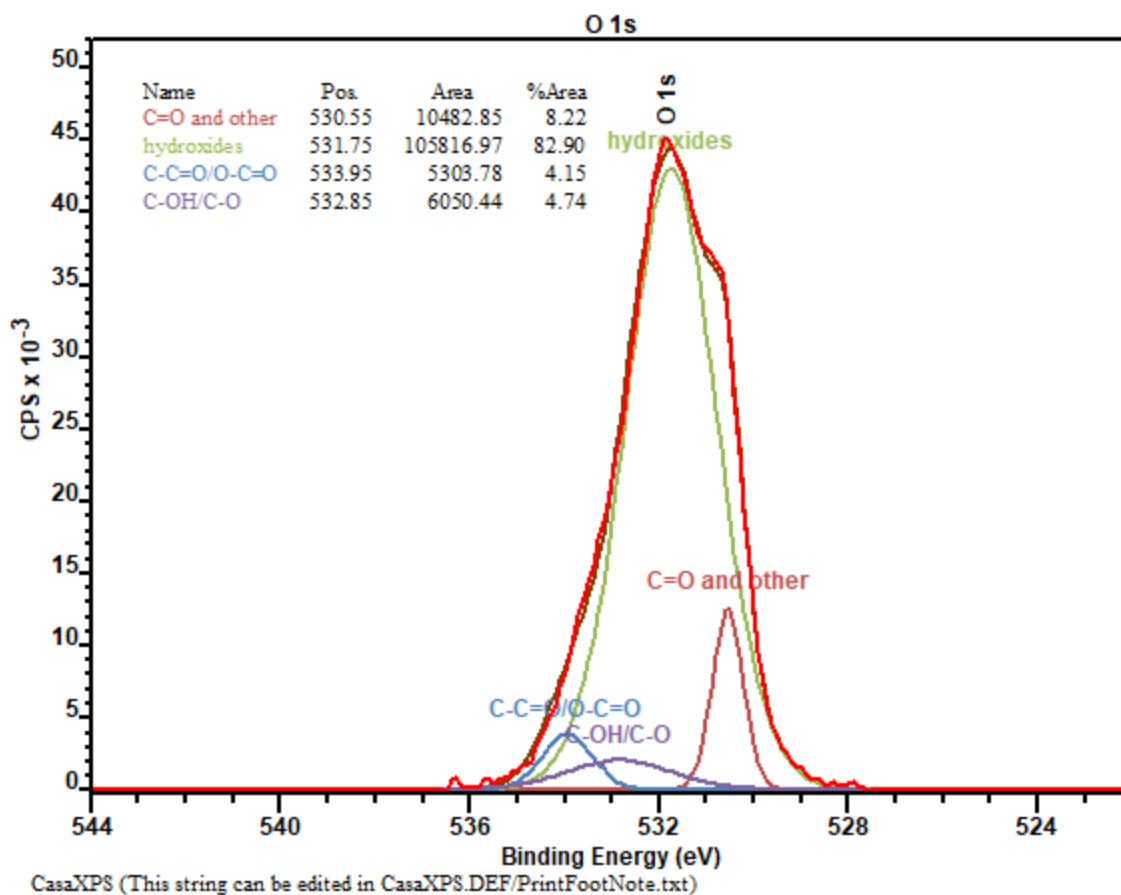
Figure 4.65. High-resolution scan for the O 1s core level peak of graphene on the Cu substrate of Sample 21.

The decomposed peak components indicate that most of the oxygen present is in the form of hydroxides.

4.3.4 Sample 22
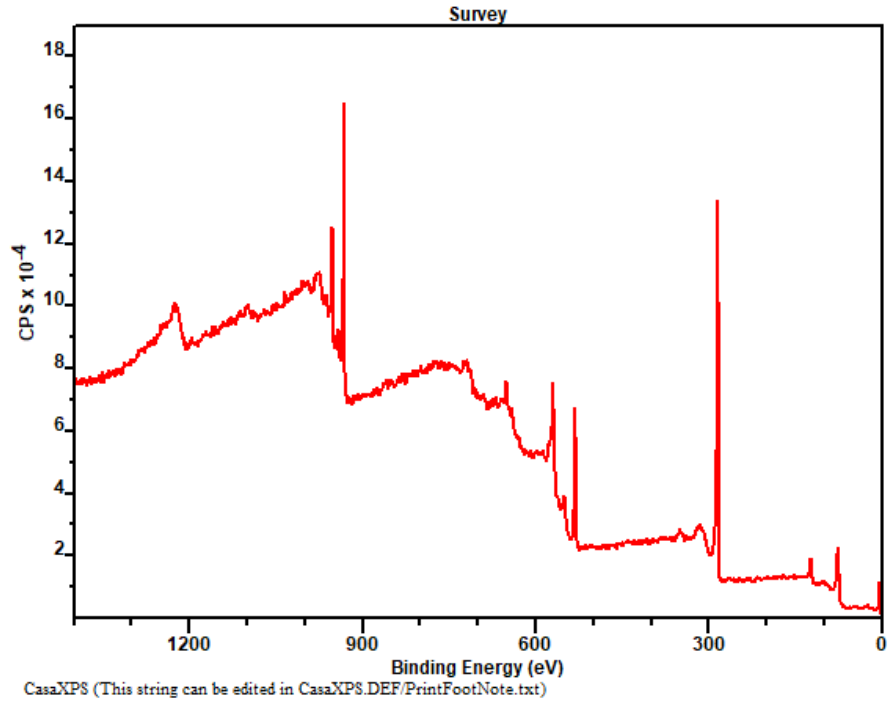
Figure 4.66. General scan for the graphene grown on the Cu substrate for Sample 22.
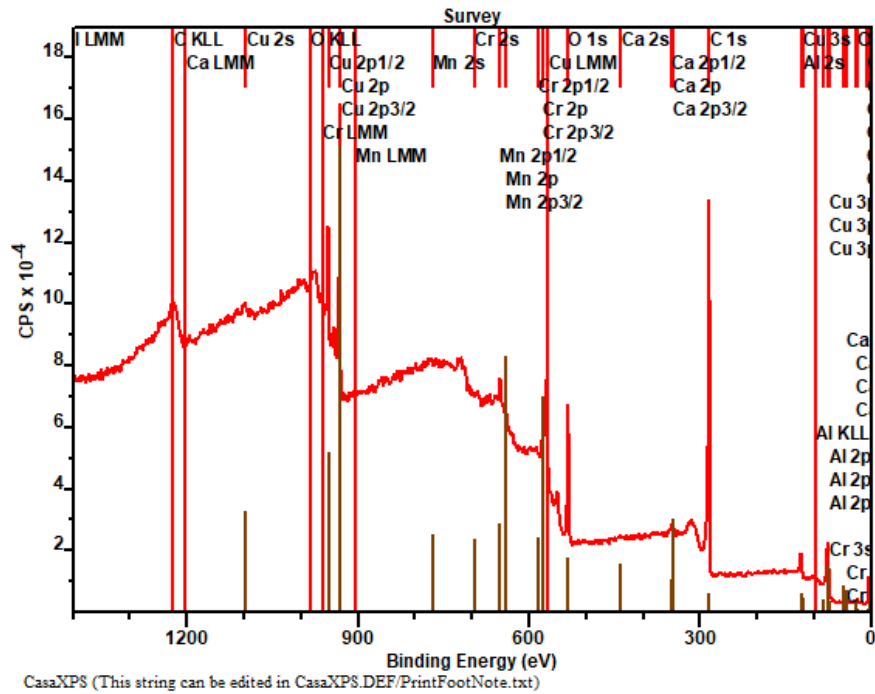
Figure 4.67. General scan for the graphene grown on the self-made Cu substrate for Sample 22 with labeled peak locations.

Figure 4.66 shows the general scan for the graphene grown on the Cu substrate for Sample 22. Figure 4.67 includes peak labels for the general scan. The identifiable peaks include C KLL, O KLL, Cu 2p ½, Cu 2p, Cu 2p 3/2, Cr 2s, Mn 2p ½, Mn 2p, Mn 2p 3/2, Cu LMM, O 1s, C 1s, Cu 3s. For the purposes of this experiment, the peaks of interest are the C 1s, Cu 3s, and O 1s core level peaks.

C 1s

Name	Pos.	Area	%Area
C sp2	284.59	195880.72	70.79
C-OH	285.69	35539.45	12.84
C-O	286.59	19051.03	6.88
C=O	287.49	11229.75	4.05
C-C=O	288.69	9860.43	3.56
O-C=O	289.99	5242.19	1.89

CasaXPS (This string can be edited in CasaXPS.DEF/PrintFootNote.txt)
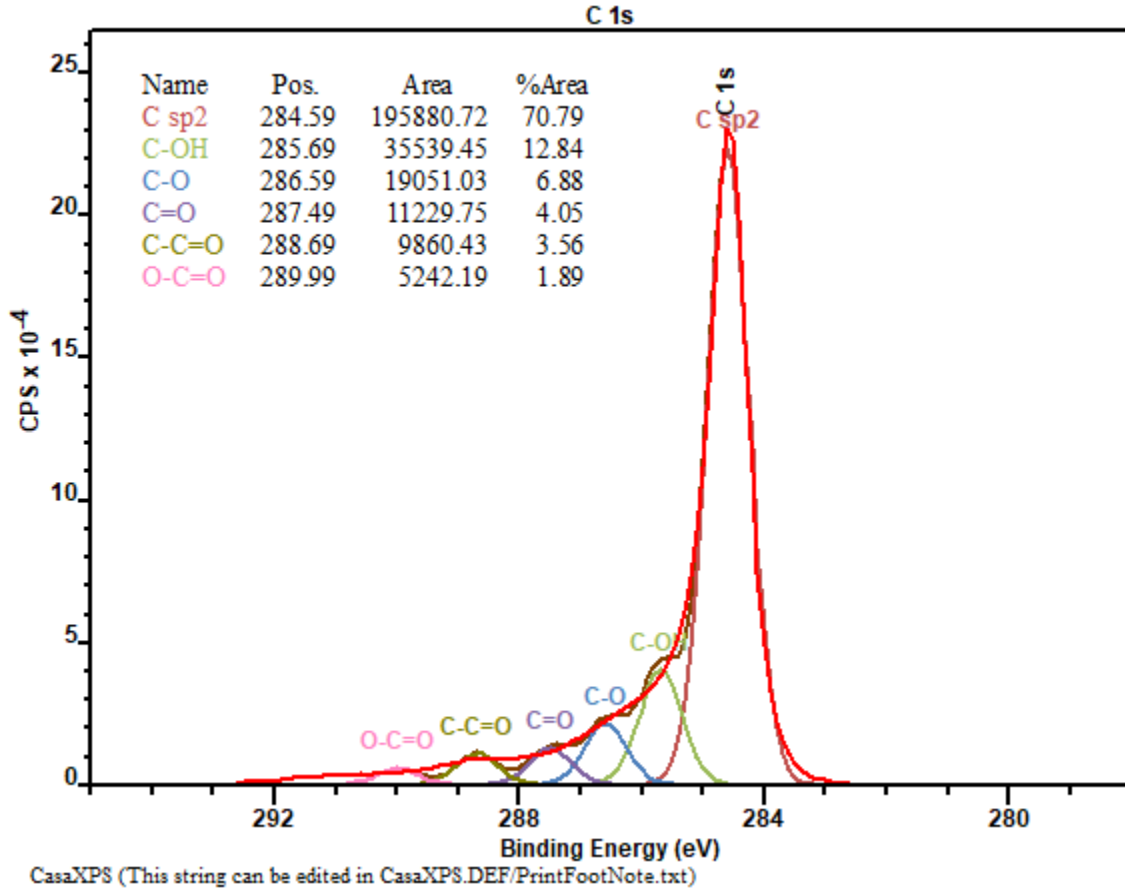
Figure 4.68. High-resolution scan for the C 1s core level peak of graphene on the Cu substrate of Sample 22.

The oxygen-related components of the decomposed peak correspond to 29.21% of the total area of the C 1s peak, indicating a certain degree of oxidation.
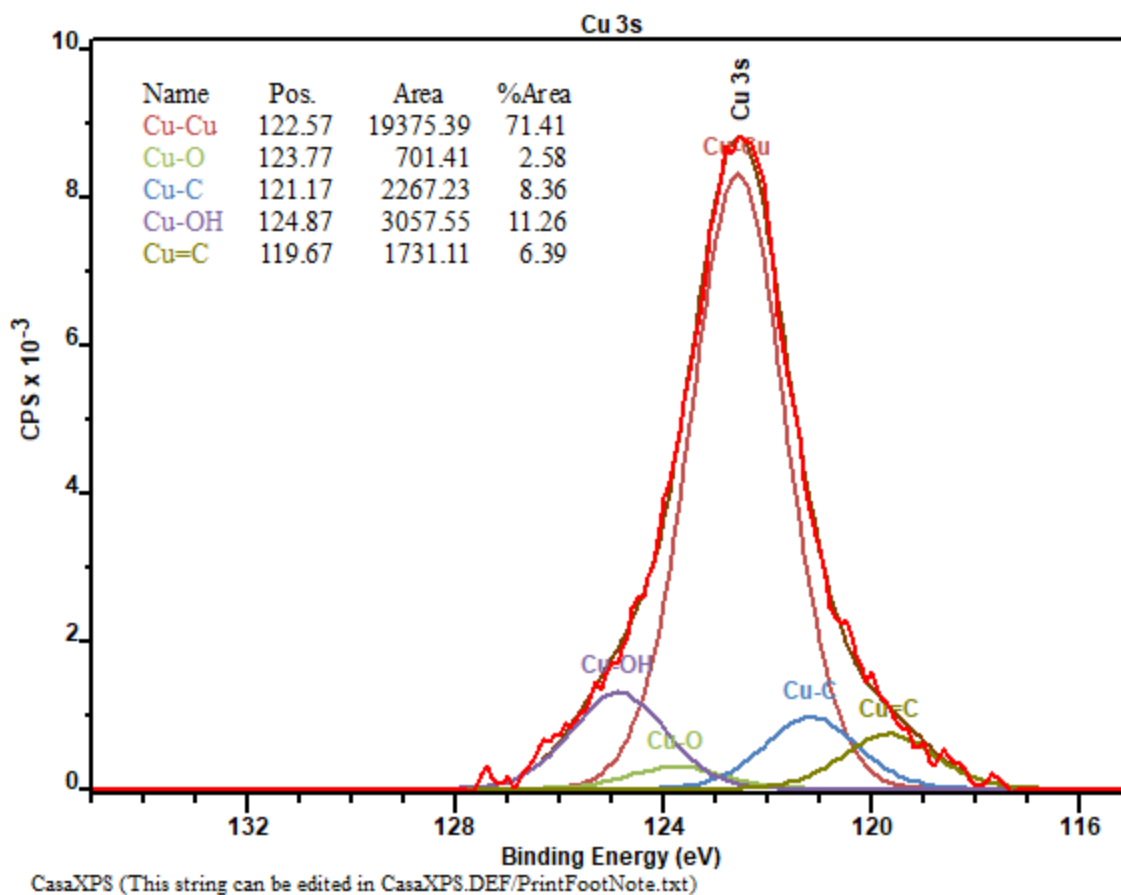
Figure 4.69. High-resolution scan for the Cu 3s core level peak of graphene on the Cu substrate of Sample 22.

The oxygen-related components of the decomposed peak correspond to 13.84% of

the total area of the Cu 3s peak, indicating a certain degree of oxidation.
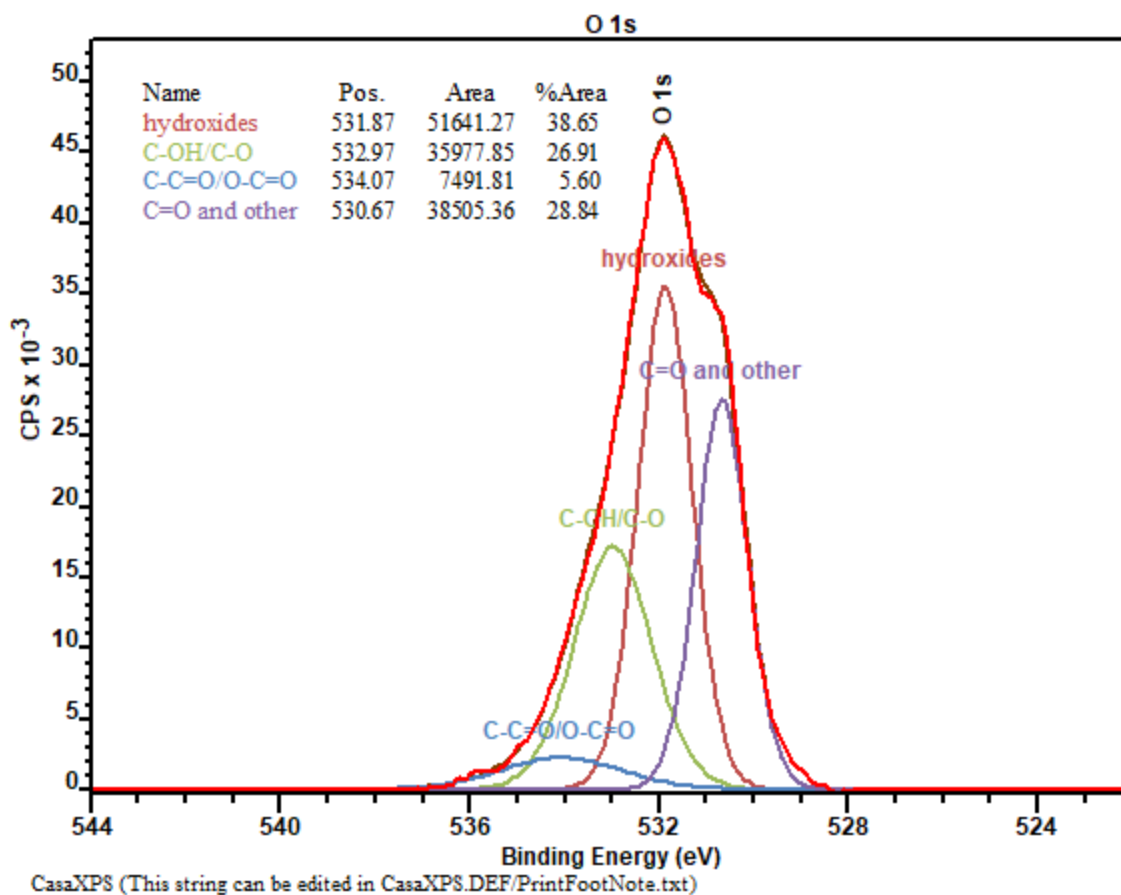
Figure 4.70. High-resolution scan for the O 1s core level peak of graphene on the Cu substrate of Sample 22.

The decomposed peak components indicate that most of the oxygen present is in the form of hydroxides.
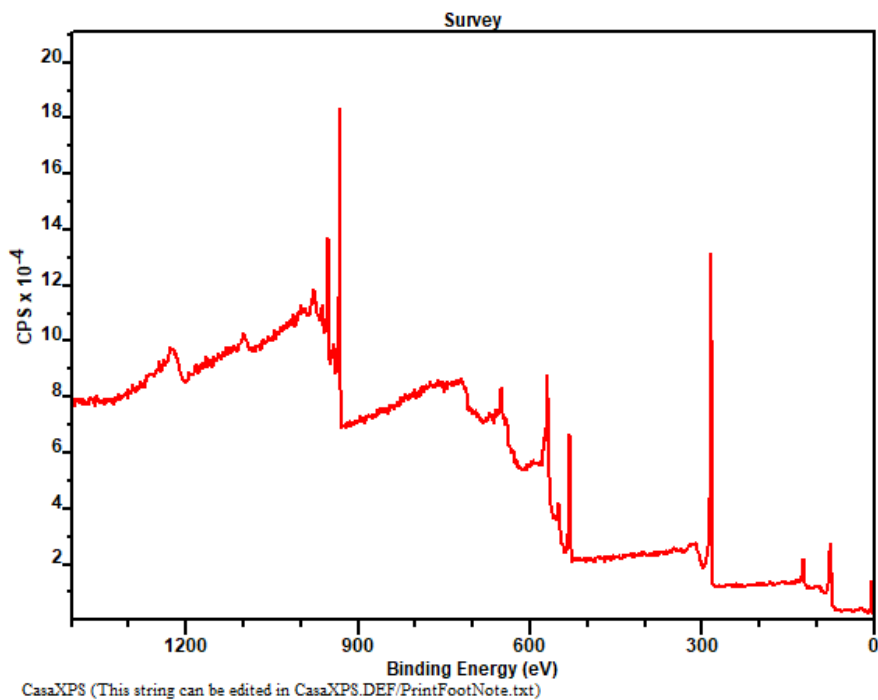
Figure 4.71. General scan for the graphene grown on the Cu substrate for Sample 23.
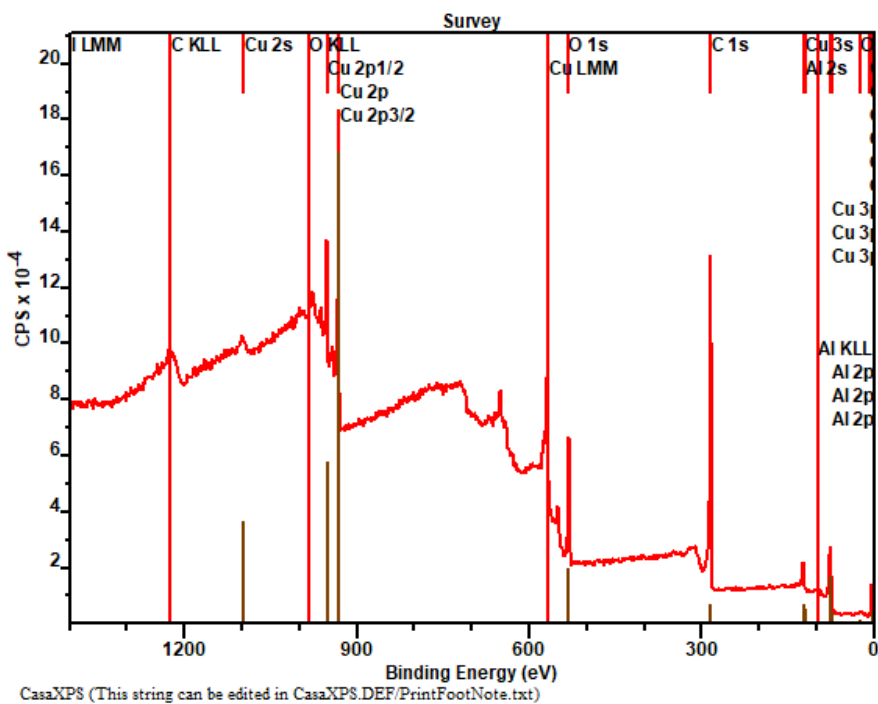

Figure 4.72. General scan for the graphene grown on the self-made Cu substrate for
Sample 23 with labeled peak locations.

Figure 4.71 shows the general scan for the graphene grown on the Cu substrate for Sample 23. Figure 4.72 includes peak labels for the general scan. The identifiable peaks include C KLL, Cu 2s, O KLL, Cu 2p ½, Cu 2p, Cu 2p 3/2, Cu LMM, O 1s, C 1s, Cu 3s. For the purposes of this experiment, the peaks of interest are the C 1s, Cu 3s, and O 1s core level peaks.

C 1s

Name	Pos.	Area	%Area
C sp2	284.57	181513.21	70.39
C-OH	285.67	44759.83	17.35
C-O	286.57	1080.04	0.42
C=O	287.47	9222.24	3.57
C-C=O	288.67	4449.93	1.72
O-C=O	289.97	16935.88	6.55

CasaXPS (This string can be edited in CasaXPS.DEF/PrintFootNote.txt)
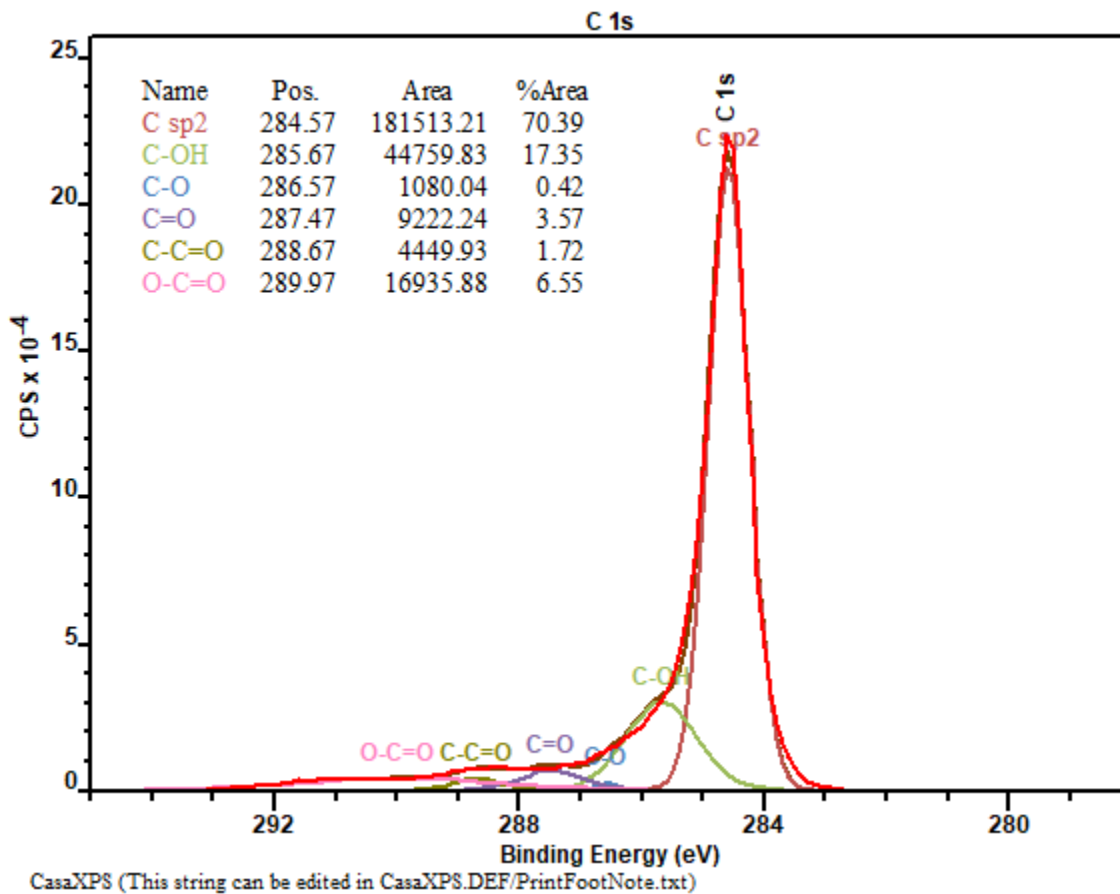
Figure 4.73. High-resolution scan for the C 1s core level peak of graphene on the Cu substrate of Sample 23.

The oxygen-related components of the decomposed peak correspond to 29.61% of the total area of the C 1s peak, indicating a certain degree of oxidation.
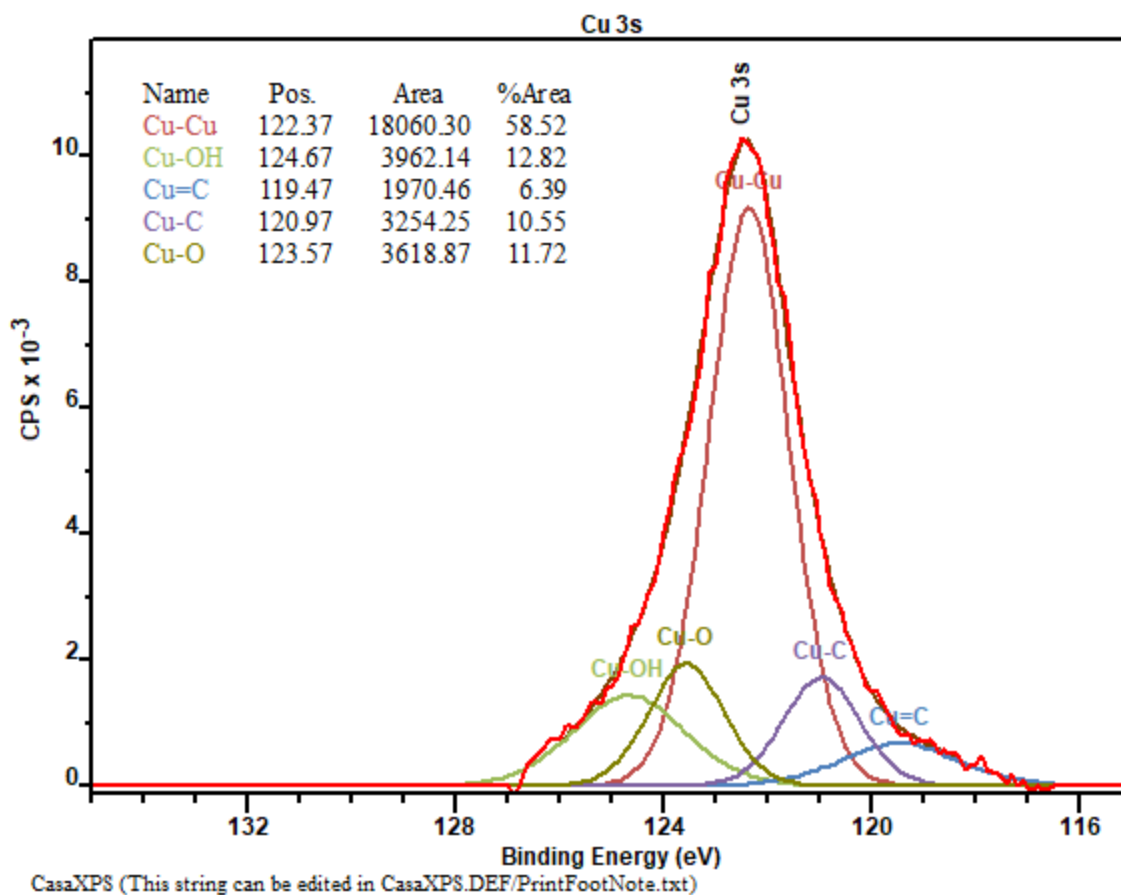
Figure 4.74. High-resolution scan for the Cu 3s core level peak of graphene on the Cu substrate of Sample 23.

The oxygen-related components of the decomposed peak correspond to 24.54% of the total area of the Cu 3s peak, indicating a certain degree of oxidation.
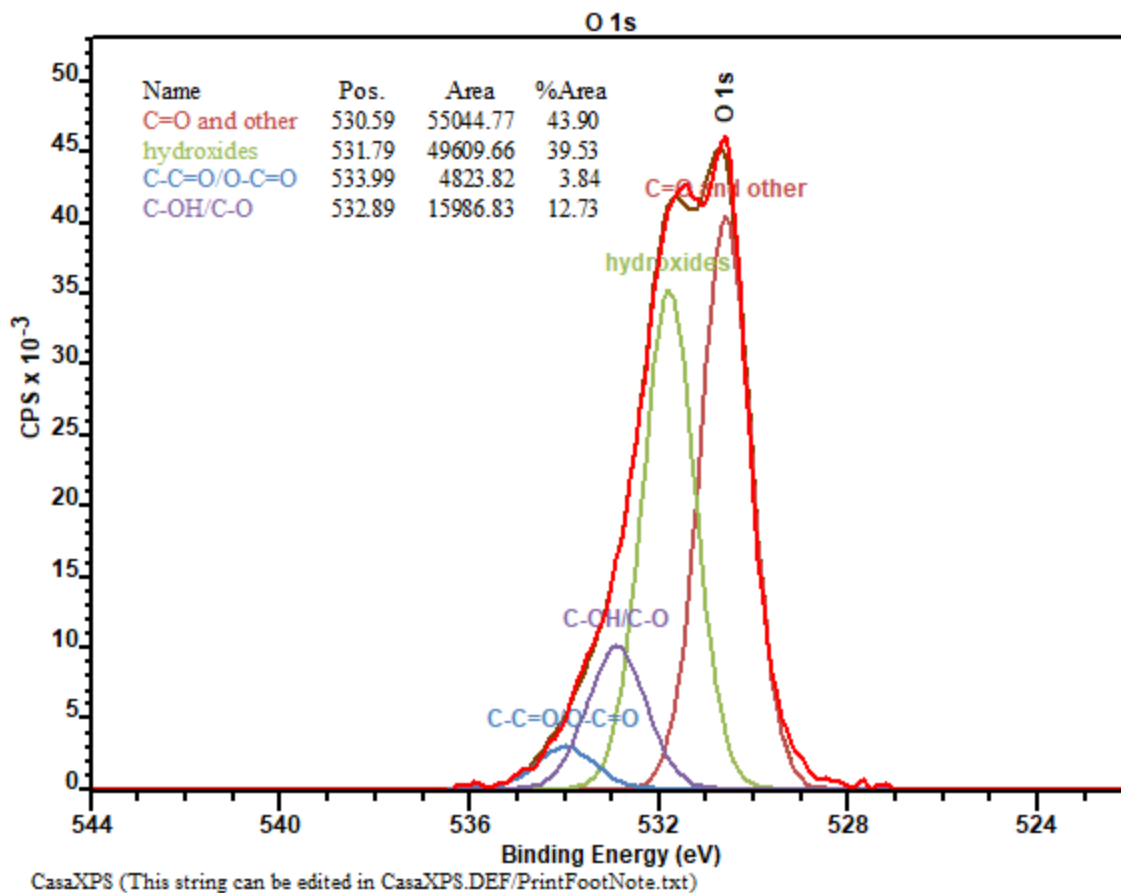
Figure 4.75. High-resolution scan for the O 1s core level peak of graphene on the Cu substrate of Sample 23.

The decomposed peak components indicate that most of the oxygen present is in the form of C=O and other.

4.3.6 Sample 24
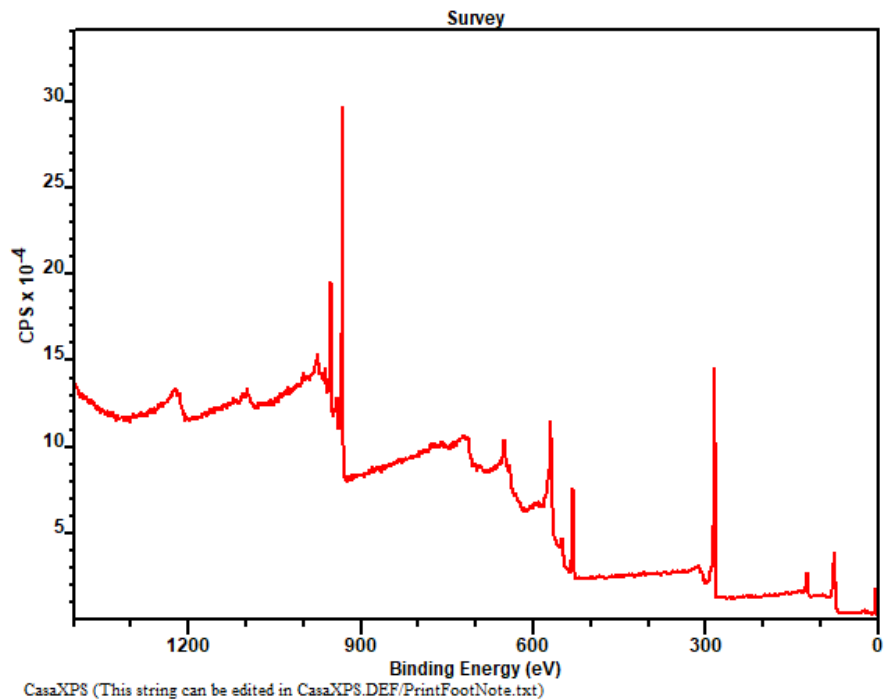
Figure 4.76. General scan for the graphene grown on the Cu substrate for Sample 24.
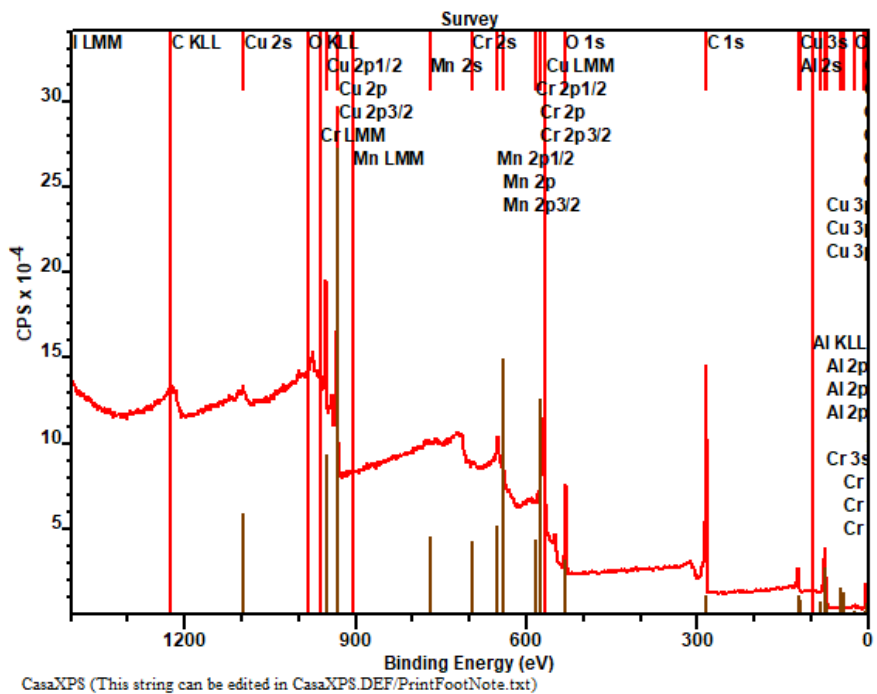

Figure 4.77. General scan for the graphene grown on the self-made Cu substrate for Sample 24 with labeled peak locations.

Figure 4.76 shows the general scan for the graphene grown on the Cu substrate for Sample 24. Figure 4.77 includes peak labels for the general scan. The identifiable peaks include C KLL, Cu 2s, O KLL, Cu 2p ½, Cu 2p, Cu 2p 3/2, Mn 2p ½, Mn 2p, Mn 2p 3/2, Cu LMM, O 1s, C 1s, Cu 3s. For the purposes of this experiment, the peaks of interest are the C 1s, and Cu 3s core level peaks.

| Name	Pos.	Area	%Area
C sp2	284.61	196259.15	66.65
C-OH	285.71	58799.68	19.96
C-O	286.61	414.55	0.14
C=O	287.51	9093.68	3.08
C-C=O	288.71	4903.02	1.66
O-C=O	290.01	25143.81	8.51
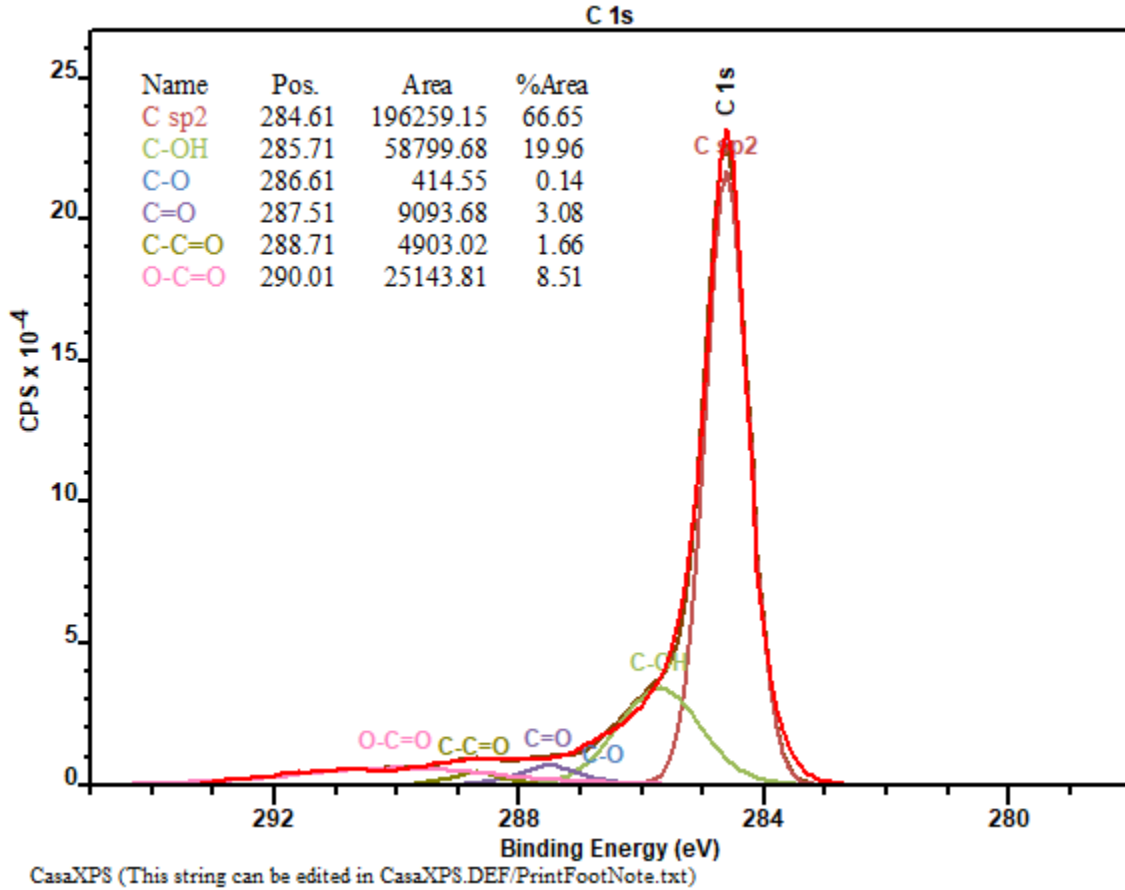
Figure 4.78. High-resolution scan for the C 1s core level peak of graphene on the Cu substrate of Sample 24.

The oxygen-related components of the decomposed peak correspond to 33.35% of the total area of the C 1s peak, indicating a certain degree of oxidation.
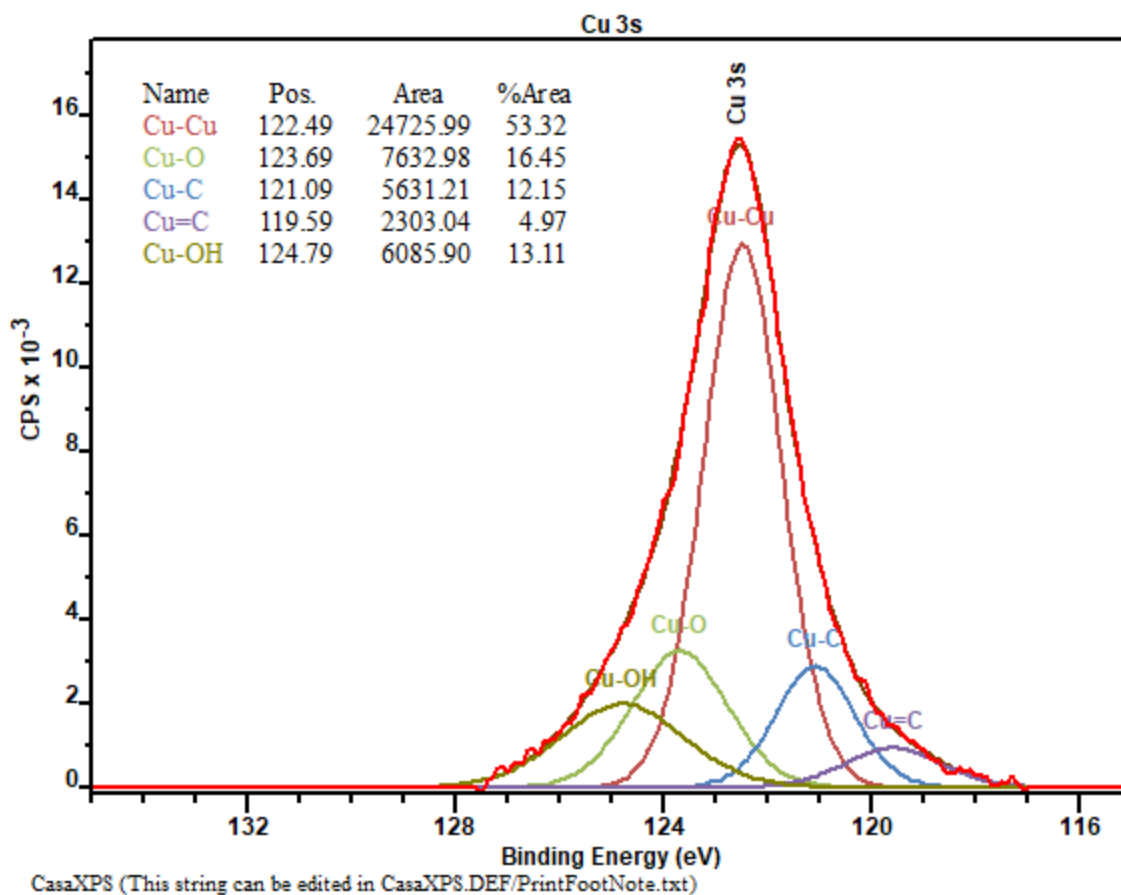
Figure 4.79. High-resolution scan for the Cu 3s core level peak of graphene on the Cu substrate of Sample 24.

The oxygen-related components of the decomposed peak correspond to 29.56% of the total area of the Cu 3s peak, indicating a certain degree of oxidation.
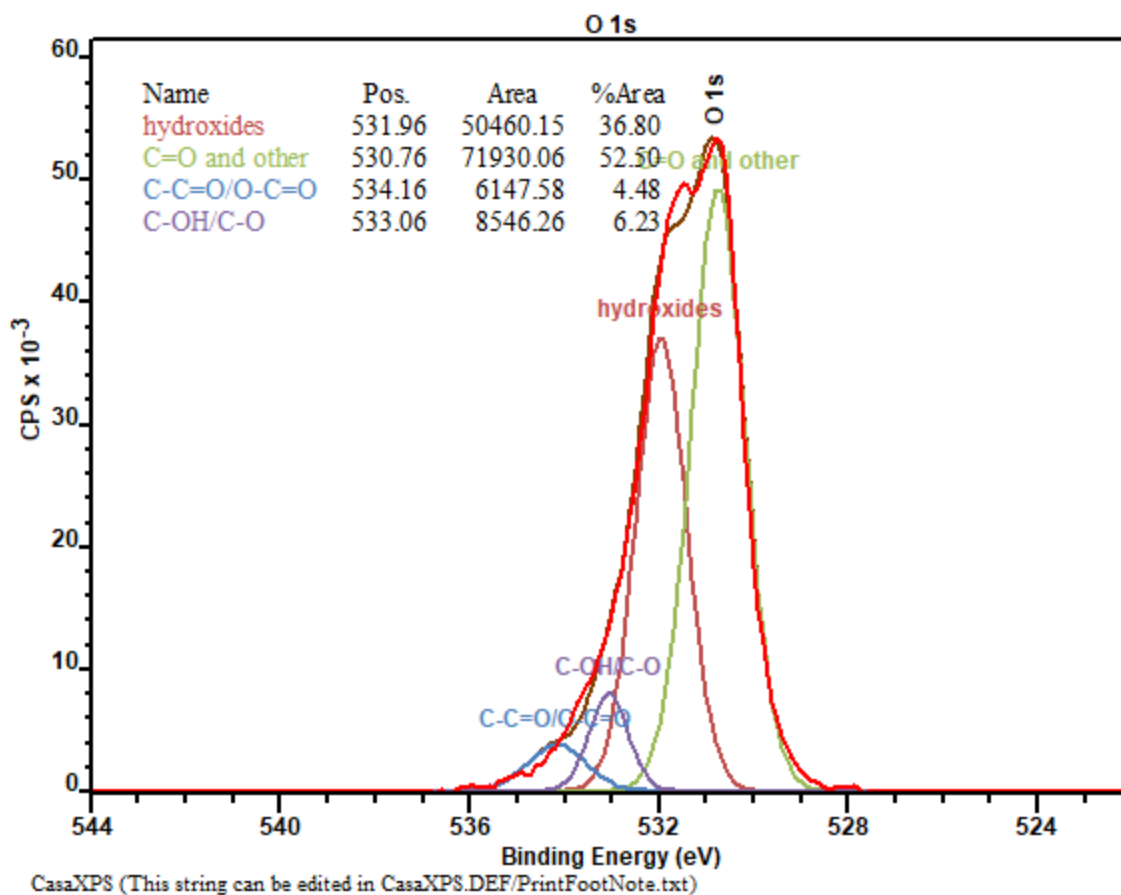
Figure 4.80. High-resolution scan for the O 1s core level peak of graphene on the Cu substrate of Sample 24.

The decomposed peak components indicate that most of the oxygen present is in the form of C=O and other.
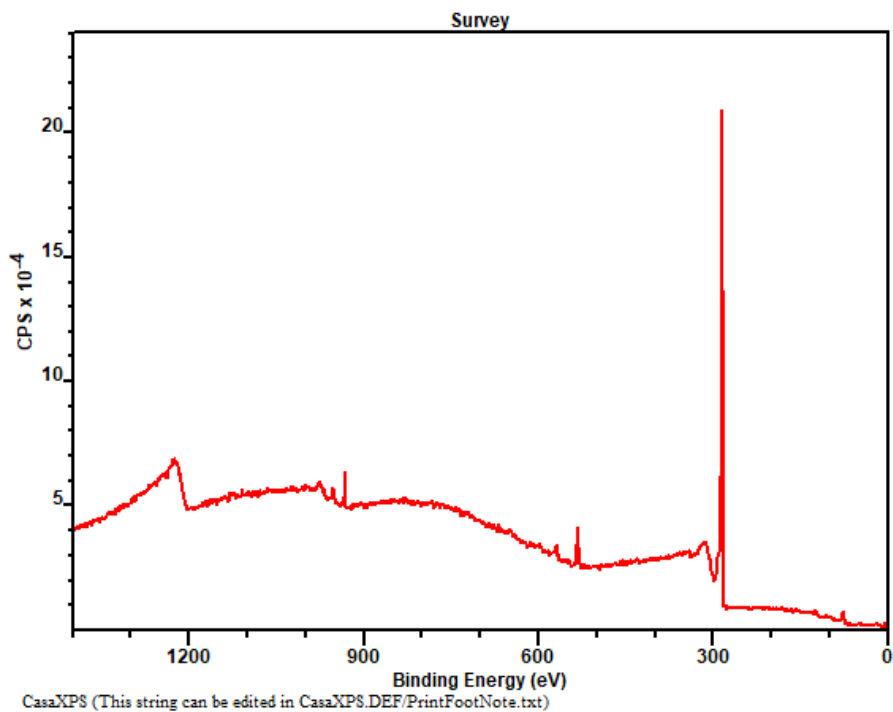
Figure 4.81. General scan for the graphene grown on the Cu substrate for Sample 25.
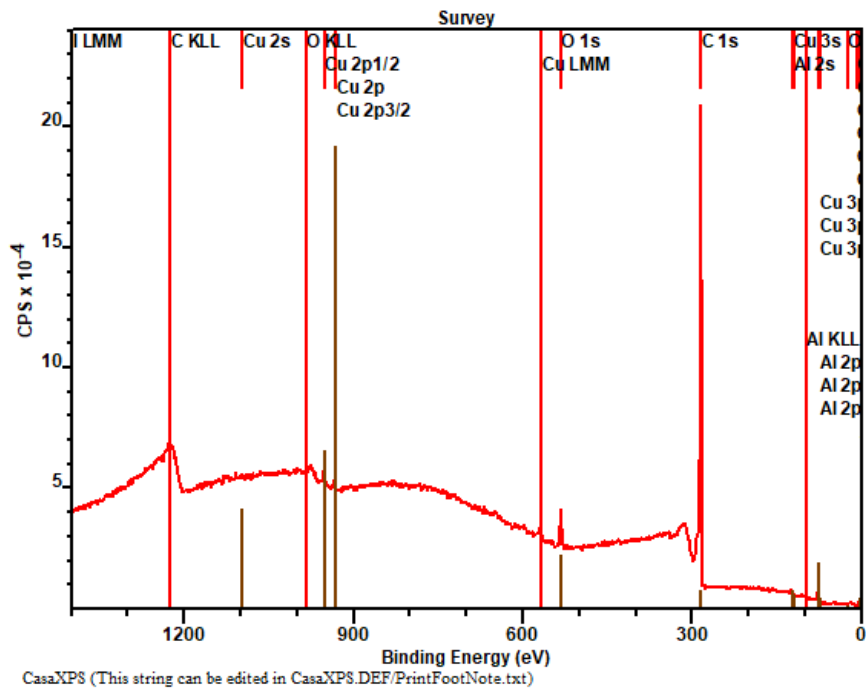

Figure 4.82. General scan for the graphene grown on the self-made Cu substrate for Sample 25 with labeled peak locations.

Figure 4.81 shows the general scan for the graphene grown on the Cu substrate for Sample 25. Figure 4.82 includes peak labels for the general scan. The identifiable peaks include C KLL, O KLL, Cu LMM, O 1s, C 1s, and Cu 3s. For the purposes of this experiment, the peaks of interest are the C 1s, O 1s, and Cu 3s core level peaks.

| Name	Pos.	Area	%Area
C sp2	284.61	287876.35	75.00
C-OH	285.71	70189.65	18.28
C-O	286.61	105.06	0.03
C=O	287.51	8015.68	2.09
C-C=O	288.51	1944.95	0.51
O-C=O	290.01	15813.13	4.11
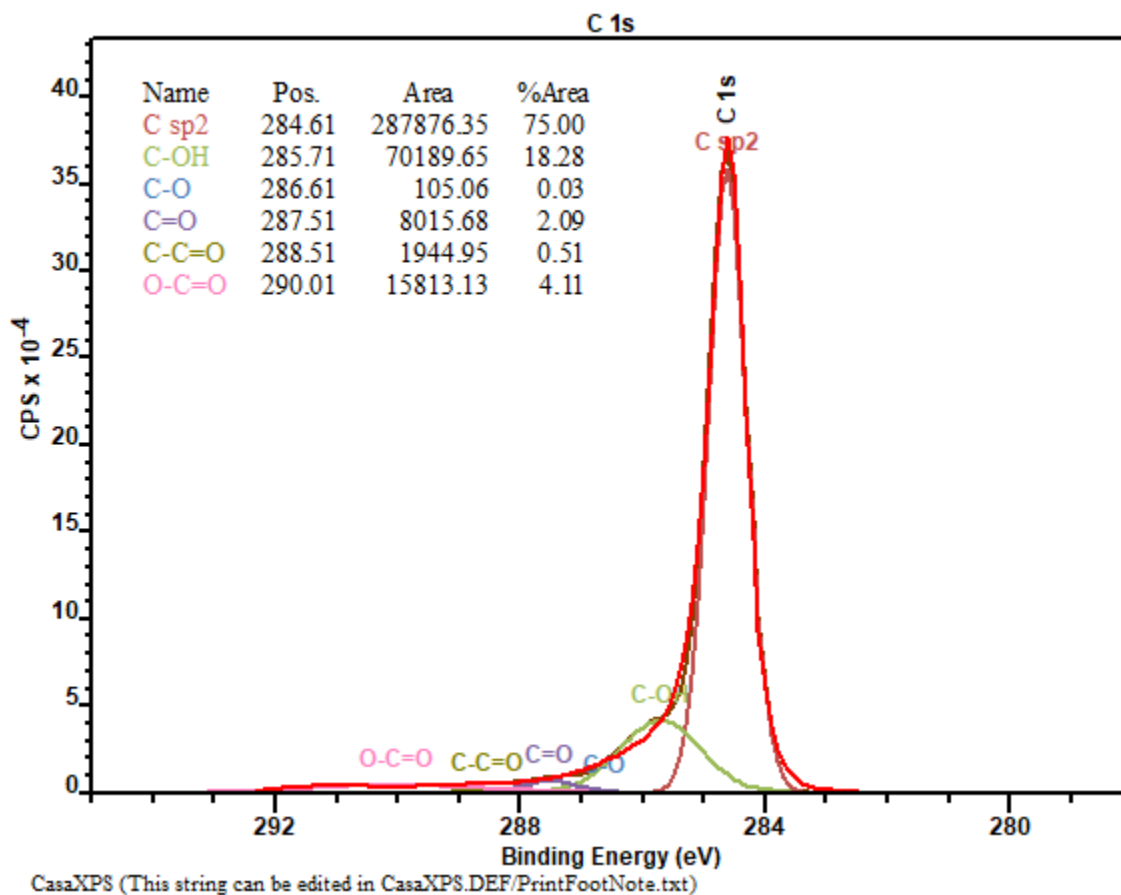
Figure 4.83. High-resolution scan for the C 1s core level peak of graphene on the Cu substrate of Sample 25.

The oxygen-related components of the decomposed peak correspond to 25% of the total area of the C 1s peak, indicating a certain degree of oxidation.
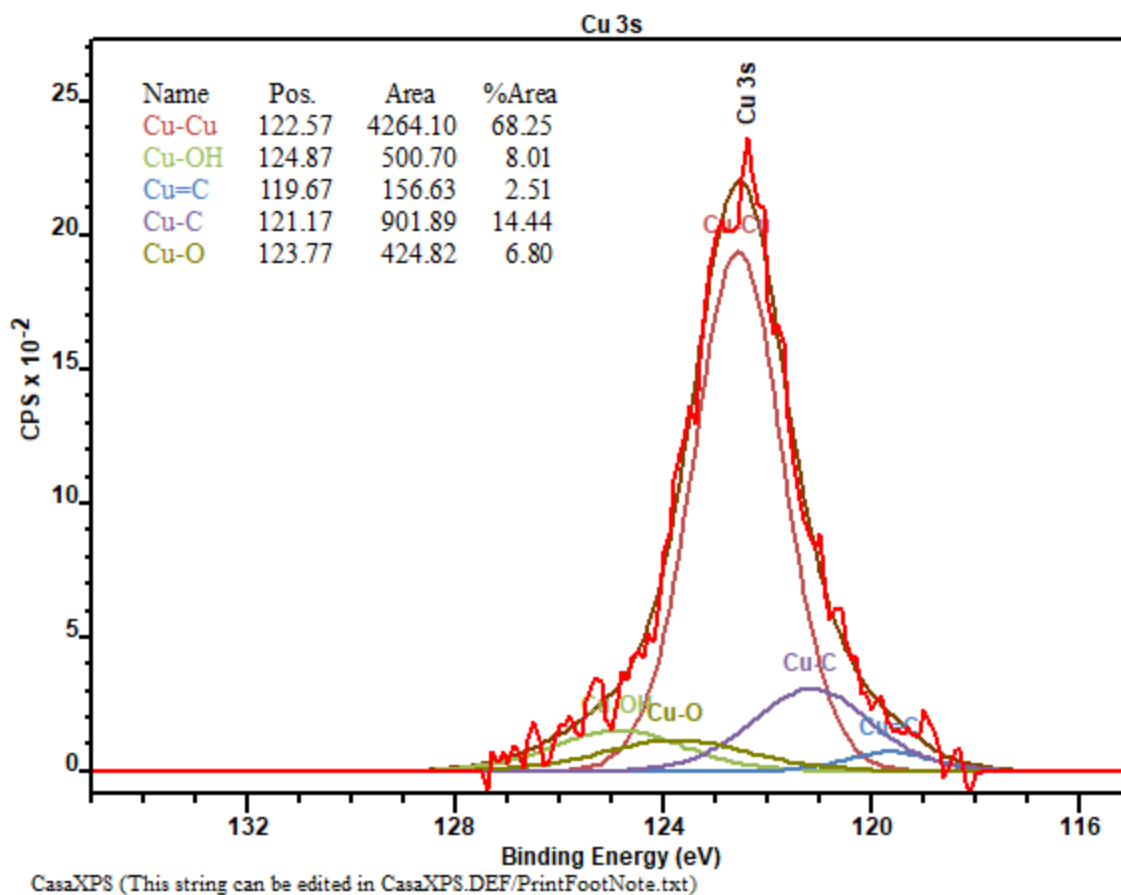
Figure 4.84. High-resolution scan for the Cu 3s core level peak of graphene on the Cu substrate of Sample 25.

The oxygen-related components of the decomposed peak correspond to 14.81% of the total area of the Cu 3s peak, indicating a certain degree of oxidation.
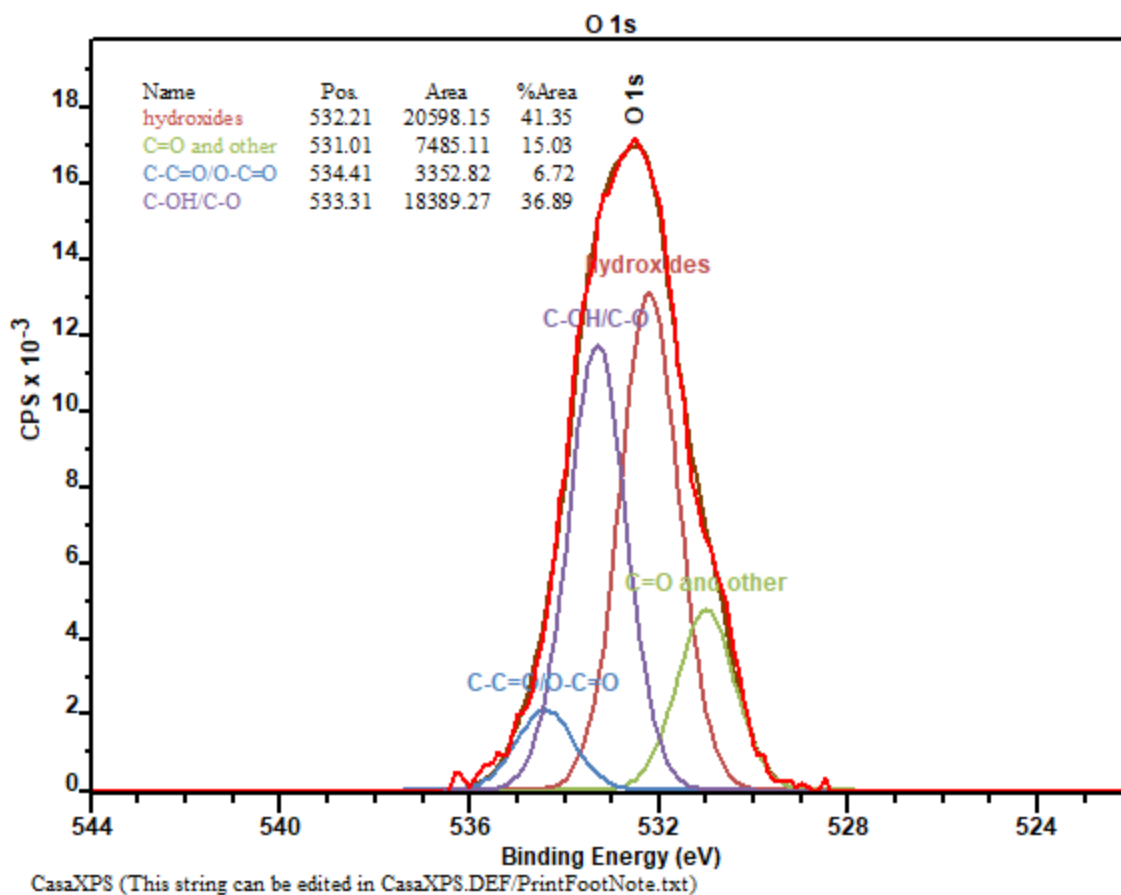
Figure 4.85. High-resolution scan for the O 1s core level peak of graphene on the Cu substrate of Sample 25.

The decomposed peak components indicate that most of the oxygen present is in the form of hydroxides.

4.3.8 Sample 26
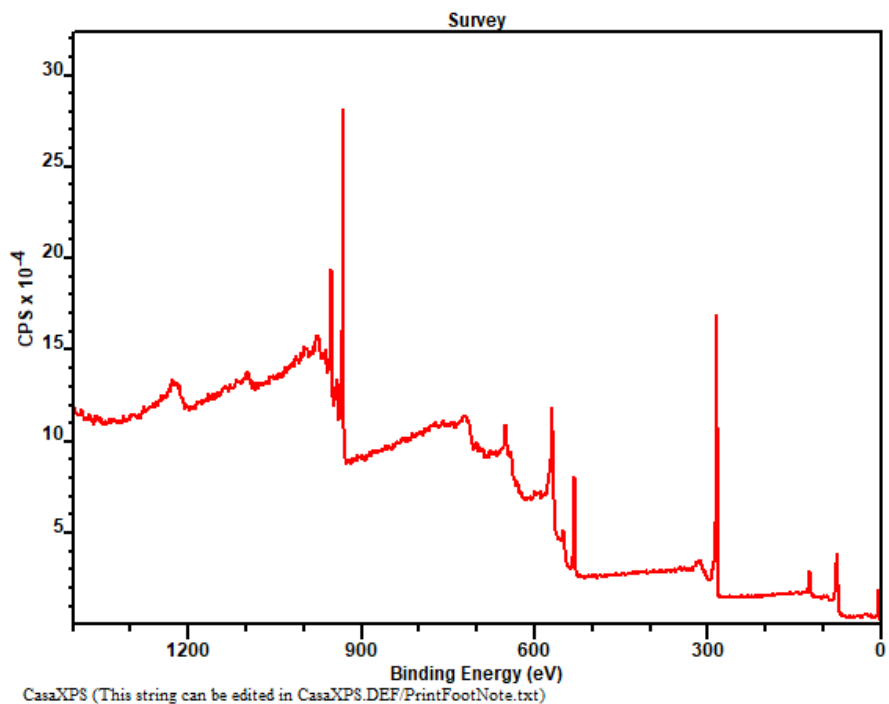
Figure 4.86. General scan for the graphene grown on the Cu substrate for Sample 26.
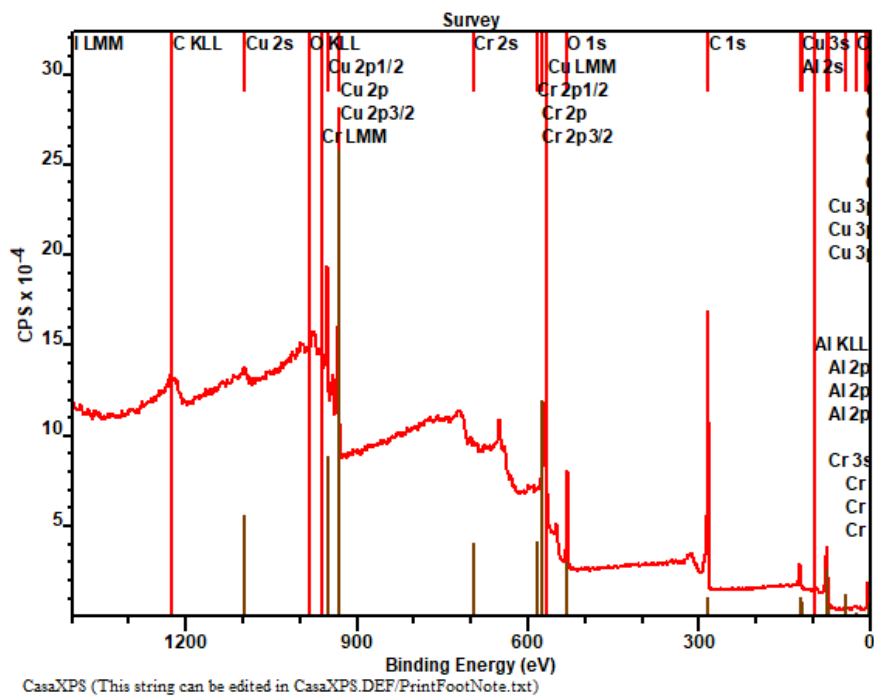

Figure 4.87. General scan for the graphene grown on the self-made Cu substrate for Sample 26 with labeled peak locations.

Figure 4.86 shows the general scan for the graphene grown on the Cu substrate for Sample 25. Figure 4.87 includes peak labels for the general scan. The identifiable peaks include C KLL, Cu 2s, O KLL, Cu 2p ½, Cu 2p, Cu 2p 3/2, Cr 2s, Cu LMM, O 1s, C 1s, and Cu 3s. For the purposes of this experiment, the peaks of interest are the C 1s, O 1s, and Cu 3s core level peaks.

Name	Pos.	Area	%Area
C sp2	284.61	236271.33	77.03
C-OH	285.71	32994.55	10.75
C-O	286.61	13544.96	4.41
C=O	287.51	8799.29	2.86
C-C=O	288.71	9962.06	3.24
O-C=O	290.01	5257.44	1.71

CasaXPS (This string can be edited in CasaXPS.DEF/PrintFootNote.txt)
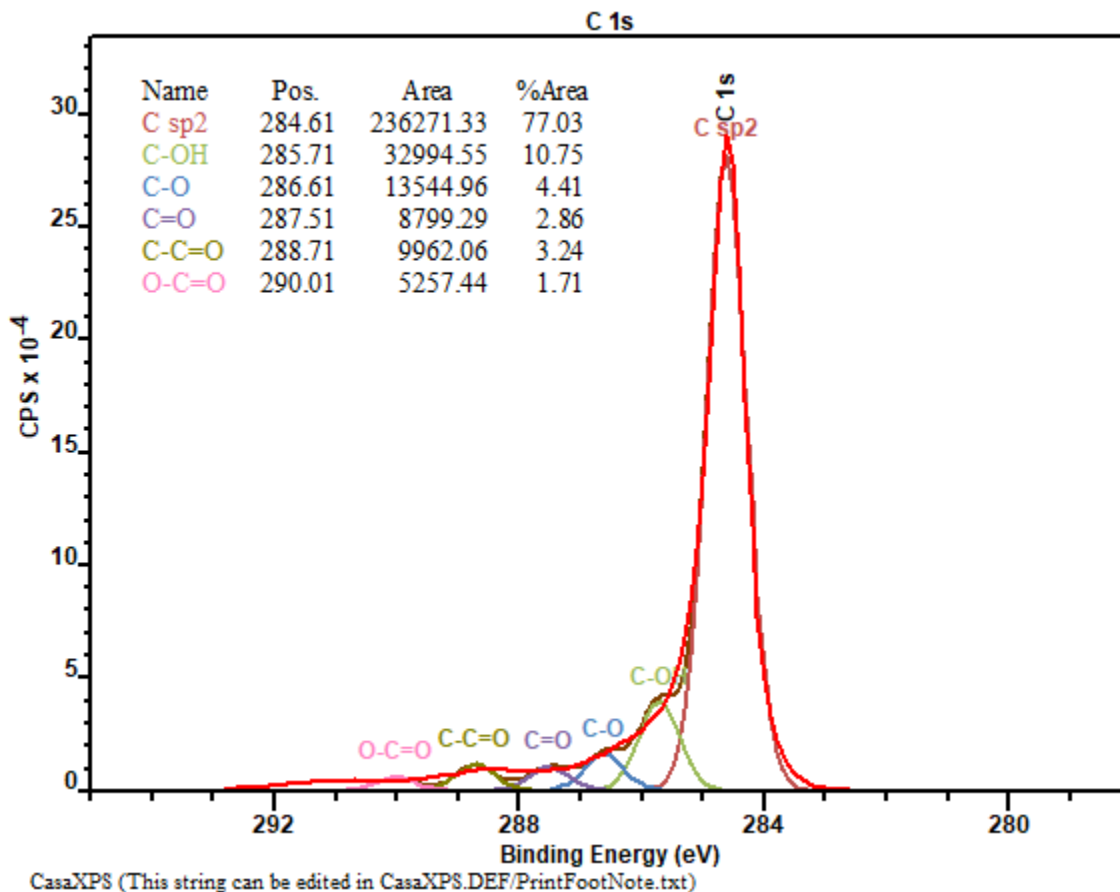
Figure 4.88. High-resolution scan for the C 1s core level peak of graphene on the Cu substrate of Sample 26.

The oxygen-related components of the decomposed peak correspond to 22.97% of the total area of the C 1s peak, indicating a certain degree of oxidation.
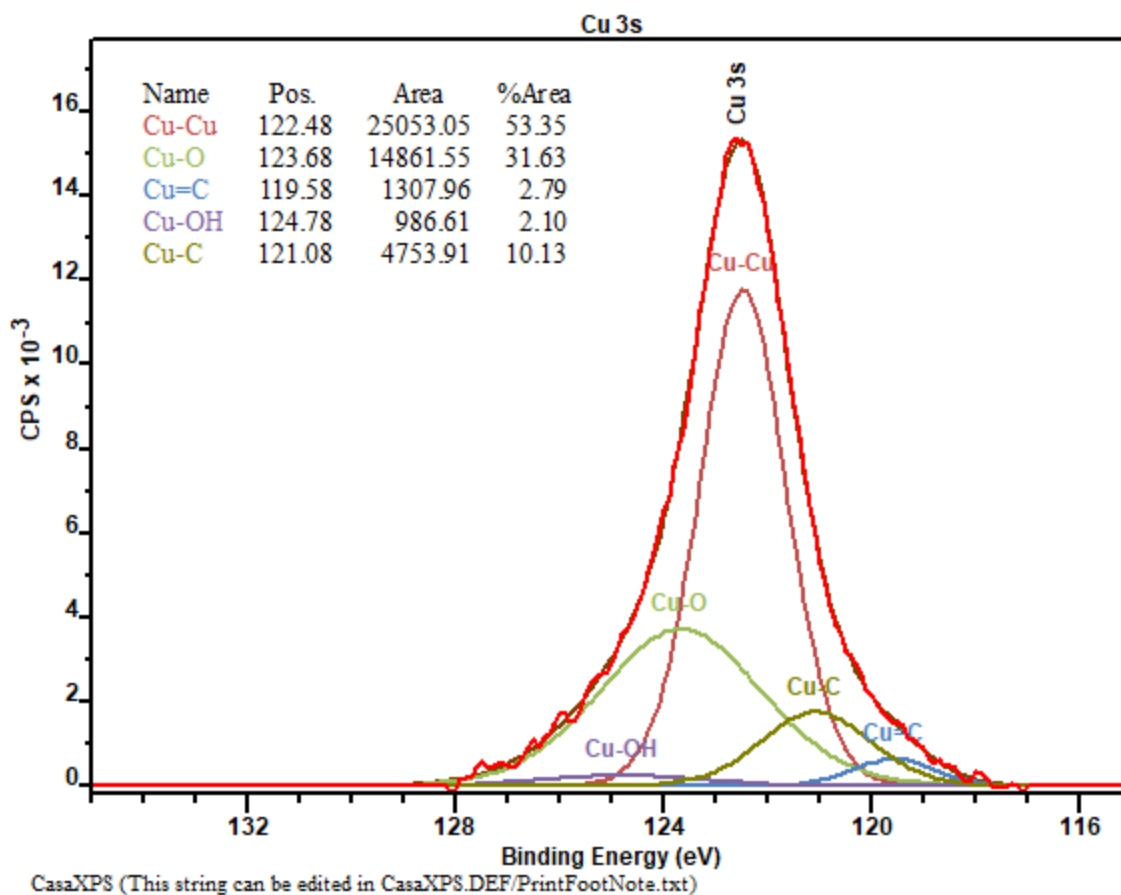
Figure 4.89. High-resolution scan for the Cu 3s core level peak of graphene on the Cu substrate of Sample 26.

The oxygen-related components of the decomposed peak correspond to 33.73% of the total area of the Cu 3s peak, indicating a certain degree of oxidation.
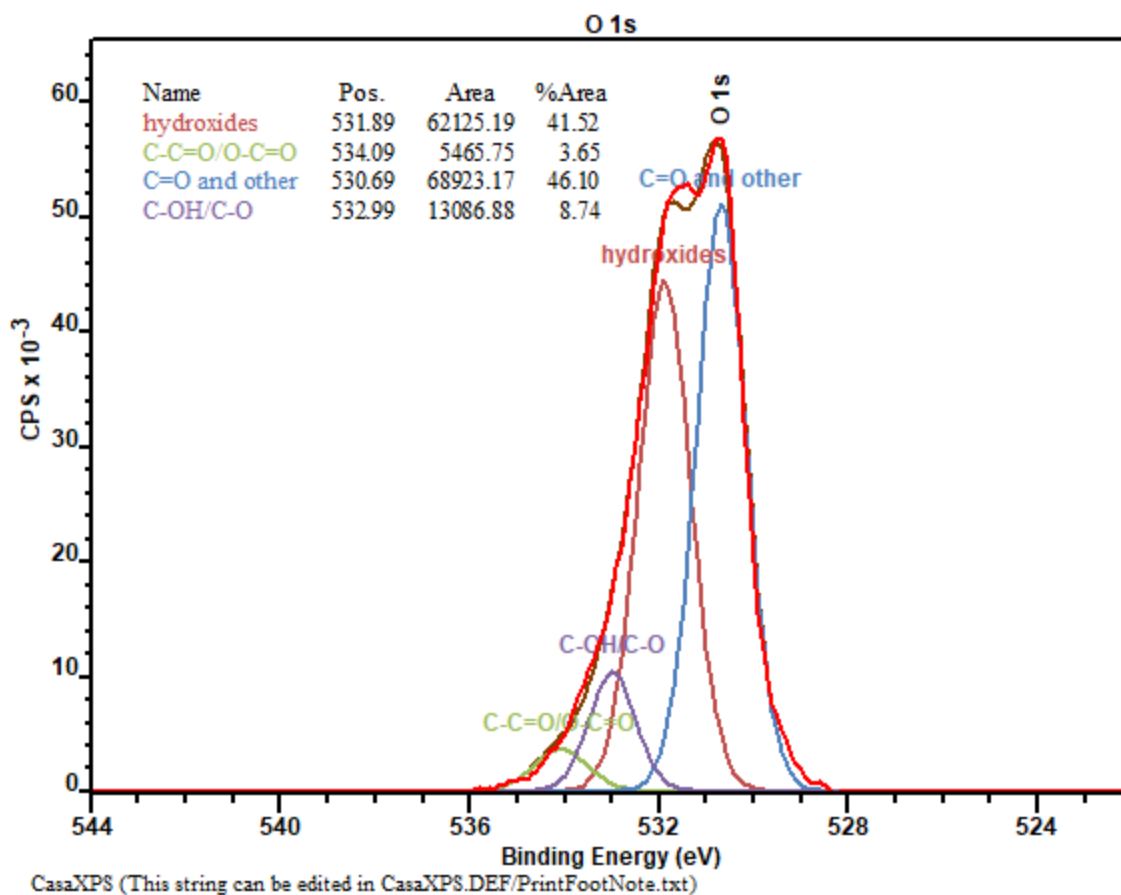
Figure 4.90. High-resolution scan for the O 1s core level peak of graphene on the Cu substrate of Sample 26.

The decomposed peak components indicate that most of the oxygen present is in the form of C=O and other.

### 4.3.9 Conclusion of XPS Data of Samples 19-26

Table 4.1: Summary of Analyzed Core Peak Levels for Samples 19-26

Sample	C 1s oxygen components	Cu 3s oxygen components	O 1s dominating oxygen component
19	44.50%	19.19%	C-OH/C-O
20	N/A	N/A	N/A
21	21.21%	21.07%	hydroxides
22	29.21%	13.84%	hydroxides
23	29.61%	24.54%	C=O and other
24	33.35%	29.56%	C=O and other
25	25.00%	14.81%	hydroxides
26	22.97%	33.73%	C=O and other

Overall, the XPS data was taken of Samples 19-26 was taken to evaluate the quality of the graphene produced. The oxygen components indicate a level of impurity or defects in the graphene produced, thus a lower quality. This section will cover the comparison of the general scans and the three core level peaks of Samples 19-26.

4.3.9.1 C 1s Core Level Peak

The C 1s core level peak was observed to determine the impact or percentage of the carbon content that contains oxygen. This peak in particular was chosen to be observed due to the well determined binding energy for the sp2 configuration.

After the XPS data was decomposed in Sample 19, it was determined that there was a relatively high composition of oxygen in the C 1s peak of 44.50%. As mentioned previously, Sample 19 had relatively good results as compared to the other samples. The results of this higher oxygen composition may suggest that the D peak in the Raman analysis will account for disorder and defects in the carbon but not oxygen content. Unfortunately, no C 1s peak was found in Sample 20 so no XPS analysis was taken. The reason for this is unclear.

The pure Cu samples showed to have the lowest oxygen content with an average 26.67% and the carbon cover samples average 27.11%. It is believed that the main cause of this oxygen content is due to a small leakage in the system as this was a consistent problem during the research process.

4.3.9.2 Cu 3s Core Level Peak

As mentioned previously, the Cu 3s core level peak was observed due to the low level of activity, flat background, as compared to other peaks. Overall, this peak was observed to determine the oxygen components within the Cu substrate to determine the

impact of oxygen. Also, while this peak was observed to determine the oxygen content, the small shifts in different oxygen configurations are difficult to distinguish with XPS.

For Sample 19, the oxygen components comprise 19.19% of the substrate observed. The average for the pure Cu samples is 19.82% and the carbon cover samples average 26.03%. This suggests that the oxygen content of the Cu/Ni samples are similar to the pure Cu samples, while the carbon cover samples contain the highest amount of oxygen components. This could be due to the carbon cover samples have a low uniformity of graphene and thus have more surface area to react with the ambient oxygen presence.

4.3.9.3 O 1s Core Level Peak

The O 1s core level peak was observed to determine the type of oxygen present in the samples. The type of oxygen, and oxygen in general, can greatly impact the mechanical and electrical properties in grown graphene and as such, the oxygen components were observed in detail using XPS.

Overall, the oxygen components appeared to either be in the form of hydroxides or C=O and other carbon complexes. However, Sample 19 showed to have C-OH/C-O as the most prominent oxygen component.

5. CONCLUSION AND FUTURE WORK

In this research, work was completed to attempt in producing a more uniform, multi-layer graphene. Initially, samples were produced to help promote the carbon absorption by moving from a tungsten base and using pure Cu. Next, samples were produced using a Cu/Ni alloy to promote the absorption of carbon into the substrate, increasing the ability to produce graphene. With this change, the tungsten base was exchanged for an Al_2O_3 base, as the tungsten base will react with the Ni to produce a Cu/Ni/W alloy. Finally, graphene samples were beginning to be produced, but with very low uniformity and quality. Several steps were taken such as increasing the baking temperature, rapid cooling, sonication to clean the Al_2O_3 base to reduce contamination, and a self-made Cu/Ni alloy. These samples were produced with varying methane flow rates to examine the effect of the graphene production.

In total, 26 samples were produced. For critical analysis, Samples 19-26 were examined using Raman spectroscopy and XPS. Samples 19 and 20 used the self-made Cu/Ni alloy with two different flow rates, Samples 21, 22, and 23 used a pure Cu substrate with varying methane flow rates, and Samples 24, 25, and 26 used pure Cu substrates with a carbon cover to help promote a temperature gradient to potentially increase the number of graphene layers produced as well as the uniformity.

The Raman spectroscopy results showed that Samples 19 and 20 had the best uniformity and quality. The spectra collected from several regions on the samples surface showed that, in general, the vast majority of the sample surface contained graphene. Also, the low D band peaks suggest a low number of defects. Between Sample 19 and Sample 20, Sample 20 showed more consistency in the graphene flakes with optical microscopy.

Both samples also showed a consistent amount of amorphous carbon. Overall, Sample 20 seems more promising in quality and uniformity as compared to all other samples.

Samples 21, 22, and 23 were produced as a control group to compare with the Cu/Ni samples and the carbon cover samples. Overall, the graphene was present on the vast majority of the sample. However, the uniformity was low. As compared to the Cu/Ni Samples 19 and 20, Samples 21, 22, and 23 also had a lower amount of amorphous carbon. Compared to the Cu/Ni samples, the pure Cu samples showed to have less uniformity of graphene, but less amorphous carbon.

Samples 24, 25, and 26 were produced using a carbon cover to produce a temperature gradient, which should theoretically promote a more uniform, multi-layer graphene. Unfortunately, results of the samples proved otherwise. Compared to Samples 21-23, the use of the carbon cover seemed to have a negative effect on the uniformity of the graphene while the amount of amorphous carbon seemed to be unaffected. In terms of quality, Samples 21-23 were better in quality and uniformity.

After completing the Raman analysis of Samples 19-26, it was determined that Samples 19 and 20 were the most successful, followed by Samples 21, 22, and 23, and finally Samples 24, 25, and 26. Again, this is due to Samples 19 and 20 displaying the highest amount of uniformity and quality. While the other samples did produce graphene, they were not of the same quality. Unfortunately, the use of the carbon cover seemed to have a negative impact on the production of higher quality and more uniform graphene.

Next, XPS was used to evaluate the quality of the graphene produced. To determine the quality, the oxygen components of the carbon and substrates were examined. A higher oxygen component would suggest a higher content of impurities and

thus a lower quality sample. Samples 19-26 were examined using XPS and were compared.

For core level peak decomposition, peaks C 1s, Cu 3s, and O 1s were used. C 1s has a well determined binding energy in the sp2 configuration, making it valuable for decomposition. The Cu 3s peak was used over the other core level peaks due to the flat background surrounding the peak. However, this peak is not useful in distinguishing between the different oxidized configurations. Fortunately, this research is concerned more with the general content. Finally, the O 1s peak is examined to determine the functional groups in the oxygen components, which can affect the mechanical and electrical properties of the graphene.

After the XPS data was decomposed, it was determined that there was a relatively high composition of oxygen in the C 1s peak of 44.50% in Sample 19. As mentioned previously, Sample 19 had relatively good results as compared to the other samples. The results of this higher oxygen composition may suggest that the D peak in the Raman analysis will account for disorder and defects in the carbon but not oxygen content. Unfortunately, no C 1s peak was found in Sample 20 so no XPS analysis was taken. The reason for this is unclear. For Sample 19, the oxygen components comprise 19.19% of the substrate observed. The average for the pure Cu samples is 19.82% and the carbon cover samples average 26.03%. This suggests that the oxygen content of the Cu/Ni samples are similar to the pure Cu samples, while the carbon cover samples contain the highest amount of oxygen components. This could be due to the carbon cover samples have a low uniformity of graphene and thus have more surface area to react with the ambient oxygen presence.

The pure Cu samples showed to have the lowest oxygen content with an average 26.67% and the carbon cover samples average 27.11%. It is believed that the main cause of this oxygen content is due to a small leakage in the system as this was a consistent problem during the research process.

Finally, the oxygen components appeared to either be in the form of hydroxides or C=O and other carbon complexes. However, Sample 19 showed to have C-OH/C-O as the most prominent oxygen component.

With the consideration of both the Raman analysis and the XPS results, Samples 19 and 20 showed to have the best results. While Sample 19 did show to have a higher oxygen content, the Raman analysis did not show any real indication of defects or peak shifts or intensity changes. This oxygen component may be localized to particular areas and not a general problem in the graphene over the sample. Next, the pure Cu samples showed to have the next best results, with the carbon cover samples with the least promising results.

The results of this research unfortunately did not produce samples which would be entirely appropriate for the replacement of carbon foils in space plasma instruments as the production of a more perfect and uniform multi-layer graphene is still needed. More work must be conducted to produce a foil which can appropriately achieve the requirements, both mechanically and electrically to replace the currently used carbon foils. A better way to produce graphene foils for these instruments would be to use the direct transfer of graphene as outlined in the literature review (Regan et al., 2010). By completing this transfer technique onto the TEM type grid, graphene layers can be stacked to achieve the required thickness. However, as mentioned previously, this method

jeopardizes the integrity of the graphene foil and causes the foil to have a higher risk of contamination, which would adversely affect the quality of the instrument.

A potential issue with the experiments conducted in this research include oxygen leaks, sample contamination, and Ni distribution with the Cu/Ni alloy. It is believed that a potential source for a lower quality of uniformity is the improper distribution of Ni within the Cu substrate. A potential solution for this is to increase the baking time during the alloy creation phase and to properly rapidly cool the sample to reduce the chance for the Cu and Ni to desegregate. Also, the use of a thinner, and more appropriate base other than the Al_2O_3 would help with the rapid cooling. A thinner base would hold less thermal energy during the graphene growth process. The rapid cooling process may be hindered by the thermal energy contained in the base. A new base which is thinner and promotes a wetting state, like the tungsten with pure Cu, would help to create a more uniform and even surface.

The technological history of mankind has been defined by the material most common and useful to everyday life. The Stone Age, the Bronze Age, the Iron Age, one can call the current age the Silicon Age. With the discovery of graphene and its incredible characteristics, modern technology could one day become based entirely around this super material and bring humanity into the Graphene Age with medical, military, industrial, mechanical and electrical applications that seem to only be limited by one's own imagination. However, humanity has not yet reached the Graphene Age and still struggles in its attempt to perfect a method to integrate the material into new technology, including space plasma instruments. With time and patience, perhaps humanity will see this new technological era. A method to produce clean graphene may prove to be a

139

suitable replacement for the carbon foils currently implemented in space plasma

instruments to have graphene in a new application and bring the world one step closer to

a Graphene Age.

REFERENCES

Aftab, S. M. A., Shaikh, R. B., Saifullah, B., Hussein, M. Z., & Ahmed, K. A. (2019). *Aerospace applications of graphene nanomaterials*.

Ahn, Y., Kim, J., Ganorkar, S., Kim, Y.-H., & Kim, S.-I. (2016). Thermal annealing of graphene to remove polymer residues. *Materials Express, 6*(1), 69-76. doi:10.1166/mex.2016.1272

Allegrini, F., Ebert, R. W., & Funsten, H. O. (2016). Carbon foils for space plasma instrumentation. *Journal of Geophysical Research: Space Physics, 121*(5), 3931-3950. doi:10.1002/2016ja022570

Arai, Y., Noto, Y., Goto, Y., Takahashi, S., Yamamoto, M., Nishiyama, T., . . . Horibe, H. (2015). Study of the decomposition mechanism of PMMA-type polymers by hydrogen radicals. *Thin Solid Films, 575*, 12-16. doi:10.1016/j.tsf.2014.10.021

Cheng, H., Gadora, K., Wang, Z., Zhang, H., Jiang, W., Chen, X., . . . Ding, Y. (2019). Functionalized nanographene oxide in biomedicine applications: bioinspired surface modifications, multidrug shielding, and site-specific trafficking. *Drug Discov Today, 24*(3), 749-762. doi:10.1016/j.drudis.2019.01.022

Childres, I., Jauregui, L., Park, W., Cao, H., & Chen, Y. Raman Spectroscopy of Graphene and Related Materials.

Delfour, L., Davydova, A., Despiau-Pujo, E., Cunge, G., Graves, D. B., & Magaud, L. (2016). Cleaning graphene: A first quantum/classical molecular dynamics approach. *Journal of Applied Physics, 119*(12). doi:10.1063/1.4945034

Giesbers, A. J. M., Bouten, P. C. P., Cillessen, J. F. M., van der Tempel, L., Klootwijk, J. H., Pesquera, A., . . . Balkenende, A. R. (2016). Defects, a challenge for graphene in flexible electronics. *Solid State Communications, 229*, 49-52. doi:10.1016/j.ssc.2016.01.002

Hawaldar, R., Merino, P., Correia, M. R., Bdikin, I., Gracio, J., Mendez, J., . . . Singh, M. K. (2012). Large-area high-throughput synthesis of monolayer graphene sheet by Hot Filament Thermal Chemical Vapor Deposition. *Sci Rep, 2*, 682. doi:10.1038/srep00682

Hinnemo, M., Ahlberg, P., Hägglund, C., Ren, W., Cheng, H.-M., Zhang, S.-L., & Zhang, Z.-B. (2016). Scalable residue-free graphene for surface-enhanced Raman scattering. *Carbon, 98*, 567-571. doi:10.1016/j.carbon.2015.11.043

Huang, M., & Ruoff, R. S. (2020). Growth of Single-Layer and Multilayer Graphene on Cu/Ni Alloy Substrates. *Acc Chem Res, 53*(4), 800-811. doi:10.1021/acs.accounts.9b00643

Huang, S., Dakhchoune, M., Luo, W., Oveisi, E., He, G., Rezaei, M., . . . Agrawal, K. V. (2018). Single-layer graphene membranes by crack-free transfer for gas mixture separation. *Nat Commun, 9*(1), 2632. doi:10.1038/s41467-018-04904-3

Islam, A. E., Zakharov, D. N., Carpena-Nuñez, J., Hsiao, M.-S., Drummy, L. F., Stach, E. A., & Maruyama, B. (2017). Atomic level cleaning of poly-methyl-methacrylate residues from the graphene surface using radiolized water at high temperatures. *Applied Physics Letters, 111*(10). doi:10.1063/1.5001479

Kim, S., Shin, S., Kim, T., Du, H., Song, M., Lee, C., . . . Seo, S. (2016). Robust graphene wet transfer process through low molecular weight polymethylmethacrylate. *Carbon, 98*, 352-357. doi:10.1016/j.carbon.2015.11.027

Kireev, D., Sarik, D., Wu, T., Xie, X., Wolfrum, B., & Offenhäusser, A. (2016). High throughput transfer technique: Save your graphene. *Carbon, 107*, 319-324. doi:10.1016/j.carbon.2016.05.058

Lee, H. C., Liu, W.-W., Chai, S.-P., Mohamed, A. R., Aziz, A., Khe, C.-S., . . . Hashim, U. (2017). Review of the synthesis, transfer, characterization and growth mechanisms of single and multilayer graphene. *RSC Advances, 7*(26), 15644-15693. doi:10.1039/c7ra00392g

Liu, H., Xing, Z., Zhang, J., Pan, J.-H., Wang, H., & Zhang, X. (2016). A Facile Chemical-Free and Universal Method for Transfer of Ultrathin Graphene-Based Films. *Advanced Materials Interfaces, 3*(18). doi:10.1002/admi.201600540

Liu, J., & Fu, L. (2019). Controllable Growth of Graphene on Liquid Surfaces. *Adv Mater, 31*(9), e1800690. doi:10.1002/adma.201800690

Liu, Y., Liu, Z., Lew, W. S., & Wang, Q. J. (2013). Temperature dependence of the electrical transport properties in few-layer graphene interconnects. *Nanoscale Res Lett, 8*(1), 335. doi:10.1186/1556-276X-8-335

Longchamp, J.-N., Escher, C., & Fink, H.-W. (2013). Ultraclean freestanding graphene by platinum-metal catalysis. *Journal of Vacuum Science & Technology B, Nanotechnology and Microelectronics: Materials, Processing, Measurement, and Phenomena, 31*(2). doi:10.1116/1.4793746

Nath, A., Koehler, A. D., Jernigan, G. G., Wheeler, V. D., Hite, J. K., Hernández, S. C., . . . Rao, M. V. (2014). Achieving clean epitaxial graphene surfaces suitable for device applications by improved lithographic process. *Applied Physics Letters, 104*(22). doi:10.1063/1.4880937

Nguyen, V. T., Le, H. D., Nguyen, V. C., Ngo, T. T. T., Le, D. Q., Nguyen, X. N., & Phan, N. M. (2013). Synthesis of multi-layer graphene films on copper tape by atmospheric pressure chemical vapor deposition method. *Advance in Natural Sciences: Nanoscience and Nanotechnology, 4*.

Regan, W., Alem, N., Alemán, B., Geng, B., Girit, Ç., Maserati, L., . . . Zettl, A. (2010). A direct transfer of layer-area graphene. *Applied Physics Letters, 96*(11). doi:10.1063/1.3337091

Wang, B., Huang, M., Tao, L., Lee, S. H., Jang, A. R., Li, B. W., . . . Ruoff, R. S. (2016). Support-Free Transfer of Ultrasmooth Graphene Films Facilitated by Self-Assembled Monolayers for Electronic Devices and Patterns. *ACS Nano, 10*(1), 1404-1410. doi:10.1021/acsnano.5b06842

Yasunishi, T., Takabayashi, Y., Kishimoto, S., Kitaura, R., Shinohara, H., & Ohno, Y. (2016). Origin of residual particles on transferred graphene grown by CVD. *Japanese Journal of Applied Physics, 55*(8). doi:10.7567/jjap.55.080305

Zhang, G., Guell, A. G., Kirkman, P. M., Lazenby, R. A., Miller, T. S., & Unwin, P. R. (2016). Versatile Polymer-Free Graphene Transfer Method and Applications. *ACS Appl Mater Interfaces, 8*(12), 8008-8016. doi:10.1021/acsami.6b00681

Zhang, Z., Du, J., Zhang, D., Sun, H., Yin, L., Ma, L., . . . Ren, W. (2017). Rosin-enabled ultraclean and damage-free transfer of graphene for large-area flexible organic light-emitting diodes. *Nat Commun, 8*, 14560. doi:10.1038/ncomms14560